THE EFFECTS OF PORE FLUIDS AND FRICTIONAL SLIDING ON SEISMIC ATTENUATION

A DISSERTATION
SUBMITTED TO THE DEPARTMENT OF GEOPHYSICS
AND THE COMMITTEE ON GRADUATE STUDIES
OF STANFORD UNIVERSITY
IN PARTIAL FULFILLMENT OF THE REQUIREMENTS
FOR THE DEGREE OF
DOCTOR OF PHILOSOPHY

By
Kenneth William Winkler
June 1979

ABSTRACT

Two aspects of seismic wave propagation are of particular interest to geophysicists. These are velocity and attenuation. From the work of others we have a reasonably good understanding of the strong effects that pore fluids and pore structure have on velocity. The goal of this study is to determine the effects that pore fluids and pore structure have on seismic attenuation, as well as to gain an understanding of the physical mechanisms involved in converting seismic energy into heat.

We have adopted an experimental approach using a bar resonance technique. One meter long bars of rock are vibrated in torsional and extensional modes at frequencies between about 500 and 1700 hertz. Confining pressure, pore pressure, degree of saturation and strain amplitude can all be varied. Our results have shown that pore fluids dominate seismic attenuation under the conditions of our experiments, conditions which are in many ways representative of the Earth's upper crust. In dry sandstone both P-waves and shear waves show relatively small amounts of attenuation. Partial saturation with water (to about 95%) causes attenuation to increase by a factor of two to four and results in P-waves being attenuated more strongly than shear waves. The transition to total saturation results in maximum shear wave attenuation, but causes a significant reduction in P-wave attenuation. In fully saturated rock, shear waves are attenuated more strongly than P-waves.

These observations are interpreted in terms of several mechanisms involving pore fluids. In fully saturated rock, viscous fluid flow between adjacent cracks results in energy loss. In partially saturated rock either intra-crack fluid flow or thermoelastic effects can explain the observations.

We have also investigated the popular attenuation mechanism involving frictional sliding at grain boundaries. Attenuation is found to be dependent on strain amplitude at large strains, in agreement with theoretical predictions of frictional models. The amplitude dependence is eliminated by moderate confining pressures, presumably because grains are being locked together and prevented from sliding. Our results indicate that frictional sliding causes significant attenuation only under laboratory conditions of large strain and low confining pressure. At the low strains and high confining pressures encountered in seismology, frictional attenuation will be negligible.

We have found that attenuation is generally much more sensitive to rock properties than is velocity. It is not yet clear whether this greater sensitivity will counter-balance the greater difficulty of obtaining precise field data. However, potential applications of our results include exploration for zones of partial saturation in the earth as indicated by anomalously high P-wave attenuation. Such zones might include hydrocarbon gas or geothermal steam reservoirs.

TABLE OF CONTENTS

CHAPTER I

INTRODUCTION

Seismic waves have provided geophysicists with their most detailed knowledge of earth structure. This is primarily because of the high resolution of seismic methods, which range from borehole stratigraphic mapping to location of the core-mantle boundary. There are two main features of seismic waves that can be studied - velocity and attenuation. Since velocity can be measured much more easily than attenuation, it has for many years provided more information than has attenuation. For instance, in reflection seismology velocities are used to help map lithologic units. Attenuation data is generally suppressed by the use of time varying signal amplification. When seismic attenuation is measured, it generally reinforces the structural features determined from velocities. The upper mantle low velocity zone, for example, is also found to be a zone of high shear wave attenuation.

Despite these successes, the great potential of seismic measurements lies not in structural determination but in the interpretation of both velocity and attenuation in terms of the physical properties of rocks. These might include lithology, porosity, pore pressure or fluid content. The relevant measurements are the velocity and attenuation of both P and

S-waves, as well as the corresponding frequency dependence. In recent years there have been significant advances in our understanding of how rock properties affect seismic velocities. In particular, crack shape and degree of saturation have been shown to be especially important. One result of this is that the petroleum industry is now trying to combine shear wave velocities with conventional P-wave velocities to detect zones of partial saturation (gas reservoirs) in the earth.

The purpose of the present study is to determine how rock properties affect the attenuation of seismic waves. In addition, we hope to discover the mechanisms by which seismic energy is converted into heat. A great amount of experimental and theoretical work has been done in the past on attenuation in rock. As with velocities, microcracks and pore fluids have been shown to influence seismic energy loss, but as yet no single mechanism has been clearly established as being an important source of attenuation. Our approach to this problem has been to develop a high precision resonance technique for measuring attenuation in the laboratory. By working at relatively low frequencies and by varying parameters such as confining pressure, pore pressure, degree of saturation and strain amplitude, we hope to gain enough insight to allow us to eventually interpret seismic observations of attenuation (and velocity) in terms of the physical properties of rock.

CHAPTER II

PREVIOUS WORK ON ATTENUATION

There exists a vast body of literature dealing with seismic attenuation in rocks, and a considerable amount of related work exists in the materials science literature. A comprehensive review of this material would be out of place here and we refer instead to several existing reviews of the subject (Knopoff, 1964; Gordon and Nelson, 1966; Jackson and Anderson, 1970; Mavko, Kjartansson, and Winkler, 1979). We shall, however, discuss some previous work that has the most direct bearing on the results to be presented in this study. In particular, this includes studies relating to frictional and pore fluid attenuation mechanisms.

One of the earliest results of laboratory studies of attenuation in rocks was the observation that Q (see Appendix A for a definition of Q) is only weakly dependent on frequency, at least over limited frequency ranges (Birch and Bancroft, 1938; Born, 1941; Bruckshaw and Mahanta, 1954; Martin (see Collins and Lee, 1956); Peselnick and Outerbridge, 1961; Pandit and Savage, 1973). Although the data gave reason for speculation that Q might be strictly independent of frequency, the precision of the measurements was certainly insufficient to support the statement "Any deviation from the law Q independent of ω would seem to be important only at high frequencies" (Knopoff and MacDonald, 1960).

Another early experimental observation was the strong influence that cracks in rock have on attenuation. This inference was made from the fact that confining pressure reduces attenuation in rocks, presumably by closing microcracks (Birch and Bancroft, 1938; Gardner et al., 1964; Gordon and Davis, 1968). The observation that attenuation in single crystal calcite is an order of magnitude less than in limestone (Peselnick and Zietz, 1959) also implies that microcracks are in some way responsible for attenuation.

The combined information of frequency "independent" Q and the role of microcracks in attenuation has been explained by many authors in terms of frictional sliding at grain boundaries or across crack faces. Since the heat generated by friction per unit slip is independent of the rate at which sliding occurs, we would expect the heat generated per stress cycle to be independent of the rate at which the cycle occurs. This nicely explains the frequency "independence" of Q. We also expect confining pressure to close cracks and lock the faces together, thereby inhibiting frictional sliding. Because of this qualitative success in explaining the observational data, many authors have interpreted their results in terms of a frictional mechanism (Born, 1941; Gordon and Davis, 1968; Birch, 1975; Lockner et al., 1977; Johnston et al., 1979). Despite these qualitative successes, there are several problems associated with a frictional mechanism. One of the most important (and probably least appreciated) was pointed out by Savage (1969). When one considers the typical strain amplitudes of seismic waves (and of many laboratory experiments) and the typical lengths of microcracks in rock, the computed slip across crack faces is less than the interatomic spacing. There is no reason to think that a macroscopic concept like friction, which is poorly understood on a microscopic scale, can be used to describe atomic level interactions. This is the realm of crystal dislocation effects (Mason, 1971). The other problem with a frictional attenuation mechanism is that it results in nonlinear wave propagation, meaning that the velocity and/or attenuation of a sinusoidal wave will depend on how it is combined with other waves. Many theoretical treatments of frictional attenuation have been given (Mindlin and Deresiewicz, 1953; Knopoff and MacDonald, 1960; White, 1966; Walsh, 1966; Mavko, 1979). While conclusions may differ, it seems likely that frictional mechanisms can be identified by cusped (as opposed to elliptical) stress-strain loops and amplitude dependent attenuation. Savage and Hasegawa (1967) have suggested that these nonlinear effects should be observable as distortion of seismic waves, but Stacey et al. (1975) have pointed out that such distortion would be so small that it would be very difficult to observe. Some nonlinear effects have been observed experimentally, such as amplitude dependent attenuation (Peselnick and Outerbridge, 1961; Gordon and Davis, 1968; Gordon and Rader, 1971) and cusped hysteresis loops (Gordon and Davis, 1968; McKavanagh and Stacey, 1974). However, Brennan and Stacey (1975) have observed the velocity dispersion predicted by linear theories of attenuation (and not by frictional mechanisms). Also, Pandit and Savage (1973) have used a theory of Lomnitz (1956,1957) to predict attenuation from observations of logarithmic creep. This again implies linear attenuation mechanisms. Thus frictional attenuation mechanisms are intimately related to the question of whether seismic attenuation is a linear or nonlinear process. In Chapter IV we will attempt to resolve this issue.

Another early observation was that attenuation in rocks is very sensitive to the presence of pore fluids. It is generally found that rocks containing pore fluids exhibit a greater amount of attenuation than dry rocks. There is, however, no agreement on the mechanism responsible for this effect. Proposed mechanisms include chemical weakening of the rock matrix (Johnston *et al.*, 1979), changes in the frictional properties of grain boundaries caused by wetting (Johnston *et al.*, 1979), macroscopic fluid flow (Biot, 1956a,b), inertial effects due to the matrix "dragging" the fluid (Biot, 1956a,b), inter-crack "squirting" flow (Mavko and Nur, 1975; O'Connell and Budiansky, 1977), intra-crack flow (Mavko and Nur, 1979), thermoelastic effects (Kjartansson and Denlinger, 1977), viscous shear relaxation (Walsh, 1969), and flow between macroscopic regions of total and partial saturation (White, 1975). Since most pore fluid attenuation mechanisms are expected to be frequency dependent, this must be considered when evaluating experimental results. However, because of the complicated nature of the pore geometry in rocks, we are not likely to observe the precise frequency dependence predicted by most simple theoretical models, and this also must be considered.

The various pore fluid attenuation mechanisms have been reviewed in detail by Mavko, Kjartansson and Winkler (1979). We will summarize them briefly before proceeding to the experimental observations. The models can be conveniently separated into those formulated in terms of macroscopic material properties (lumped parameters) (Biot, 1956a,b; White, 1975; Stoll and Bryan, 1970; Stoll, 1974,1977) and those developed in terms of rock microstructure (Walsh, 1968,1969; O'Connell and Budiansky, 1977; Mavko and Nur, 1979; Kjartansson and Denlinger, 1977).

Biot (1956a,b) developed a comprehensive theory of wave propagation in fluid saturated porous media. Although the resulting equations are rather formidable, White (1975) shows how the resulting attenuation can be understood physically. Both P and S-waves cause relative motion between the pore fluid and the rock matrix due to inertial effects. As the matrix is accelerated, the fluid lags behind, resulting in viscous dissipation of mechanical energy. In addition, P-waves (and not shear waves) create pressure gradients between the peak and the trough of the wave. Pore fluid will flow along this pressure gradient, controlled by the permeability and governed by Darcy's Law (Darcy, 1856; Bear, 1972). This macroscopic flow also results in viscous dissipation of energy. Because the macroscopic pressure gradient opposes the inertial pressure gradient, shear waves are expected to be attenuated more strongly than P-waves. Biot's theory predicts a significant amount of attenuation only for high permeability rocks or sediments at ultrasonic frequencies. At lower frequencies the expected losses are negligible (White, 1965; Stoll, 1974; Johnston *et al*., 1979).

White (1975) has developed a model involving macroscopic flow between regions of total saturation and regions of undersaturation. Compressive stresses create large pressure gradients at the boundaries between these regions, and the resulting fluid flow causes viscous dissipation of energy. This model predicts significant attenuation of P-waves and no attenuation of shear waves. As with Biot's theory, White's model ignores the microstructure of the rock.

An alternative approach to this problem is to consider the interaction of the seismic wave and the pore fluid on the scale of individual pores in the rock. Three basic mechanisms are shear relaxation, flow between adjacent pores, and flow within partially saturated pores. Walsh (1968,1969) and O'Connell and Budiansky (1977) have considered viscous shear relaxation in fully saturated pores and Mavko and Nur (1979) have done the same in partially saturated pores. This mechanism is most easily understood in terms of a parallel-walled crack. Shearing stresses will cause the crack faces to move parallel to one another, thereby shearing the fluid contained between them. This results in viscous heating of the fluid and loss of seismic energy. The frequency dependence of this mechanism is also easily understood. At high frequencies the fluid will support relatively high shear stresses, thus tending to "glue" the crack faces together and minimizing the shear displacement. This will minimize the attenuation. At low frequencies the fluid supports negligible shear stresses and displacement is a maximum. Again, attenuation is minimized. At some intermediate frequency both shear stresses and displacements will be significant and attenuation will be a maximum. Because of this frequency dependence, theory shows that shear relaxation is probably insignificant in water-saturated rocks below megahertz frequencies. However, the mechanism may result in significant attenuation at seismic frequencies in rocks containing a high viscosity melt phase.

Intercrack, or "squirting", flow has been discussed by Mavko and Nur (1975) and O'Connell and Budiansky (1977). As fluid-saturated rock is stressed, cracks at different orientations to the principle stress axes (or cracks with different shapes) will be compressed by different amounts. This results in pore pressure variations between cracks. Fluid will flow between cracks to re-establish pore pressure equilibrium, and this flow causes viscous dissipation of energy. O'Connell and Budiansky (1977) have shown that this mechanism may result in significant attenuation at frequencies ranging from high seismic to low ultrasonic.

The last flow mechanism to be discussed is that described by Mavko and Nur (1979). If each crack is partially saturated, compression of the crack will cause the liquid droplets to flow into regions occupied by gas. This will apparently result in a significant amount of attenuation in the thinnest cracks and will be important at seismic frequencies. Because this mechanism responds simply to crack compression, it predicts about twice as much attenuation in bulk compression as in pure shear.

The third type of mechanism we will discuss does not involve viscous flow. Kjartansson and Denlinger (1977) have presented a model involving thermal relaxation of pore fluids. In fully saturated rock, relaxation occurs because of the difference between the adiabatic and isothermal bulk moduli of the pore fluid. As the rock is stressed, the pore fluid compresses by an amount determined by the adiabatic bulk modulus. The adiabatic compression increases the temperature of the pore fluid. Heat then flows from the fluid into the rock. This cools the fluid and it compresses further by an amount determined by the isothermal bulk modulus. The irreversible flow of heat from the fluid into the rock represents a loss of energy to the seismic wave. For water saturated rock this mechanism is expected to be significant at elevated temperatures (>150°C). This mechanism can also be applied to partially saturated rock, in which case the thermal relaxation occurs in the vapor phase. This version of the model predicts increasing attenuation with increasing saturation, followed by elimination of the mechanism at total satuation. Pore pressure will also affect the magnitude of the predicted attenuation.

We can now review the experimental work that has been done on attenuation in rocks in light of the theories that we have just discussed. Most of this work has been done in the laboratory, although a few field measurements have also been made. Because of the great variety of experimental methods, frequency ranges, rock types, and sample environments that have been used, there is no obvious way in which to organize this background material. We have chosen for convenience to discuss previous results in approximately the chronological order in which the work was done.

In one of the first studies of attenuation in rocks, Birch and Bancroft (1938) made the two fundamental observations that attenuation decreases with increasing confining pressure and that Q is approximately independent of frequency. A resonant bar technique was used on several samples of Quincy granite, the longest having a length of 244 cm. Several resonance modes were used to cover the frequency range from 140-4500 hertz. Confining pressures up to 4 kb were obtained, and the resulting decrease in attenuation was explained by crack closure. Although the precision of these measurements was about 20%, this was adequate to detect the first order effects in which the authors were interested.

Although Birch and Bancroft were apparently not concerned with the moisture content of their samples, the important effect of water on attenuation was soon discovered by Born (1941). Working with sandstone bars (again using a resonance technique) he found that over the frequency range 1-10 khz Q was independent of frequency in dry rock. However, the addition of a small amount of water (<1%) added a frequency dependent component of attenuation to what was observed in dry rock. Simple extrapolation of Born's results to higher frequencies or greater degrees of saturation soon leads to unreasonably low values of Q. However, the data does indicate that small amounts of water in rock can have a large influence on the magnitude of attenuation. Born concluded that the constant Q observed in dry rock indicated an unspecified "solid friction" mechanism and that the additional frequency dependent loss in wet rock was due to a viscous loss mechanism.

A very interesting technique for measuring attenuation was used by Bruckshaw and Mahanta (1954). While driving a bar in flexure they measured the phase difference between the driving force and the resulting displacement and then computed the attenuation. They found the Q's of various rocks to be almost independent of frequency over the range 40-120 hz, thus extending the observation of Birch and Bancroft (1938) to lower frequencies.

During the 1950's several field studies were done in an attempt to measure attenuation *in situ* at seismic frequencies. Ricker (1953) reported on an experiment done in the Pierre shale in Colorado in which he observed pulse width increasing as the square root of distance. This observation supported Ricker's theory of wavelet propagation, with the implication that $Q \propto \omega^{-1}$. However, his interpretation of the data has not been accepted without reservation (Collins and Lee, 1956; Kjartansson, 1979). Collins and Lee (1956) reported on an experiment performed in the Pottsville sandstone in Pennsylvania using Fourier spectral techniques. Although their data was consistent with Q being independent of frequency from 400-900 hz, it was not accurate enough to be conclusive.

The most complete field study was done by McDonal et al. (1958) in the Pierre shale studied by Ricker (1953). Both P and S-waves were studied using Fourier techniques. Contrary to Ricker's result, McDonal et al. found that the Q's of both P and S-waves were substantially independent of frequency (P 50-450 hz; S 20-125 hz). They also found that $Q_p:Q_s \approx$ 32:10. This is the only field experiment of this type in which shear waves have been studied.

In addition to their field study, Collins and Lee (1956) presented data taken by J.L. Martin showing attenuation in limestone bars. Martin found that in fully saturated rock attenuation was approximately independent of frequency over the range 100-4400 hz. This result would not be expected from the results of Born (1941) which showed water contributing a frequency dependent component of attenuation. In neither study were complete experimental details given, so we cannot comment on the relative quality of the data.

Peselnick and Zietz (1959) used an ultrasonic pulse-echo technique to measure P and S-wave attenuation in several fine-grained limestones. They found that Q was approximately independent of frequency over the range 3-15 Mhz. They also measured attenuation in single-crystal calcite and found it to be an order of magnitude less than in polycrystalline, low porosity (<1%) limestone. This represents further evidence that cracks or grain boundary contacts are in some way responsible for seismic attenuation. In a subsequent series of experiments, Peselnick and Outerbridge (1961) used a combination of techniques to measure shear attenuation in dry Solenhofen limestone over the extremely large frequency range from 4 hz to 9 Mhz. They found that attenuation was approximately constant from 4 hz to 18,000 hz and then increased by a factor of four at 9 Mhz. They also observed that attenuation increased with strain amplitude at the strains measured ($>10^{-6}$). This was an important observation to which we shall return.

In an attempt to model partial melt in the asthenosphere, Spetzler and Anderson (1968) measured attenuation in $NaCl \cdot H_2O$ as frozen bars were heated through the eutectic temperature, thus causing partial melt of the brine. Besides the possibility of frictional or fluid flow energy losses, an additional mechanism involving phase changes induced by the stress wave may have been involved. Thus the results are not easily related to saturated rocks. This is also true regarding the results of Stocker and Gordon (1975), who studied attenuation in partially melted metal alloys.

Wyllie _et_ _al_. (1962) measured attenuation as a function of degree of saturation in resonating bars of alundum (Al_2O_3) at frequencies of about 10 khz. They found that attenuation increased almost linearly with degree of saturation in the low frequency range of Biot's theory ($f/f < 0.15$, where f_c is a characteristic frequency in the theory). They also claim that their data verifies Biot's theory in the low frequency range. However, the data they present in support of this was actually taken in the high frequency range. Wyllie _et al_. also apply Biot's theory to data for partially saturated rock, although it is not at all clear that this is valid. The data in this paper should be re-interpreted in light of the flow mechanisms proposed in the last few years (O'Connell and Budiansky, 1977; Mavko and Nur, 1979; Kjartansson and Denlinger, 1977). However, two definite conclusions can be made. One is that attenuation increases monotonically with degree of saturation to high degrees of saturation. It is not clear what happens at total saturation. The other conclusion, not emphasized by the authors, is that attenuation is greater for extensional resonance than for torsional resonance. We will see later that this has important implications regarding attenuation mechanisms. These results were extended to Berea sandstone by Gardner _et al_. (1964) who also showed that confining pressure reduces attenuation in partially saturated rock. Total saturation was not achieved in this study. Unconsolidated sands and glass beads were also studied and found to have an order of magnitude less attenuation than in consolidated sandstone. Presumably this indicates that clays and/or cementing materials contribute to attenuation in rock, perhaps through the action of absorbed water. Similar results were obtained by Gardner and Harris (1968) who found that small amounts of clay added to clean sand caused a large increase in the observed attenuation. This increase varied with the type of clay used.

In a series of papers, Mason has interpreted high frequency measurements of attenuation in dry rocks using mechanisms involving crystal dislocations (Mason, 1969, 1971a,b; Mason and Kuo, 1971; Mason *et al*., 1970). These studies were very important because in each rock studied (Westerly granite, Solenhofen limestone and Pennsylvania slate), a significant peak in attenuation was found between about 0.5 - 5 Mhz. This observation throws serious doubt on the validity of extrapolating ultrasonic measurements into the seismic frequency range. It also shows that at least part of the attenuation in dry rock (perhaps all of it, according to Mason's theory) cannot be explained with a frequency independent frictional mechanism.

Another important paper was presented by Gordon and Davis (1968). The effects on attenuation of strain amplitude, confining pressure, pore pressure, temperature, frequency and water saturation were all studied with varying degrees of completeness. Two observations were particularly significant. Attenuation measured as a function of strain amplitude was found to be relatively constant at small strains ($<10^{-6}$) and increased at larger strains. Thus the strain dependence observed by Peselnick and Outerbridge (1961) was found to occur only at large strains. Gordon and Davis (1968) also measured attenuation using very low frequency (to 1 mhz) quasi-static stress cycles. Besides observing frequency independent Q in dry rock from 1-100 mhz, they also observed stress-strain loops which had pointed (or cusped) ends rather than being elliptical. The cusped loops, taken at strains $>10^{-5}$, indicated a nonlinear attenuation mechanism, although the observation was made somewhat ambiguous by the use of triangular rather than sinusoidal loading cycles. At slightly lower strains, using sinusoidal loading cycles, Gordon and Rader (1971) also observed cusped stress-strain loops. McKavanagh and Stacey (1974) extended these measurements to lower strains (10^{-6}) and still observed cusped loops. However, Brennan and Stacey (1977) made further improvements in the technique and found that the stress-strain loops did become elliptical at strains below 10^{-6}. Taken together with the amplitude dependence of Q, this implies that nonlinear attenuation may be limited to large strains ($>10^{-6}$).

In addition to the elliptical loops found at low strains, Brennan and Stacey (1977) also observed the velocity dispersion predicted by linear theories of attenuation. As a further test of linearity, Pandit and Savage (1973) used a theory due to Lomnitz (1957) to predict values of Q from creep experiments. The predictions were in good agreement with values measured at sonic frequencies. This provides strong evidence that attenuation is a linear phenomenon, at least under the conditions of the experiment.

In attenuation mechanisms involving viscous flow, frequency (ω) and viscosity (ν) always appear together as the quantity $\omega\nu$. Therefore the procedure of varying viscosity at a fixed frequency is equivalent to varying frequency at a fixed viscosity. This was done by Nur and Simmons (1970) and Nur (1971) who presented data taken at ultrasonic frequencies in granite and limestone in which the viscosity of the pore fluid was varied over several orders of magnitude. In each rock a distinct peak was found in a plot of attenuation vs. viscosity. An inflection in velocity vs. viscosity coincided with the attenuation peak. The authors interpreted these peaks as being due to a shear relaxation mechanism (Walsh, 1969). O'Connell and Budiansky (1977) have interpreted the same data in terms of inter-crack flow. Results similar to those of Nur were observed by V. Clark and reported by Gordon (1974).

Motivated by observations of very low attenuation in the lunar crust, Tittmann and his colleagues (Tittmann *et al*., 1972, 1973, 1974, 1975, 1976; Tittmann, 1977, 1978) have shown that in materials ranging from lunar and terrestrial rocks to a ceramic and porous glass, ultra-high vacuum (to 10^{-10} torr) combined with heat treatments to 300°C can decrease attenuation by roughly two orders of magnitude over the values at ambient room conditions. Experiments have been done at ~10 khz using a free resonance technique and at ~50 hz using a mass-loaded resonance. The cause of this decrease in attenuation has been linked to trace amounts of volatiles, particularly water vapor, found in the samples, but the mechanism responsible for these effects has not yet been identified.

CHAPTER III

EXPERIMENTAL TECHNIQUE

Introduction

As discussed in Chapter II, several methods are available by which attenuation in rocks may be measured. In this study we have used a bar resonance technique similar in principle to those used by Birch and Bancroft (1938), Born (1941), Wyllie *et al*. (1962), and Gardner *et al*. (1964). Basically, a bar of rock is made to vibrate in one of its normal modes, either torsional, extensional or flexural. The bar is then modelled as a damped harmonic oscillator (see Appendix C for details) and attenuation is measured either from the sharpness of a resonance or from the rate at which vibrations of the bar decay with time. In this study we have only made use of torsional resonance modes (controlled by the shear modulus) and extensional modes (controlled by Young's modulus).

We have made several improvements in the resonance technique over the versions used by previous investigators, and our most important observations have resulted directly from these improvements. In particular, we have the ability to control pore pressure within the sample independently of confining pressure. While this capability is fairly standard in ultrasonic experiments, it has never been done before in a resonance experiment. By controlling pore pressure we are able to make the transition from slight undersaturation to total saturation.

We have also made an effort to improve the precision and accuracy of the measurements. By using large samples (length ~1 meter) we have minimized external energy losses relative to the losses within the rock. External losses have been determined by measuring the attenuation in an aluminum bar with jacketing and confining pressure. Samples of various shapes and sizes were used to make sure that geometrical effects were not influencing the measurements. To improve the precision (reproducibility) of the measurements, we have made extensive use of the resonance peak shapes. Theory predicts smooth, nearly symmetric, peak shapes (see Appendix C), but various system resonances often tend to distort the sample resonances. We have been able to isolate and eliminate virtually all of these system resonances. If an occasional system resonance does occur during an experiment, it is readily identified from the peak shape. Data is not taken unless a pure resonance is observed. These efforts have resulted in a precision of ~2-3% and an absolute accuracy of ~5-10%.

Our experiment consists basically of three systems - mechanical, pressure and electrical. These systems interact to varying degrees. The mechanical system consists of everything that is placed inside the pressure vessel. This includes the sample and its support, the driving electromagnets, sensing transducers, jacketing and pore fluid inlet. The pressure system consists of the pressure vessel, the confining pressure and pore pressure media, pumps, pressure gauges, and the vacuum system. The electrical system includes various components to drive the electromagnets and detect the sample vibrations, and an oscilloscope and X-Y plotter for displaying the output signal. A schematic drawing of the system is shown in Figure (3-1). A list of the components is given in Appendix D.

Mechanical System

The samples (one meter long, thin rectangular bars) are supported horizontally by rigidly clamping them at their midpoints. The midpoint is a node of the fundamental resonance mode and of all odd harmonics, so the effect of the clamp on the sample is minimized. A special clamp was developed (Figure (3-2)) that minimizes coupling between the sample and the supporting aluminum frame. To drive the bar in extension, a small disk magnet is epoxied to one end of the bar. A bar-shaped electromagnet is mounted directly opposite the disk magnet (Figure (3-3)). As the electromagnet is driven by a sine wave, it alternately attracts and repels the disk magnet, thus applying a sinusoidal driving force to the end of the bar. The mass of the disk magnet is negligible compared to

Figure (3-1). This is a schematic drawing of the experimental arrangement with emphasis on the electronics.

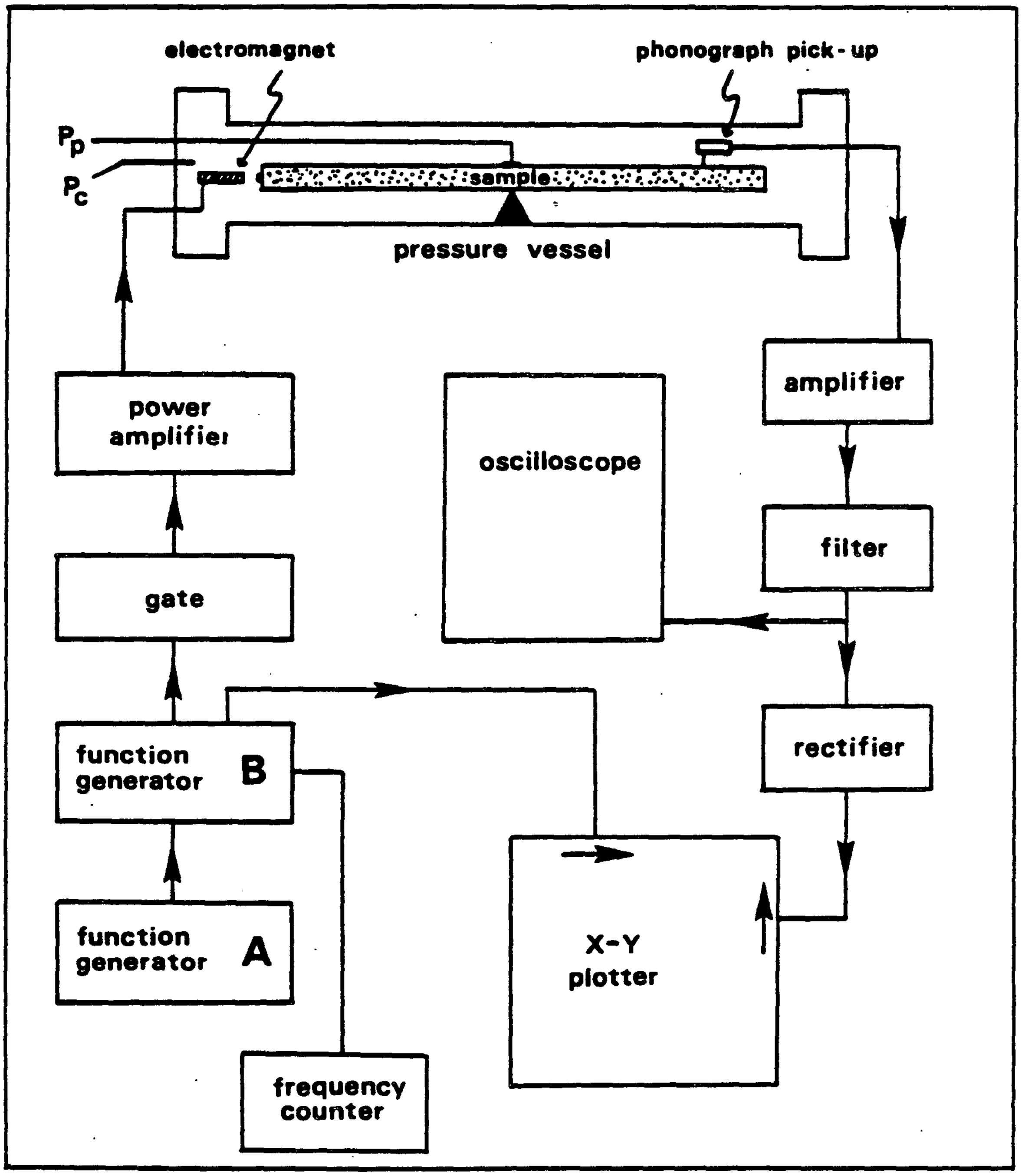

Figure (3-2). This clamp supports the sample at the center of the bar (a node of the fundamental resonance modes). The pore fluid connection is above the clamp.

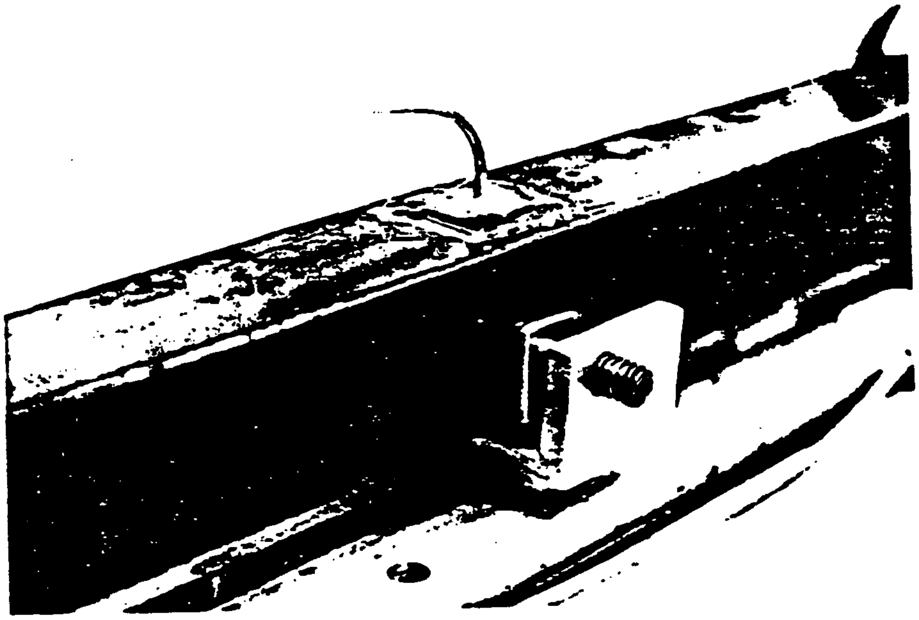

Figure (3-3). Permanent magnet (cemented to sample) and electromagnet used to drive extensional resonance.

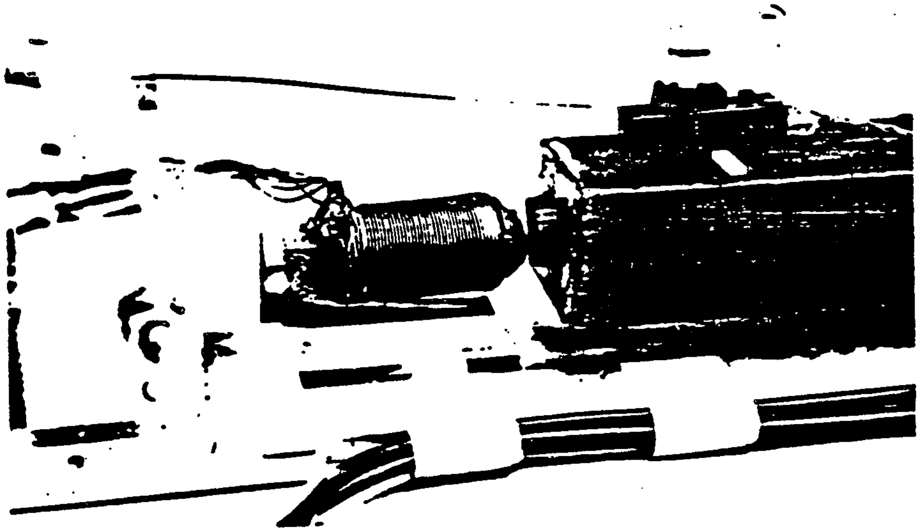

the mass of the bar (<0.1%) and no correction has been made for it. To drive the sample in torsion, a small bar magnet is epoxied horizontally across the opposite end of the bar. Two U-shaped electromagnets are mounted in parallel vertical planes directly off the end of the sample such that each pole of the bar magnet is located within the gap of one of the U-shaped magnets (Figure (3-4)). The electromagnets are connected in series and driven with a sine wave. Since the magnetic fields in the gaps of the electromagnets are always in the same direction, the net result is to apply a torque to the end of the bar. The electromagnets were carefully made to have the same dimensions and number of windings so that a balanced torque is applied. All three electromagnets are mounted on supports that allow precise positioning in three directions.

The vibrations of the bar are detected with crystal phonograph pick-ups (Figure (3-5)). These contain piezoelectric transducers that produce a voltage proportional to displacement. The pick-ups are coupled to the sample through standard phonograph needles. Since the pick-ups respond most strongly to motion at right angles to their longest dimension, they can be oriented to selectively detect either extensional or torsional motion of the bar. In extension, the motion of the bar is along its length. In torsion, the motion is perpendicular to the bar. We therefore have two pick-ups mounted on the frame, one at each end of the bar where displacement is a maximum. To minimize electrical noise, each pick-up is mounted at the opposite end of the bar from its corresponding driving electromagnet. The pick-ups are mounted on the ends of

Figure (3-4). Arrangement of magnets used to drive torsional resonance modes.

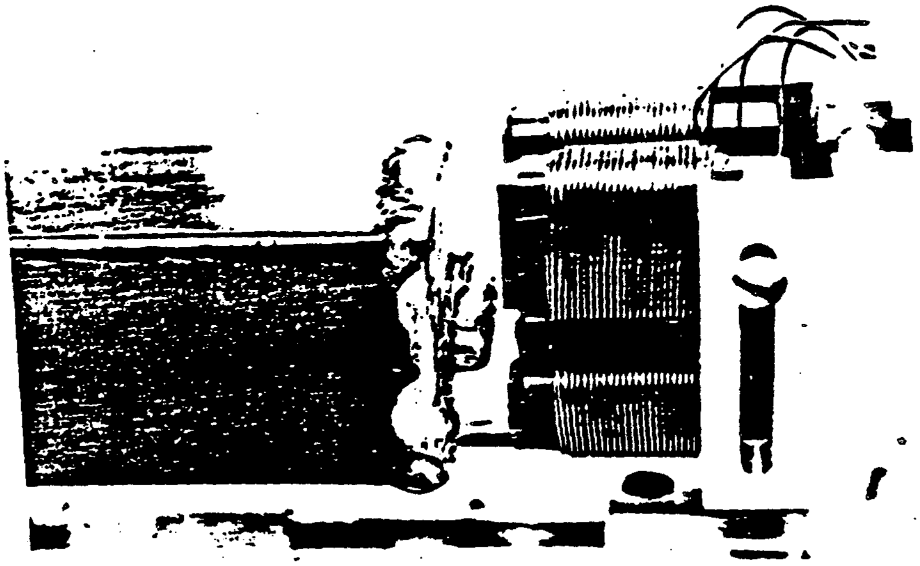

Figure (3-5). Crystal phonograph pick-up mounted on plastic arm.

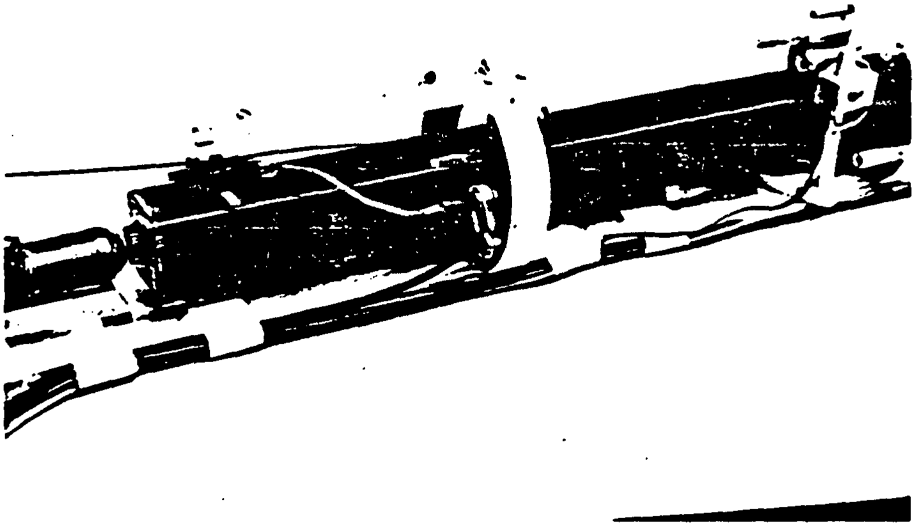

light plastic arms that are suspended above the sample with rubber bands. These are necessary to minimize mechanical coupling between the frame and the pick-ups. With a suitable arrangement of electromagnets, either pick-up can be lifted off the bar when not being used. Strain amplitude was calibrated using semiconductor strain gages mounted on both an aluminum sample and a sandstone sample. For the sandstone sample, a hole was cut in the jacketing material (heat-shrink tubing) near the support and the strain gage was epoxied directly to the rock. For both samples, the response of the pick-ups was found to be linear over the entire range used in this study. This range corresponds to strains in a one meter long sample of from 10^{-8} to 2.6×10^{-6}. The frequency response of the pick-ups has not been calibrated, though we assume it is reasonably flat at the frequencies we are working at (which are in the sonic range for which the pick-ups were designed). However, since virtually all of our data has been taken from fixed frequency resonance decays, these measurements are completely insensitive to any frequency dependence of the pick-up response.

Jacketing the sample proved to be the most difficult problem to solve. Various epoxy coatings were tried but were found to have large mechanical and chemical effects on the properties of the bar. The rigid coatings increased the velocities and decreased the attenuation of the bar. It was even found that simply by placing an open can of epoxy next to an unjacketed bar of sandstone, the vapors would enter the rock and significantly affect the measured properties.

Copper foil had similar adverse effects. Although it proved to be the most reliable jacketing material, it also significantly affected the properties of the bar. For instance, very thin 0.002 inch copper foil increased the velocities and Q's of partially saturated sandstone by 20-30%. The effect is stronger in torsion than in extension. While an error of this magnitude may be acceptable in some types of experiments, it masks the more important effects that we are looking for, in particular, the relative size of extensional and shear attenuation. We should point out that this effect of copper jacketing may not be observed if the more common procedure is followed of jacketing high Q materials and looking for a damping effect of the jacketing.

The best jacketing that we have found is a combination of heat-shrink tubing and epoxy (see Appendix D for specifications). Although not as reliable as copper foil, it has an acceptably small effect on the velocities and attenuation of the bar. In practice, the sample is placed within a length of tubing and a heat gun is used to shrink the tubing onto the sample. Heating of the sample itself is negligible. A hole is cut into the jacket at the midpoint of the bar and the pore pressure connection (described below) is epoxied onto the sample. The permanent magnets are epoxied onto the ends of the samples and at the same time epoxy is used to seal the ends of the bar. The entire sample is then coated with an extremely thin epoxy coating which serves to seal any micropores existing in the tubing. With care (and patience) this jacketing can be made to hold 350 bars confining pressure of nitrogen. It will not keep out helium, which, as discussed below, is more desirable than nitrogen.

To couple pore fluid into the sample, capillary tubing is silver-soldered into a hole in a small copper plate (0.010" thick; 0.5" square). This plate is then epoxied onto the sample at the midpoint (which is a clamped node). With copper jacketing, the plate is soldered directly to the jacket. The capillary tubing runs along the frame and leaves the pressure vessel through a port in an endplug.

Pressure System

The pressure system is fairly simple. The pressure vessel consists of a steel pipe with 0.5 inch wall thickness. The inner length (excluding endplugs) is 52 inches and the inner diameter is 3.5 inches. The pressure rating is 350 bars. This allows for a 5X safety factor, the weakest point being the bolts holding the endplugs. Confining gas (nitrogen or helium) is bled from a standard gas bottle (2400 psi) through a gas intensifier into the pressure vessel. Confining pressure is monitored with a Heise gauge. The confining gas may also be fed into the pore pressure line, though this is rarely done.

Pore fluid (liquid) is supplied by a reservoir pressurized by air line pressure (~100 psi). When the sample is saturated, a piston intensifier is used to control the pore pressure. Pore pressure can be monitored approximately with an Ashcroft pressure gauge, but for greater precision a Celesco differential pressure gauge is used to measure the difference between confining and pore pressures. (The Ashcroft gauge has recently been replaced with a more accurate Heise gauge.) Both confining and pore pressure measurements are believed accurate to ±2 bars.

A vacuum pump can also be connected to the pore pressure line, and pressures on the order of 0.1 mm Hg can be obtained. This method is rather inefficient because of the large sample volume and small cross-section of the capillary tubing. It does, however, allow us to obtain a reproducible "dry" state.

Electrical System

The electrical system is shown schematically in Figure (3-1). It consists of two parts - the driving section and the detection section. Two types of drives are used depending on whether a resonance peak or resonance decay is desired. To plot a resonance peak, function generator A puts out a very low frequency triangle wave that drives the voltage controlled oscillator (VCO) input on function generator B. This causes function generator B to output a time-varying sinusoidal signal that sweeps over a range of frequencies. This signal is fed through an open gate to a power amplifier. The amplifier provides enough current to drive the electromagnets which drive the bar. This swept-frequency input causes the sample to pass through a resonance peak. The amplifier output can be directed to either the extensional or torsional driving electromagnets.

An alternative method of driving the bar is to turn off function generator B and connect function generator A directly to the gate. (This is done simply because function generator A is a better instrument than B.) Function generator A is then set at a resonance frequency of the bar. The gate is held open until the bar has reached steady-state resonance. The gate then closes, shutting off the driving voltage, and the vibrations of the bar decay with time. For each driving technique, the sinusoidal driving signal is also sent to a frequency counter which measures the frequency at which the sample is being driven.

The detection system is identical for both resonance peak and resonance decay measurements, although the detected signal is analyzed in different ways. The phonograph pick-ups put out a voltage of 1-10 millivolts. Because of the high output impedance of the pick-ups, this signal is immediately amplified by 100X. The signal is then bandpass filtered to eliminate low frequency (<300 hz) acoustic noise and high frequency electrical transients. The pass band is always wide enough so that frequencies of interest are negligibly affected. We have checked to make sure that none of our measurements are significantly affected by the response of any of the electronic equipment. After being filtered, the output signal is sent in one of two directions. To plot a resonance peak the output is taken to an X-Y plotter which plots the rms value of the AC signal on the vertical axis. At the same time, a DC signal proportional to the output frequency is taken from function generator B and used to drive the horizontal axis of the X-Y plotter. The result is a plot of resonance amplitude vs. frequency (see Figure (4-2) for examples). To view a resonance decay, the filtered signal is sent to an oscilloscope. The resulting trace shows the vibration of the bar vs. time - in principle, an exponentially decaying sinusoid (Figure (3-6)). This trace is photographed, hand digitized, and an exponential is fit to the envelope of the signal using a standard linearized least squares algorithm.

Discussion

Resonance techniques have the potential for providing high precision (~1%), reasonably accurate (~5%) measurements of attenuation in rocks. However, the method is subject to many possible sources of error and great care must be taken to minimize these. When measuring attenuation in rock, we are interested in determining the ratio $\Delta E/E$ where ΔE is the

Figure (3-6). Oscilloscope traces showing exponential decays of sample oscillations. Top, low attenuation. Bottom, large attenuation.

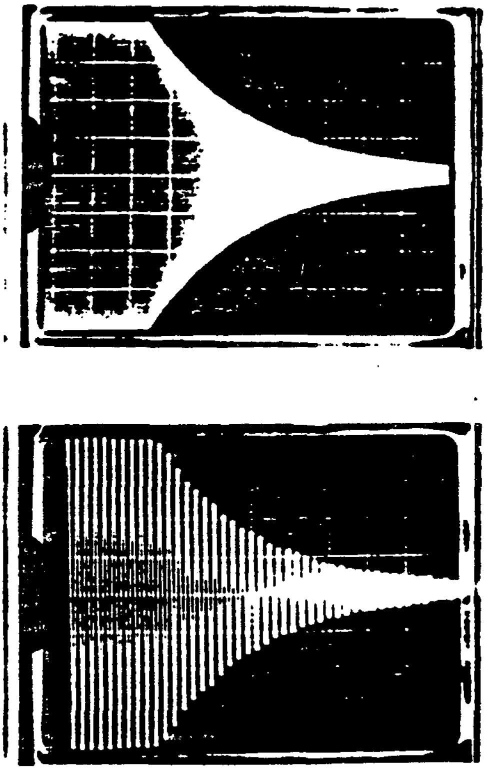

mechanical energy converted into heat in the sample in one stress cycle and E is the maximum mechanical energy in the sample during the cycle. What we actually measure is $\Delta E'/E'$, where $\Delta E'$ is the heat generated in the entire system in one stress cycle and E' is the maximum energy in the system. The system includes the sample, jacketing, support, pick-ups, confining gas, etc., or in short, everything that interacts with the sample. To measure $\Delta E/E$ accurately we must make $\Delta E \approx \Delta E'$ and $E \approx E'$. To make $E \approx E'$ we must make sure that most of the mechanical energy of the system is contained within the sample. This is difficult to calibrate precisely, but we can make a step in this direction simply by making the sample large with respect to its surroundings. We have done this by using one meter long samples.

To make $\Delta E \approx \Delta E'$ we must minimize all energy losses to the surroundings. This is easily calibrated by using an aluminum sample. Zemanek and Rudnick (1961) have used a technique similar to ours to show that at a frequency of 1 khz the Q of aluminum is greater than 200,000. Compared to damping in rocks this is effectively infinite Q or zero energy loss. Therefore whatever Q we measure for an aluminum sample represents energy losses to the surroundings. In Table (4-1) we show for aluminum $Q \approx 35{,}000$, which implies negligible losses to the surroundings. When we compare this to $Q \approx 23$ for lucite we see that we have come very close to making $E = E'$ and $\Delta E = \Delta E'$, at least at room pressure with no jacketing.

To determine the effect that the jacketing and confining pressure medium have on the measurements, we ran two simple experiments. In the first experiment an aluminum bar (100 x 2.22 x 2.22 cm) was jacketed with heat-shrink tubing and epoxy as described above. Attenuation and resonance frequencies were measured at various confining pressures (P_c). Following are the extensional resonance frequency (f_e), extensional Q (Q_e), torsional resonance frequency (f_t) and torsional Q (Q_t). All were taken from the fundamental resonance modes with nitrogen as the confining pressure medium.

$P_c = 0$ bars $f_e = 2474$ hz $Q_e = 1952$
$f_t = 1361$ hz $Q_t = 1190$

$P_c = 36$ bars $f_e = 2476$ hz $Q_e = 4058$
$f_t = 1360$ hz $Q_t = 2586$

$P_c = 99$ bars $f_e = 2476$ hz $Q_e = 2795$
$f_t = 1355$ hz $Q_t = 2406$

$P_c = 107$ bars $f_e = 2475$ hz $Q_e = 2573$
$f_t = 1355$ hz $Q_t = 2402$

Next, helium was used as the confining pressure medium.

P_c = 0 bars	f_e = 2477 hz	Q_e = 1540
	f_t = 1358 hz	Q_t = 1823
P_c = 37 bars	f_e = 2476 hz	Q_e = 2359
	f_t = 1362 hz	Q_t = 2280
P_c = 82 bars	f_e = 2477 hz	Q_e = 3372
	f_t = 1362 hz	Q_t = 2521
P_c = 102 bars	f_e = 2477 hz	Q_e = 2934
	f_t = 1362 hz	Q_t = 2385

Several points can be made from this data. If we assume that the velocities and attenuation in aluminum are insensitive to the pressures we have used, then we see that the velocities (proportional to f_e and f_t) are negligibly affected by any coupling to the confining gas. However, Q_e and Q_t are significantly affected, if we assume that the intrinsic Q's of aluminum are on the order of 200,000. The important point, however, is that except at $P_c = 0$, both Q_e and Q_t are greater than 2000. In a rough sense this means that our measurements on rock will have an error of less than 10% for Q's of 200 and an error of less than 1% for Q's of 20. We consider this to be acceptable. Another point to make is that the values of Q at $P_c = 0$ are somewhat anomalous.

This is presumably caused by poor coupling between the jacket and the sample, so in our experiments with rock we always try to maintain at least a small amount of confining pressure on the samples. Note also in the above data that there is no significant difference between the data taken with nitrogen and with helium.

Although we have evaluated energy losses to the confining gas experimentally, these losses can also be estimated theoretically. Browne and Pattison (1957) have done this and basically have verified our observations that the damping effect of the gas is not a critical problem at the pressures we are working at.

To test the effect of a jacketing material having high Q such as copper foil, a low Q sample must be used. In a second experiment we jacketed a sample of Berea sandstone (101.6 x 2.54 x 2.54 cm) with heat-shrink tubing and 0.002" copper foil. The heat-shrink tubing was necessary to prevent grains from puncturing the copper. The sample was pressurized, partially saturated with water and then removed from the pressure vessel. The following measurements were obtained.

heat-shrink tubing plus copper foil	$f_e = 816$ hz	$Q_e = 26$
	$f_t = 500$ hz	$Q_t = 60$

The copper foil was then carefully removed from the sample.

heat-shrink tubing	$f_e = 677$ hz	$Q_e = 21$
	$f_t = 408$ hz	$Q_t = 48$

Finally, the heat-shrink tubing was also removed.

no jacket f_e = 646 hz Q_e = 21
f_t = 397 hz Q_t = 46

Some of the variation in the above measurements was undoubtedly caused by handling the sample, but we believe most of the variation was caused by the jacketing. Notice that removal of the copper foil caused a 20-25% reduction in the measured values, while removal of the heat-shrink tubing caused a further average reduction of only 3%. The interpretation is that the copper foil is storing a significant amount of elastic energy, making $E' > E$, and so making the measured system Q significantly larger than the intrinsic Q of the rock. A systematic error of 20-25% is probably acceptable for some types of work. However, we are particularly interested in relative variations of Q_e and Q_s on the order of 25-35% and so cannot tolerate the effect of the copper jacketing.

As a result of these calibration efforts, we estimate the average accuracy of our measurements at about 5-10%. Low Q measurements are more accurate than high Q measurements.

We have estimated the precision of our data from various measures of reproducibility. For example, on a well-shaped resonance peak (signifying a pure resonance mode) the value of Q found from the width of the peak agrees to within ~1% with the value found from a decay of resonance. Several measurements taken on a single resonance decay generally agree to within ~1%. Measurements taken on a given sample at different times under identical conditions usually agree to within 3-4%. As a conservative estimate we will take the precision of any measurement on a pure resonance as being 2-3%. We have found that a convenient way of estimating the precision of a given measurement is to calculate the standard deviation of Q determined from a linearized least squares fit of a decaying exponential to a resonance decay. See, for example, Bevington (1969, p.114).

The final problem we will discuss is that of gas resonances. We have found that when using nitrogen as the confining pressure medium, the resonance peaks occasionally become distorted. This distortion occurs at various combinations of gas pressure, resonance frequency, and sample geometry. Although we have not been able to determine the precise source of this distortion, we have found that it can be eliminated by using helium as the confining medium. This was the main reason for our unsuccessful effort to develop copper jacketing, since heat-shrink tubing will not seal out helium. Presumably some sort of resonance is being set up in the nitrogen, but not in helium because of its higher velocity and the resulting longer wavelength of sound. As a result of this problem, during a few experiments some of the extensional data was contaminated by gas resonances (the effect does not occur with torsional modes). Whenever this occurred, the data was discarded. We might note that this same problem was encountered by Gardner *et al*. (1964), in the only other experiment of this type.

Sample Descriptions

Massilon Sandstone

Massilon sandstone is a medium-grained quartzose sandstone of Mississippian age obtained from Briar Hill Stone Co., Glenmont, Ohio. It contains 88% quartz, 5% clay, 3% feldspar, and 4% amorphous silica. The porosity is 22%, the grain density is 2.66 g/cm^3, and the permeability to water at zero confining pressure is 740 millidarcies.

Berea Sandstone

Berea sandstone is a fine to medium grained graywacke of Mississippian age obtained from Cleveland Quarries, Amherst, Ohio. Two types of Berea sandstone were used in this study, denoted as Berea (350) and Berea (600).

Berea (350) contains 82% quartz, 6% clay, 2% feldspar, 2% dolomite, and 6% amorphous silica. The porosity is 22%, the grain density is 2.67 g/cm^3, and the permeability is 380 millidarcies.

Berea (600) contains 84% quartz, 4% clay, 2% feldspar, 1% pyrite, and 8% amorphous silica. The porosity is 21%, the grain density is 2.65 g/cm^3, and the permeability is 620 millidarcies.

Sierra White Granite

Sierra White granite is a fine-grained, grayish-white, muscovite-biotite granite obtained from Raymond Quarry, Raymond, Cal. through the American Monument Company, Colma, Cal. Its absorption (porosity ?) is 0.27%, and the bulk density is 2.64 g/cm^3. An approximate chemical analysis is 74% silica, 15% alumina, 2% iron oxides, 3% lime, 5% soda and potash, and 0.3% combined water.

Vycor 7930

Vycor porous glass was obtained from Corning Glass Works. It has 28% porosity, a bulk density of ~1.5 g/cm^3, an average pore size of 4 nm, a typical grain size of 50 nm, and appears under the SEM to be composed of a packing of nearly spherical beads. Vycor is composed of 96% silica. It has an extremely large adsorbing surface of 250 square meters per gram.

Our samples of aluminum and lucite are of unknown composition.

Because sample size and shape are important in a resonance experiment, sample geometry is given in Table (3-1) along with conversions between resonance frequency and velocity. These conversion factors were calculated from the formulae and tables given by Spinner and Tefft (1961).

Table (3-1). Sample dimensions and frequency/velocity conversion factors.

Sample	Dimensions (cm)	V_e/f_e (km/sec/hz)	V_s/f_t (km/sec/hz)
Massilon sandstone	100 x 2.0 x 1.9	2.000	2.181
Berea sandstone	101.6 x 2.54 x 2.54	2.032	2.213
Sierra White granite	101.6 x 2.54 x 2.54	2.032	2.213
Vycor glass	91.4 x 1.5 diameter	1.828	1.828
Lucite	98.7 x 1.51 diameter	1.974	---
Aluminum	100 x 2.22 x 2.22	2.000	---

CHAPTER IV

FRICTIONAL ATTENUATION MECHANISMS

Introduction

Far more information about the constitution of the earth is obtained from seismic studies than all other geophysical methods combined. Of the two main aspects of wave propagation - velocity and amplitude - velocities have been used to obtain most of our knowledge of the earth. Attenuation data is of much more limited use, partly because it is difficult to obtain, but more importantly because it is difficult to interpret in terms of rock properties. This is due primarily to our lack of understanding of the physical processes involved in the attenuation of seismic waves. We are, of course, not considering apparent attenuation caused by geometrical spreading, partial reflections, etc., but are only interested in those processes that actually convert seismic energy into heat.

Many investigators using a variety of techniques have studied the attenuation of acoustic waves propagating through rock. Although much data has been collected, no well-defined mechanism of energy loss has yet been firmly established on both experimental and theoretical grounds. One of the most intuitively appealing and widely discussed mechanisms proposed for seismic energy loss is based on simple Coulomb friction. In this mechanism the passing wave causes sliding at grain boundaries or across crack faces, thereby doing work against friction and converting seismic energy into heat. Since frictional heating per stress cycle is rate independent, it seems to account for the reported observation that the specific dissipation function, Q, is nearly independent of frequency. Friction also seems to explain why the introduction of cracks into a crystalline solid increases attenuation. The most severe criticism of a frictional mechanism is, however, that the mechanism is inherently nonlinear. This means that the velocity and attenuation of a sinusoidal wave will depend on how it is combined with other waves. It has been found that at large strain amplitudes ($>10^{-6}$) nonlinear effects such as cusped hysteresis loops (Gordon and Davis, 1968; McKavanagh and Stacey, 1974) and amplitude dependent velocity and attenuation (Peselnick and Outerbridge, 1961; Gordon and Davis, 1968; Gordon and Rader, 1971) can be observed, but these effects disappear at strains more typical of seismic waves.

Using both theoretical arguments and experimental results, several authors (Savage and Hasegawa, 1967; Savage, 1969; Mason et al., 1970; Tittmann et al.; 1972) have expressed doubts about the validity of a frictional attenuation mechanism. For instance, Savage (1969) has suggested that frictional effects should be important only at large strains where displacements across crack faces are large enough that the concept of macroscopic friction is valid. Despite these criticisms, frictional losses are often used to interpret experimental observations (Birch, 1975; Lockner *et al.*, 1977; Johnston *et al.*, 1979). To clarify the role of friction in seismic wave attenuation, we carefully investigated the dependence of velocity and Q on strain amplitude. We were able to identify the range of conditions for which frictional losses may be significant and our results show that the frictional mechanism is generally not important for seismic waves in the earth.

Theory of Frictional Losses

Two types of frictional attenuation models have been proposed. Walsh (1966) developed a model based on thin elliptical cracks in which frictional sliding occurs between crack faces. Models based on spheres in contact were developed by Mindlin and Deresiewicz (1953) and by White (1966). Recently Mavko (1979) reviewed these theories and extended the contact model to more general geometries. The most significant feature of Mavko's model (which it shares with that of Mindlin and Deresiewicz) is that it predicts Q^{-1} to be proportional to strain amplitude. It has been found experimentally that frictional behavior is often described by an equation of the form (Jaegar and Cook, 1976)

$$\sigma_f = S + \gamma\sigma_n$$

where σ_f is the frictional force, S is the cohesive shear strength, γ is the coefficient of friction, and σ_n is the normal stress across the sliding surfaces. The contact models predict that attenuation will decrease as either γ or S increases. Attenuation will also decrease as σ_n increases and the sliding interfaces are effectively locked together.

In addition to the effects on attenuation, all frictional models predict that stress-strain loops will have discontinuities in slope at maximum strain. This is a static hysteresis effect. As stress reverses direction there is a simultaneous reversal of elastic strain and a delayed reversal of sliding strain.

Past Observations of Frictional Losses

Several of the predicted effects of frictional attenuation models have been observed. Energy loss has been found to increase with strain amplitude at large strains in rock (Gordon and Davis, 1968) as well as between sliding glass and metal surfaces (Mindlin et al., 1951; Goodman and Brown, 1962) It has been shown that at low strains ($<10^{-6}$) attenuation is nearly constant (Gordon and Davis, 1968) and that variation with strain amplitude occurs only at larger strain. Some attenuation in metals at large strain is associated with dislocation mechanisms, but this does not explain all of the observations.

Discontinuities in the slope of stress-strain loops have been observed in large strain quasi-static experiments (Gordon and Davis, 1968; McKavanagh and Stacey, 1974). These have been described as cusped loops. It has recently been shown (Brennan and Stacey, 1977) that as strain amplitude decreases, the cusped loops become elliptical at strains approaching 10^{-6}. It is interesting that two of the effects predicted by frictional attenuation models, amplitude dependent Q and cusped hysteresis loops, both seem to disappear below the same strain amplitude.

It is also commonly observed that increasing confining pressure causes attenuation to decrease (Birch and Bancroft, 1938; Gardner et al., 1964). While this is predicted by frictional models, it is also predicted by many other possible mechanisms of energy loss and so by itself does not provide evidence for frictional loss.

New Observations of Frictional Losses

We are using the well established bar resonance technique (Birch and Bancroft, 1938; Gardner et al., 1964). to measure both attenuation and velocity in long, thin bars of rock. (Experimental details will be found in Chapter III.) A unique feature of our experiment is that pore pressure is controlled independently of confining pressure. This has not previously been achieved in a resonance experiment. The length of the samples ($\sim$1 meter) puts the fundamental resonance frequencies at roughly 500 - 1500 hz. Sample dimensions are given in Table (3-1). Resonance frequencies are measured to one hertz and converted to velocities using the relation $v = 2Lf$ where L is the length of the bar. Geometric corrections given by Spinner and Tefft (1961) are negligible for our samples in extensional resonance. Strain amplitudes are measured with crystal phonograph pick-ups calibrated against semiconductor strain gages. Attenuation measurements can be made either by plotting resonance peaks ($Q = f/\Delta f$) or by measuring the time constant of resonance decays ($\tau = Q/\Delta f$). Before using either technique, resonance peak shapes were carefully observed to insure the purity of the resonances. For convenience, all attenuation data presented in this chapter was taken with the resonance decay technique (except as noted in Figure (4-1)). The precision of the attenuation measurements is 2-3% and the estimated absolute accuracy is 5-13%. Both torsional (shear modulus) and extensional (Young's modulus) resonance modes show similar nonlinear behavior at large strains. Only extensional data (taken at the fundamental resonance) will be presented here.

Data for dry Massilon sandstone as a function of resonant strain amplitude is shown in Figure (4-1). At strains below 5×10^{-7} both attenuation (Q^{-1}) and velocity are nearly independent of strain amplitude, whereas at relatively large strains ($>10^{-6}$) there is a clear increase in attenuation and decrease in velocity. Of the two measured quantities, Figure (4-1). Variation of attenuation (Q_e^{-1}) and velocity with strain amplitude for dry Massilon sandstone in extensional resonance. The star indicates the value found from the resonance peak half-width using the relation $Q^{-1} = \Delta f/f$.

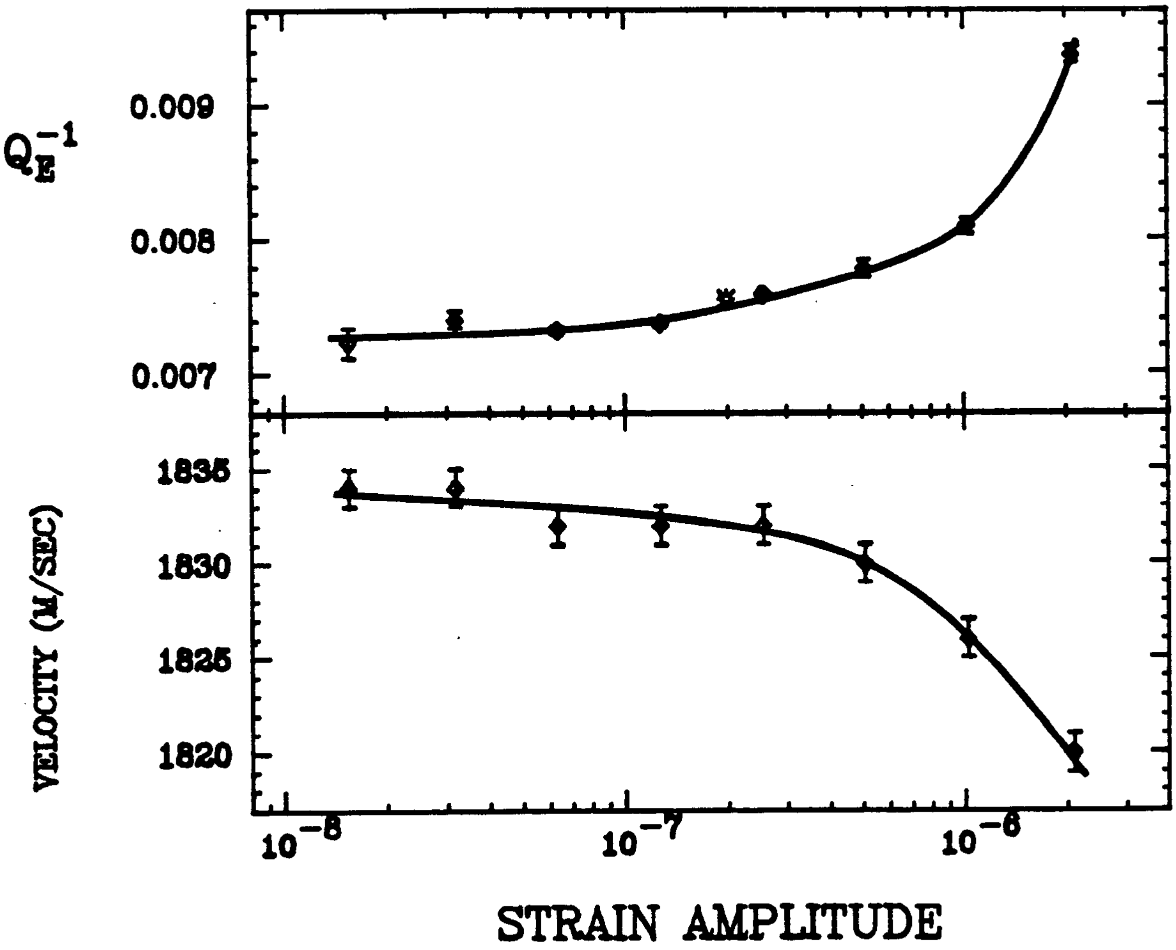

Figure (4-2). Normalized extensional resonance peaks taken at two strain levels. Asymmetric peak was taken at large strain and is evidence of non-linear behavior.

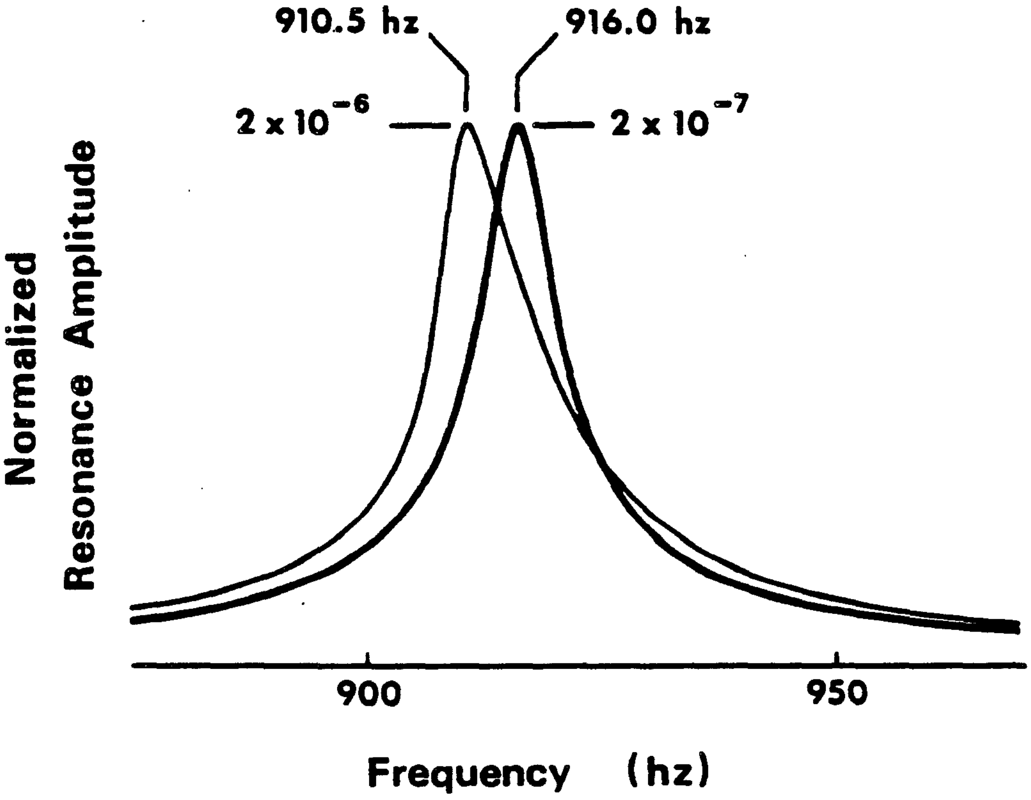

Q^{-1} is more sensitive to strain amplitude than is velocity, varying by 19% and 0.7%, respectively. The similarity of the curve shapes suggest an underlying relationship between the amplitude dependence of Q^{-1} and velocity. An interesting consequence of this behavior is shown in Figure (4-2), where we have plotted the displacement amplitude of extensional resonance peaks vs. frequency for a sample of Massilon sandstone. The peak at 910.5 hz was recorded at a maximum strain amplitude of 2×10^{-6} whereas the peak at 916 hz was recorded at a maximum strain of 2×10^{-7}. The amplitudes were normalized for plotting, but the horizontal axis is the same for both peaks. The low strain peak is symmetric and has the shape predicted for a damped harmonic oscillator. The value of Q found from the half-width of this peak, using the relation $Q = f/\Delta f$ derived for a damped harmonic oscillator, is, as expected, in excellent agreement with the Q found from resonance decay. In contrast, the peak taken at higher strain is shifted to lower frequency, is broader, and is not symmetric. The frequency shift is explained by the velocity variation shown in Figure (4-1) (since velocity is proportional to the resonant frequency), and the broadening is caused by the increasing attenuation at higher strain. The asymmetry can also be explained by the variation in velocity: Any two points on the resonance peak at a given strain amplitude will be symmetric about a central frequency that is determined by the velocity of the bar at that strain. As strain amplitude increases, leading to a velocity decrease, the frequency of symmetry shifts to lower frequencies, producing an overall asymmetric peak. This data clearly shows the amplitude dependence, and therefore the nonlinear behavior, of seismic wave propagation at large strains. At low strains the symmetry of the resonance peak shows that nonlinear effects are either absent or negligible. (Theory predicts slightly asymmetric peaks even in completely linear systems, with displacement peaks skewed towards higher frequencies (see Appendix C or Heuter and Bolt (1955)). Close examination of Figure (4-2) will reveal this asymmetry in the low strain peak, but this in no way affects our arguments or conclusions.)

We have further investigated these nonlinear effects by varying effective stress - the difference between confining pressure and pore pressure. Data for a jacketed sample of Berea sandstone, with helium used for both confining pressure and pore pressure, is shown in Figures (4-3) and (4-4). As confining pressure is increased from 10 to 50 bars (curves A - D), the variation of both Q^{-1} and velocity with strain amplitude gradually decreases. At a constant confining pressure of 50 bars (curves D and E) increasing pore pressure restores the dependence on strain amplitude.

The effects of changing water content on Q^{-1} in Berea sandstone are shown in Figure (4-5). The data for partially saturated rock at very low saturation was obtained at ambient room conditions. The data for 'dry' rock was obtained after drying the sample in a vacuum oven, and the data for almost fully saturated rock after saturating the sample with distilled water. The most apparent feature is that the addition of water greatly increases the attenuation. This effect, which is associ-

Figure (4-3). Attenuation in dry Berea (350) sandstone as a function of strain amplitude, confining pressure (P_c) and pore pressure (P_p). Helium was used as the pressure medium. (A) P_c = 10 bars; (B) P_c = 20 bars; (C) P_c = 30 bars; (D) P_c = 50 bars; (E) P_c = 50 bars, P_p = 30 bars.

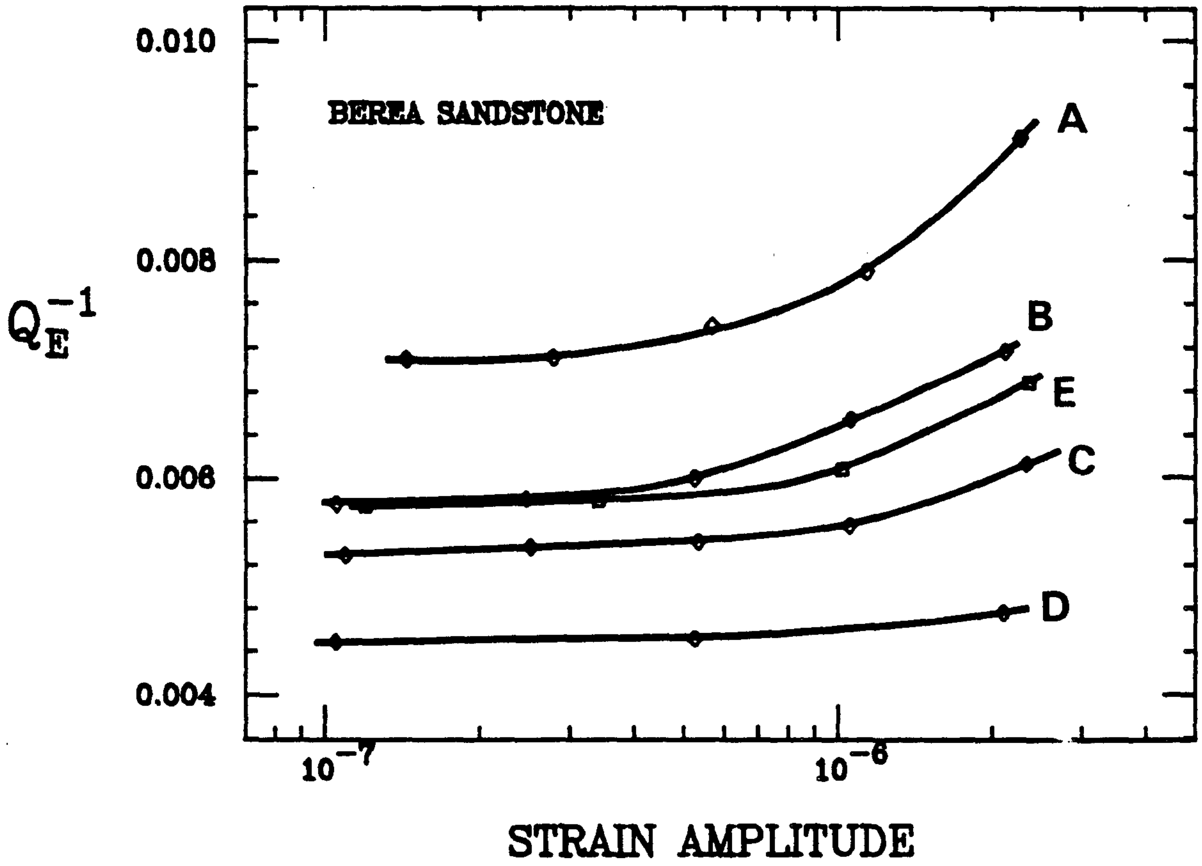

Figure (4-4). Extensional velocity of Berea (350) sandstone vs. strain amplitude. Data corresponds to the attenuation data shown in Figure (4-3).

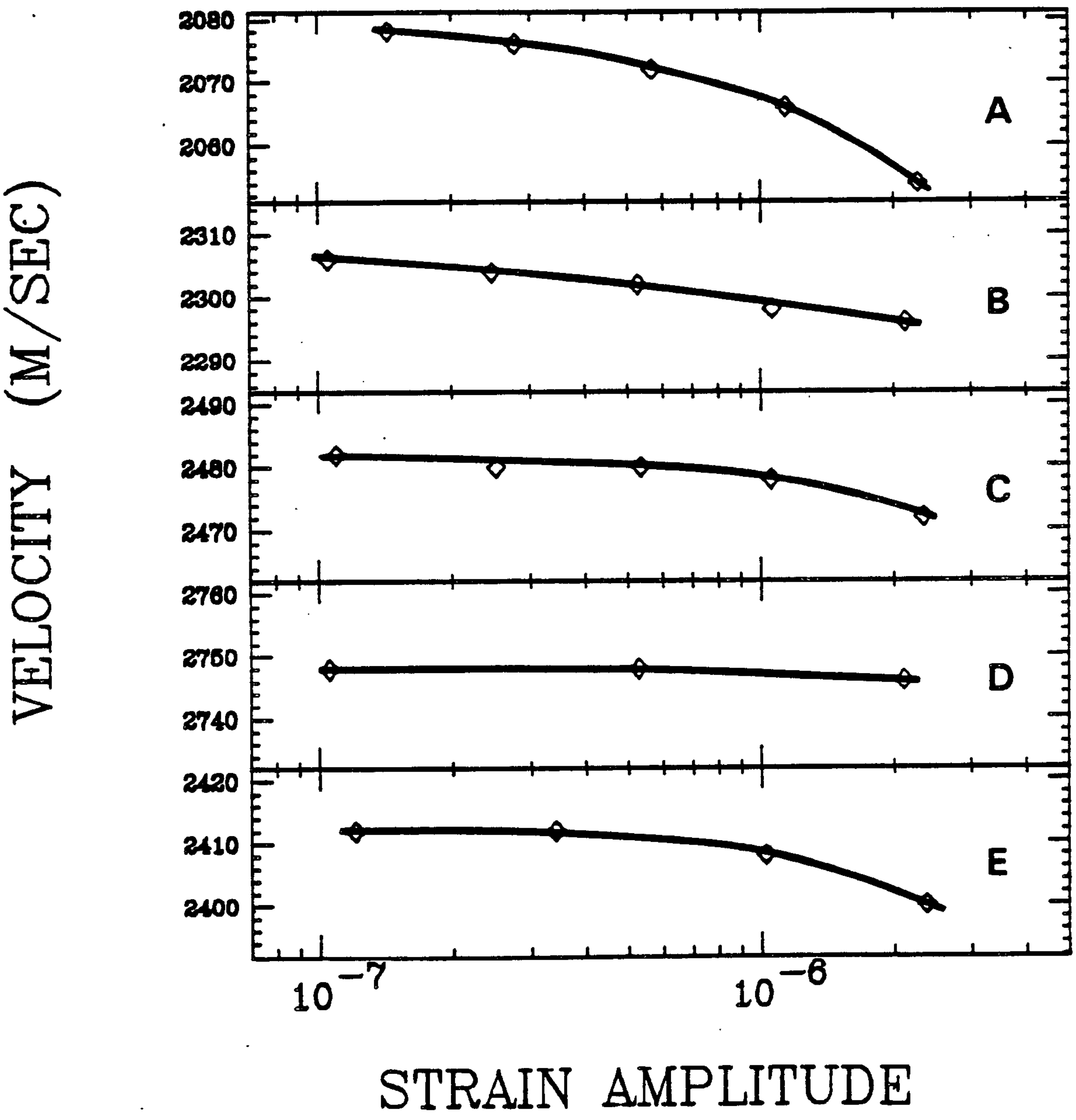

Figure (4-5). Attenuation in Berea (350) sandstone vs. strain amplitude. Brackets indicate frictional component of energy loss. (A) almost fully water saturated; (B) lightly saturated; (C) dry.

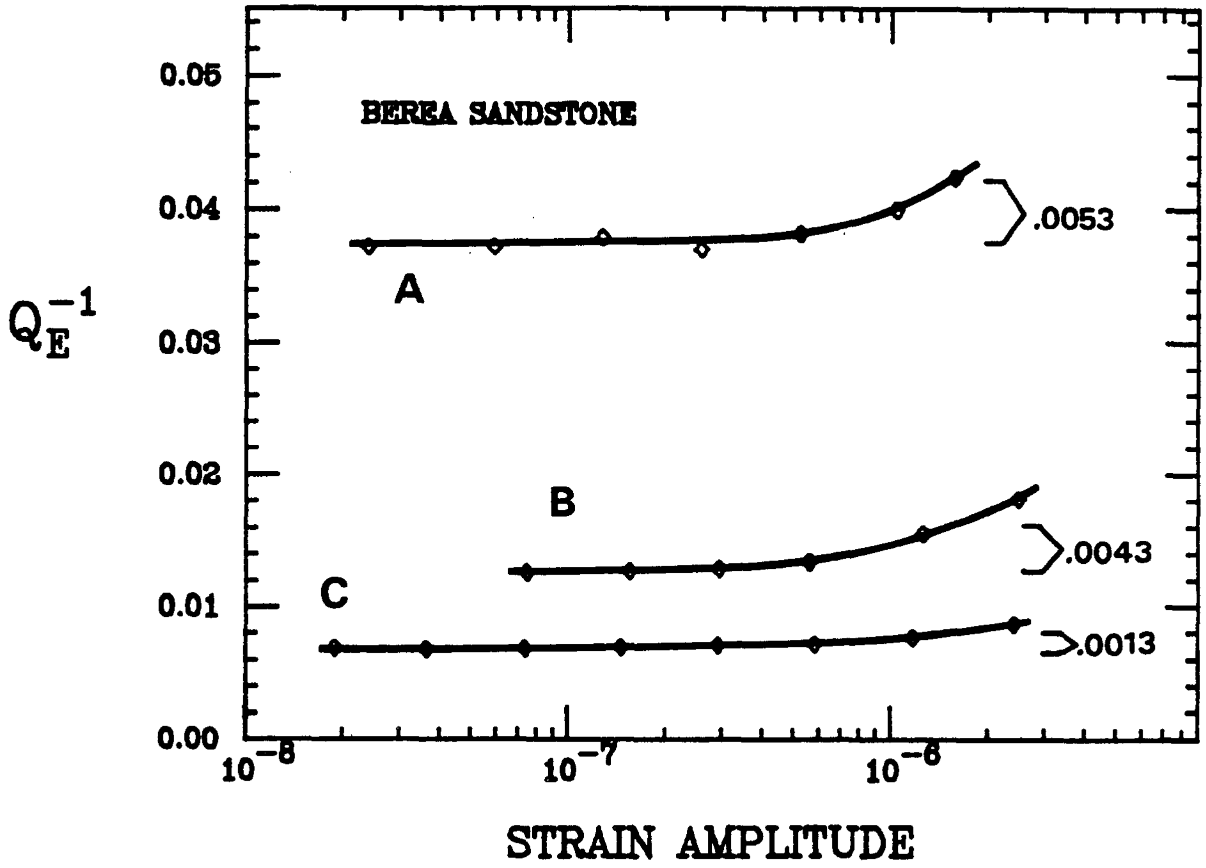

ated with a fluid flow mechanism, will be discussed more thoroughly in Chapter V. Of greater interest here is that the addition of a small amount of water greatly increases the variation of Q^{-1} with strain amplitude, whereas continued addition of water causes a smaller additional variation in Q^{-1} This is indicated by the brackets in Figure (4-5) which show the difference between Q^{-1} at a strain of 1.7×10^{-6} and the constant value of Q^{-1} at low strains.

To find out which structural features of a material are related to these nonlinear effects, we experimented with materials having physical compositions different from sandstone. In Table (4-1) is shown data for a variety of materials measured at both large and small strain amplitudes. Lucite and aluminum show no evidence of any change in velocity or attenuation with strain (to within experimental uncertainty) although their respective Q's span more than three orders of magnitude and their internal structures are quite different. (The values of Q for aluminum are probably underestimates because they are at the limits of sensitivity of our system.) There is also no variation in the values for dry Vycor glass. Under the scanning electron microscope Vycor appears to be composed mainly of glass beads of approximately 50 nm diameter. The contacts were beyond the resolution of the SEM used, (86,000X), but presumably the particles are welded together since they formed simultaneously from the melt. The flat cracks and partially cemented grain boundaries commonly found in rocks are probably scarce in Vycor. Table (4-1) also includes data for a room dry granite sample which shows the same nonlinear effects found in sandstone.

Table (4-1). Tests for nonlinear behavior in various materials (negligible changes of Q_e and V_e are found for materials where frictional mechanisms are inoperative).

Material	Strain Amplitude	Q_e	Velocity (m/sec)
Lucite	1.43×10^{-6}	23.4 ± 0.3	2108
	3.04×10^{-8}	23.2 ± 0.4	2108
Vycor	2.84×10^{-6}	437 ± 2	3345
	1.58×10^{-8}	435 ± 4	3345
Aluminum	2.41×10^{-6}	34,800 ± 300	5102
	2.46×10^{-8}	35,200 ± 400	5102
Sierra White granite	1.44×10^{-6}	185 ± 1	3629
	4.15×10^{-8}	204 ± 1	3637
Massilon sandstone	2.10×10^{-6}	107 ± 1	1820
	1.55×10^{-8}	138 ± 2	1834
Berea sandstone	2.10×10^{-6}	103 ± 3	1937
	2.30×10^{-8}	140 ± 2	1955

Discussion

The data we have presented, together with the existing data we have discussed, provide strong support for the existence of a frictional attenuation mechanism in rock at large strain amplitudes and low effective stresses. Every predicted feature of the contact frictional loss mechanism has been observed experimentally. At large strains ($>10^{-6}$) Q^{-1} increases with increasing strain amplitude and the amount of the variation in Q^{-1} is strongly influenced by effective stress. Fifty bars is enough to virtually eliminate the strain dependence at the strains and in the rocks which we have used.

The effect of water on the amplitude dependence of Q^{-1} is probably caused by water changing the frictional properties of the sliding interfaces. Evidence for this is found in Figure (4-5). Adding a small amount of water to the sample presumably wets most of the internal surfaces, causing a slight increase in the low strain, linear attenuation (a fluid flow mechanism) and a large increase in the nonlinear, frictional component of attenuation. The addition of more water fills the remaining pore space, thus enhancing the flow losses but only slightly increasing the frictional energy loss.

Unfortunately, neither theory nor experimental data is sufficiently developed to predict how water will affect grain boundary friction. Data taken by Horn and Deere (1962) show that water increases the coefficient of friction, γ, of massive minerals such as quartz and feldspar, but reduces γ of layer-lattice minerals such as mica and chlorite. Since our sandstone samples contain both mineral types (including ~6% clay minerals), we cannot predict how the γ involved in the frictional loss mechanism will be affected by water. Further complicating the matter, Byerlee (1967) found that on ground granite surfaces water has no effect on γ but instead reduces the cohesive shear strength, S, by a factor of five. Mavko's (1979) theory may provide a clue to the effect of water on grain boundary friction. The theory predicts that water can increase the frictional energy loss only by decreasing either γ or S. Since most sliding surfaces in sandstone and granite are probably between massive minerals, the theory suggests that the results of Horn and Deere do not apply to grain boundary friction. However, Byerlee's results do explain our observations and imply that water reduces the cohesive shear strength of internal sliding contacts in rock.

The observations of cusped stress-strain loops (Gordon and Rader, 1971; McKavanagh and Stacey, 1974) at strains greater than 10^{-6} also indicate that frictional sliding is occurring. It is significant that all of the evidence for a frictional attenuation mechanism disappears below strains on the order of 10^{-6}. The cusped loops become elliptical and Q^{-1} becomes independent of strain amplitude. The implication is that at low strains attenuation is caused only by linear loss mechanisms. At larger strains, nonlinear frictional losses become observable. This leads to the question of why a strain of 10^{-6} or larger is needed to observe frictional attenuation. We can assume that displacements across crack surfaces must be at least comparable to interatomic spacings ($\sim 10^{-8}$ cm) for friction to be present. A shear strain ϵ will produce a displacement d across the sides of a crack of length L given roughly by $d=\epsilon L$. If $d = 10^{-8}$ cm and $\epsilon = 10^{-6}$, then we find that $L = 10^{-2}$ cm. A crack length of 10^{-2} cm may well be a rough upper bound to the majority of crack lengths found in rock. Hadley (1976) reported that in Westerly granite only 7% of the observed cracks had lengths greater than 10^{-2} cm and none were longer than 3×10^{-2} cm. Therefore, at strains below 10^{-6}, sliding displacements between crack faces are so small in the majority of cracks that friction does not adequately describe the interaction. As strain increases above 10^{-6}, frictional sliding begins to occur at more and more cracks and attenuation increases.

Unlike Q, the nonlinear behavior of velocity at high strain has not yet been explained in terms of a frictional mechanism, but it is reasonable to expect the effective moduli to decrease as slip occurs at grain contacts (as observed in Figures (4-1) and (4-4)). Mavko and Kjartansson (1978) have attempted to relate the amplitude dependence of velocity to the amplitude dependence of Q by analyzing the shape and orientation of cusped stress-strain hysteresis loops.

After eliminating friction as a loss mechanism at low strains, we still have to account for the observed energy loss at low strain amplitudes in "dry" rock. We must also explain the change in attenuation that occurs as cracks are closed under confining pressure (Birch and Bancroft, 1938; Gardner *et al*., 1964; Gordon and Davis, 1968) or created through thermal cracking (Gordon and Davis, 1968) or dilatancy (Lockner *et al*., 1977). Unfortunately, we do not know yet what mechanism is responsible for these losses. The data collected by Tittmann *et al*. (1972) showing the strong effect that trace amounts of volatiles have on attenuation probably has a direct bearing on this mechanism. Another possibility is some form of grain boundary relaxation (Gordon and Nelson, 1966; Jackson and Anderson, 1970) or a dislocation mechanism similar to those discussed by Mason *et al*. (1970,1978). Whatever the cause may be, it is reasonably certain that the mechanism does not involve any macroscopic concept of friction.

Conclusion

On both experimental and theoretical grounds it seems clear that frictional energy losses occur in rock at room pressure only at strains greater than approximately 10^{-6}. This is far greater than strain amplitudes generally encountered in seismology except in regions near seismic sources. Even there the effect of confining pressure will virtually eliminate frictional energy losses in the earth. Consequently, wave attenuation caused by frictional sliding is not important in seismology.

The mechanism by which cracks influence attenuation at low strains in "dry" rock needs to be re-examined. The concept of frictional energy loss is so firmly established (on intuitive grounds) that the term "internal friction" is often interpreted literally to mean a frictional energy loss. Though the choice of words is unfortunate, "internal friction" is simply a general term for energy absorption and does not imply any particular mechanism. It must be kept in mind that actual frictional energy loss is a large strain, low pressure phenomenon that is often observed in the laboratory, but seldom observed in the earth.

CHAPTER V

PORE FLUID ATTENUATION MECHANISMS

Introduction

It has been recognized for many years that pore fluids, water in particular, have a strong effect on seismic attenuation. Born (1941) and Tittmann *et al*. (1972) have shown that even trace amounts of water (<1%) can significantly affect attenuation measurements in the laboratory. Wyllie *et al*. (1962) and Gardner *et al*. (1964) have shown that attenuation increases monotonically with degree of saturation to very large degrees of saturation. Total saturation was not achieved, however. Nur and Simmons (1970), Nur (1971) and Gordon (1974) have observed peaks in attenuation as the viscosity of the pore fluid was varied. Toksoz *et al*. (1979) have shown that at ultrasonic frequencies complete water saturation causes increased attenuation relative to that in dry rock, with the effect being larger for shear waves than for P-waves. An important, though overlooked, point, is that in partially saturated rock, $Q_e^{-1} > Q_s^{-1}$ (Wyllie *et al*., 1962; Gardner *et al*., 1964). This implies that $Q_p^{-1} > Q_s^{-1}$ (see Appendix B). However, in fully saturated rock, $Q_p^{-1} < Q_s^{-1}$ (Toksoz *et al*., 1979). This difference must have some implication for attenuation mechanisms.

Although experimental data is rather sparce, many theoretical models have been proposed to describe mechanisms by which pore fluids may contribute to seismic attenuation. Biot (1952) has considered inertial effects and macroscopic flow, but the resulting energy losses are probably insignificant below ultrasonic frequencies (White, 1965). Viscous shear relaxation has also been shown to be a high frequency (or high viscosity) mechanism (Walsh,1969; O'Connell and Budiansky, 1977) and is not important below ultrasonic frequencies for water saturated rocks. Inter-crack "squirting" flow (Mavko and Nur, 1975; O'Connell and Budiansky, 1977) may be important at low frequencies in fully saturated rock. White (1975) has presented a model for energy loss in macroscopically partially saturated rock that may be important in the earth. However, it is probably not generally important in the laboratory where an attempt is usually made to avoid inhomogeneous distributions of pore fluid. A flow model based on partial saturation of individual cracks has been discussed by Mavko and Nur (1979), and a thermoelastic partial saturation mechanism has been presented by Kjartansson and Denlinger, (1977). Both models make similar predictions as to the relative size of shear and compressive energy losses, and either may explain the observations of Born (1941) and Gardner et al. (1964) that increasing fluid saturation causes increasing attenuation. These mechanisms have all been discussed in greater detail in Chapter II.

Experimental Results

We will first discuss a series of three experiments performed on a sample of Massilon sandstone (see Chapter III for a sample description). In the first experiment the sample was dry and jacketed with heat-shrink tubing. The confining pressure medium was nitrogen. After cycling confining pressure to eliminate hysteresis effects, attenuation and velocity data was taken vs. confining pressure. The rock was then evacuated to a pressure of ~0.1 torr, then partially saturated with distilled water (pore pressure ~7 bars), and confining pressure was again varied. To achieve total saturation it was necessary to increase pore pressure to about 15 bars, so in the third experiment we held confining pressure constant at 345 bars and varied the pore pressure. Because attenuation and velocity are functions of effective stress (in saturated rock), this procedure is equivalent to varying confining pressure in fully saturated rock. We do not have precise control over the degree of saturation when partially saturated, but we have estimated this in several ways, as discussed below.

We will first consider the velocity measurements because these help in understanding the attenuation data. Figure (5-1) shows the measured shear and extensional velocities. We have the usual observation of velocities increasing with pressure due to crack closure. Notice that shear velocity is minimum in fully saturated rock and extensional velocity is minimum in partially saturated rock. Extensional velocities, however, are of limited practical interest, so we have used the data in Figure (5-1) to calculate P-wave velocities using the relation

$$V_p^2 = V_s^2(4V_s^2-V_e^2)/(3V_s^2-V_e^2)$$

Both P-wave and shear wave velocities are shown in Figure (5-2). Notice that shear wave velocities decrease continuously as the degree of saturation increases. However, P-wave velocities decrease as the rock goes from dry to partial saturation, and then sharply increase as the rock becomes fully saturated. This sort of behavior has often been observed at ultrasonic frequencies (Elliot and Wiley, 1975; Domenico, 1976; Gregory, 1976) but this is the first such observation at frequencies below one kilohertz. (Note - Gordon and Rader (1971) reported that at millihertz frequencies the extensional velocity in fully saturated rock was less than in dry rock. They then interpreted this observation to imply that P-wave velocity was also less in fully saturated rock. However, our results show that even though the extensional velocity is less in fully saturated rock than in dry rock, the P-wave velocity may still be a maximum. Also, the samples used by Gordon and Rader were apparently unjacketed with no confining pressure, in which case the unrealistic boundary conditions on pore fluid flow will probably invalidate their results.)

The causes of the effects seen in Figure (5-2) are fairly well understood, at least qualitatively. As water is added to the rock, the over-

Figure (5-1). Shear (S) and extensional (E) velocities in dry (D), partially saturated (PS), and fully saturated (FS) Massilon sandstone. Pore fluid is water.

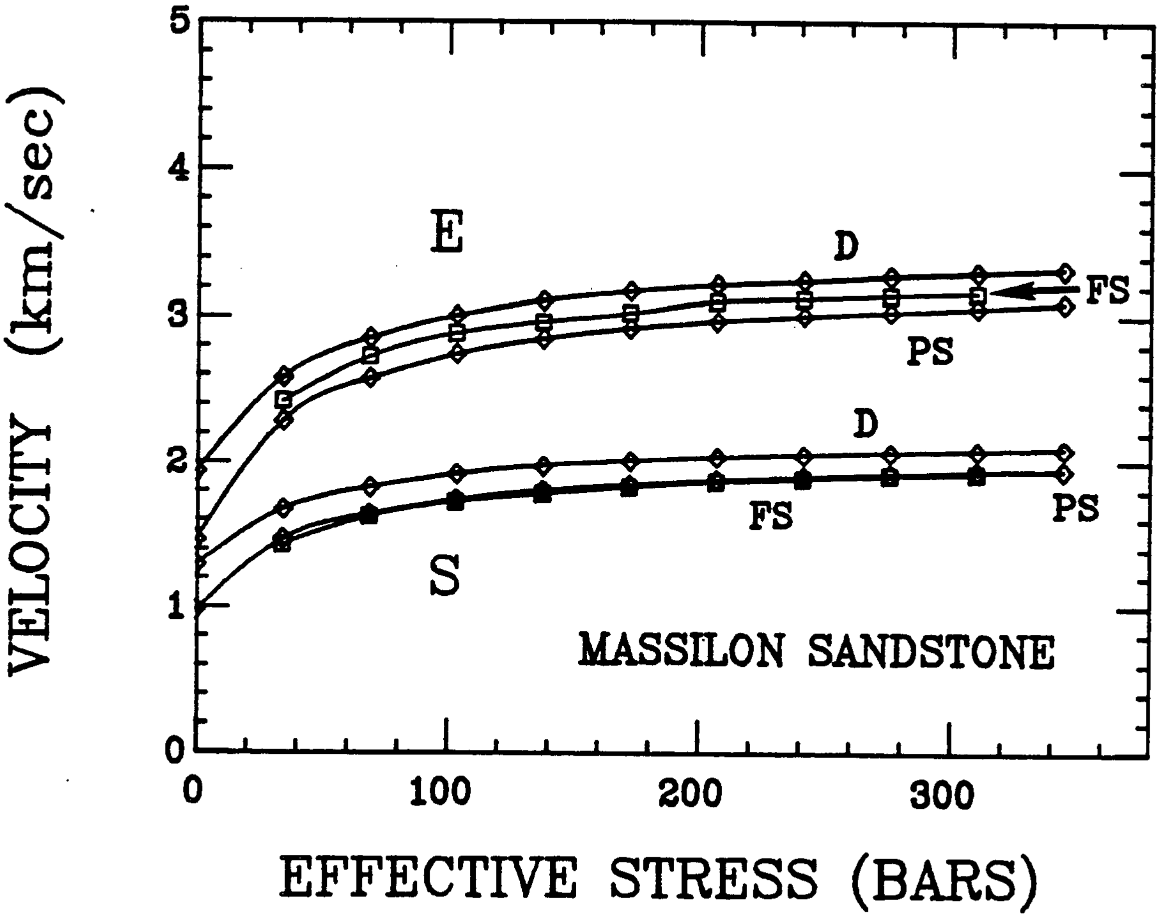

Figure (5-2). Shear velocities (S) and computed P-wave velocities (P) in dry (D), partially saturated (PS), and fully saturated (FS) Massilon sandstone.

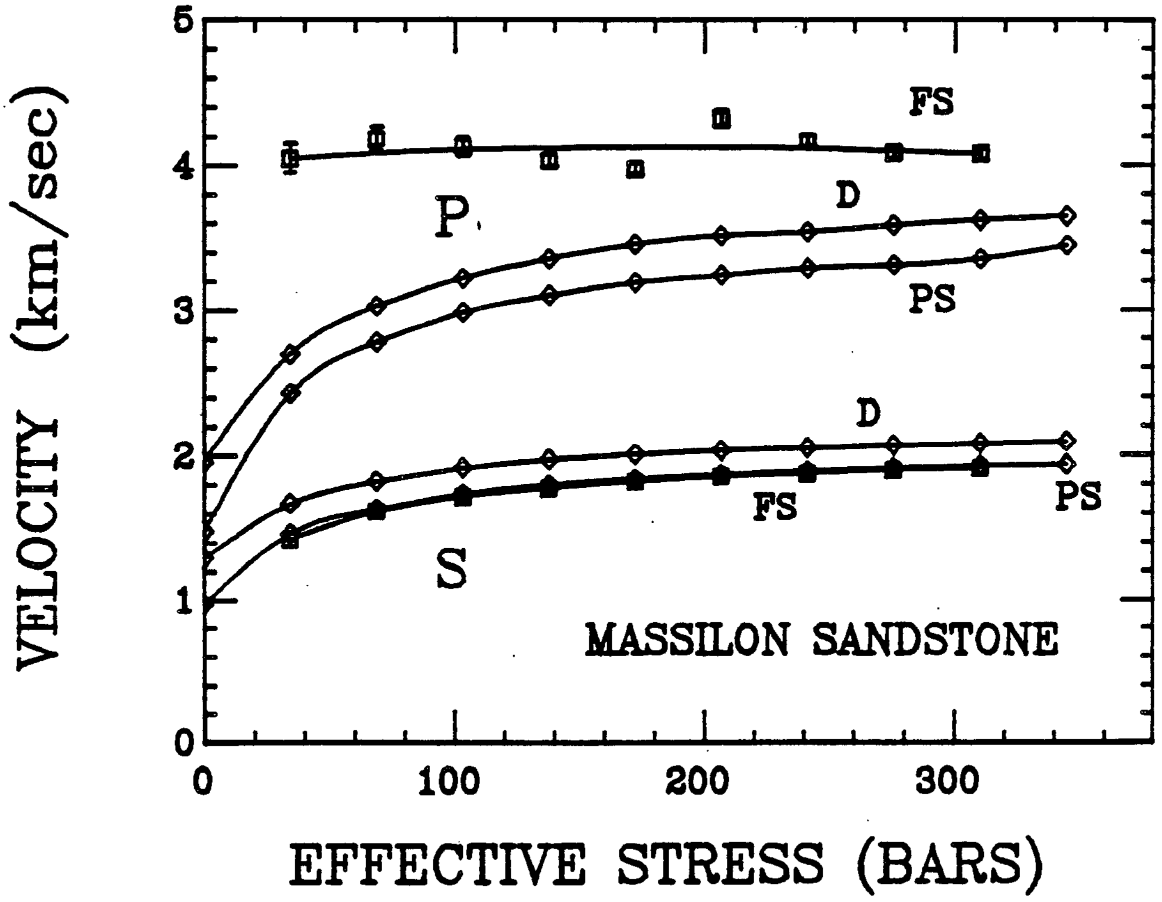

all density increases, thus reducing the velocities of both P and S-waves. As total saturation is reached, the pores in the rock become less compressible. This increases the effective bulk modulus of the rock but has no effect on the effective shear modulus. Therefore P-wave velocity increases at total saturation while shear wave velocity reaches a minimum. We can make use of this behavior to estimate the degree of saturation in our partially saturated rock. Notice that the shear velocity in the fully saturated rock is only very slightly less than in the partially saturated rock. If we assume that shear velocity is simply varying with the density of the rock, then we can estimate the degree of saturation as approximately 95%. Another way to place a minimum value on the degree of saturation is to assume thaat the rock was full of air before pumping water into it. Then at a pore pressure of 7 bars the air will occupy roughly one seventh of its original volume, giving 86% overall saturation. Since in fact much of the air was removed from the sample, the degree of saturation must be greater than 86%. Finally, the transition from partial to total saturation is accomplished by pumping only 2-3 cubic centimeters of water into the sample. Since the total pore volume is ~84 cubic centimeters, this implies only 2-4% undersaturation. Therefore 95% degree of saturation is a reasonable estimate.

We have also used the observed increase in P-wave velocity as our main evidence that we have in fact achieved total saturation. Presumably the small increase in pore pressure causes any gas remaining in the rock to dissolve into the water. Our concern with determining the degree of saturation is prompted not so much by our interest in velocities as by an interest in understanding the attenuation data that follows.

Figures (5-3 and 5-4) show the attenuation data that was taken simultaneously with the velocity data in Figure (5-1). Attenuation decreases with increasing effective stress, and as with velocities, this is presumably caused by crack closure. Notice in Figure (5-3) that shear attenuation is minimum in dry rock, increases by a factor of 2-4 in partially saturated rock, and is maximum in fully saturated rock. Error bars are approximately ±1% and have not been shown. Extensional attenuation is shown in Figure (5-4). Here again, attenuation is minimum in dry rock and increases by a factor of 3-6 in partially saturated rock. Partial saturation has a larger effect on extensional attenuation than on shear attenuation. However, we find that extensional attenuation in fully saturated rock is less than in partially saturated rock. This is opposite to what we found for shear attenuation. Although this may seem like a small effect, it will be seen to have very important implications.

With the four measurements of velocities and attenuation in both shear and extension, we can use the equations in Appendix B to calculate the attenuation of P-waves and of bulk compressional deformation. However, before using these equations we must be sure we have satisfied the assumptions upon which they are based, namely, small attenuation, isotropy and linearity. The maximum attenuation observed in this study was $Q^{-1} \sim 0.057$, $(Q \sim 17)$, which satisfies our requirement of small attenuation. Anisotropy is less than 3% as measured by the velocities of ultrasonic P and S-waves. All data presented in this chapter was taken at strains below those at which nonlinear, frictional effects are observed (see Chapter IV). One additional requirement is that Q be only weakly dependent on frequency. This is because extensional and shear Q's are measured at different frequencies ($f_e \approx 1.5 f_t$), and we use both to calculate Q_p^{-1} and Q_k^{-1}. We have used higher harmonics of the fundamental resonance to verify that Q is only weakly dependent on frequency over the frequency range of this study. Of course, this method yields measurements at only a few relatively widely spaced frequencies. However, very weak dependence of attenuation on frequency has been fairly well established by previous investigators (discussed in Chapter II), so our assumption of constant Q should not result is significant errors in the calculations. The weak dependence of velocity on frequency is also well established.

Figure (5-5) shows the P-wave attenuation calculated from the shear and extensional data. The small uncertainties in the original data have propagated through the calculations and are now worth showing. The reason for the relatively large error bars on some of the data is that extensional attenuation is dominated by shear attenuation (~80%) and so both together give rather poor resolution on P-wave and bulk compressional attenuation. A few of the calculated values are negative, which is physically impossible. These probably result from systematic errors in the data and should simply be interpreted as very small values of attenuation. Despite these uncertainties in the data, the main features are fairly clear. Once again, attenuation is minimum in dry rock. Partial saturation causes a substantial increase in P-wave attenuation and then total saturation causes a sharp reduction in attenuation. This is analogous to the reversal in P-wave velocity with degree of saturation shown in Figure (5-2). In Figure (5-6) we show the computed bulk compressional attenuation which basically amplifies the effects seen for P-wave attenuation.

Figures (5-3 to 5-6) have all been plotted on different vertical scales so that we can emphasize relative variations of a particular mode of attenuation with degree of saturation. In Figures (5-7 to 5-9) we have re-plotted the same data using identical vertical scales, but with each figure showing a different state of saturation. This helps us to compare the data for different attenuation modes.

To summarize these results, both shear and bulk compressional attenuation are minimum in dry rock. Attenuation for both modes increases substantially when the rock is partially saturated, with bulk compression being affected about twice as much as pure shear. However, as total saturation is achieved, bulk compressional attenuation is significantly reduced while shear attenuation reaches a maximum.

Figure (5-3). Shear attenuation in dry (D), partially saturated (PS), and fully saturated (FS) Massilon sandstone.

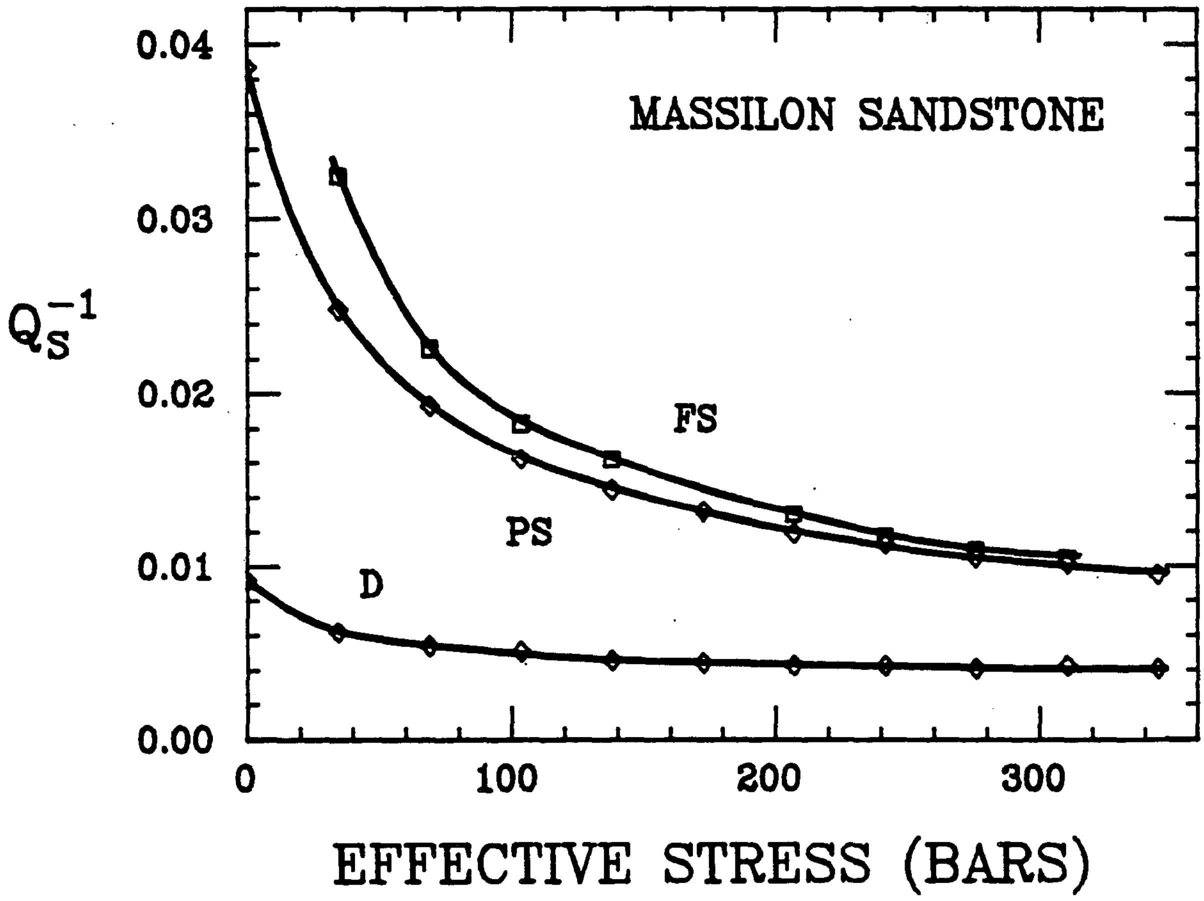

Figure (5-4). Extensional attenuation in dry (D), partially saturated (PS), and fully saturated (FS) Massilon sandstone.

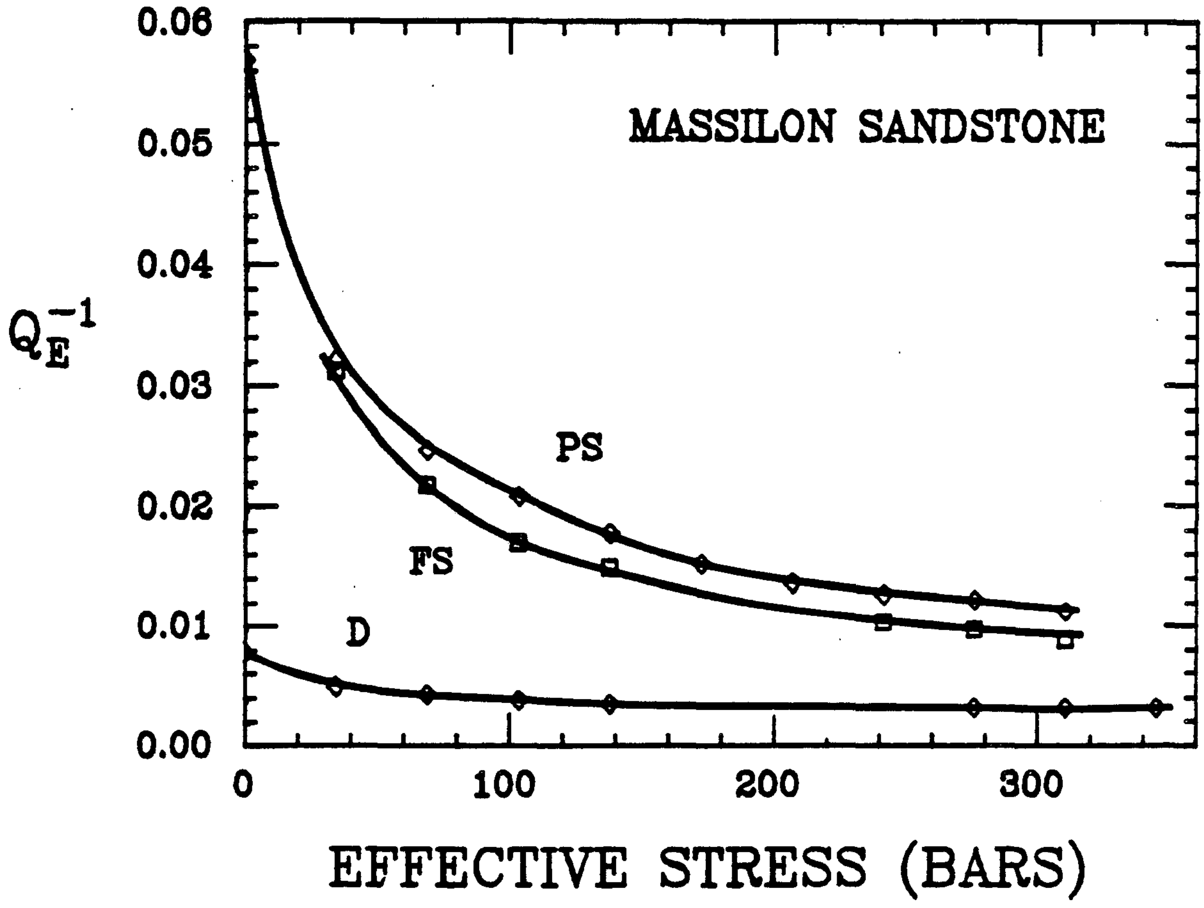

Figure (5-5). Computed P-wave attenuation in dry (D), partially saturated (PS), and fully saturated (FS) Massilon sandstone.

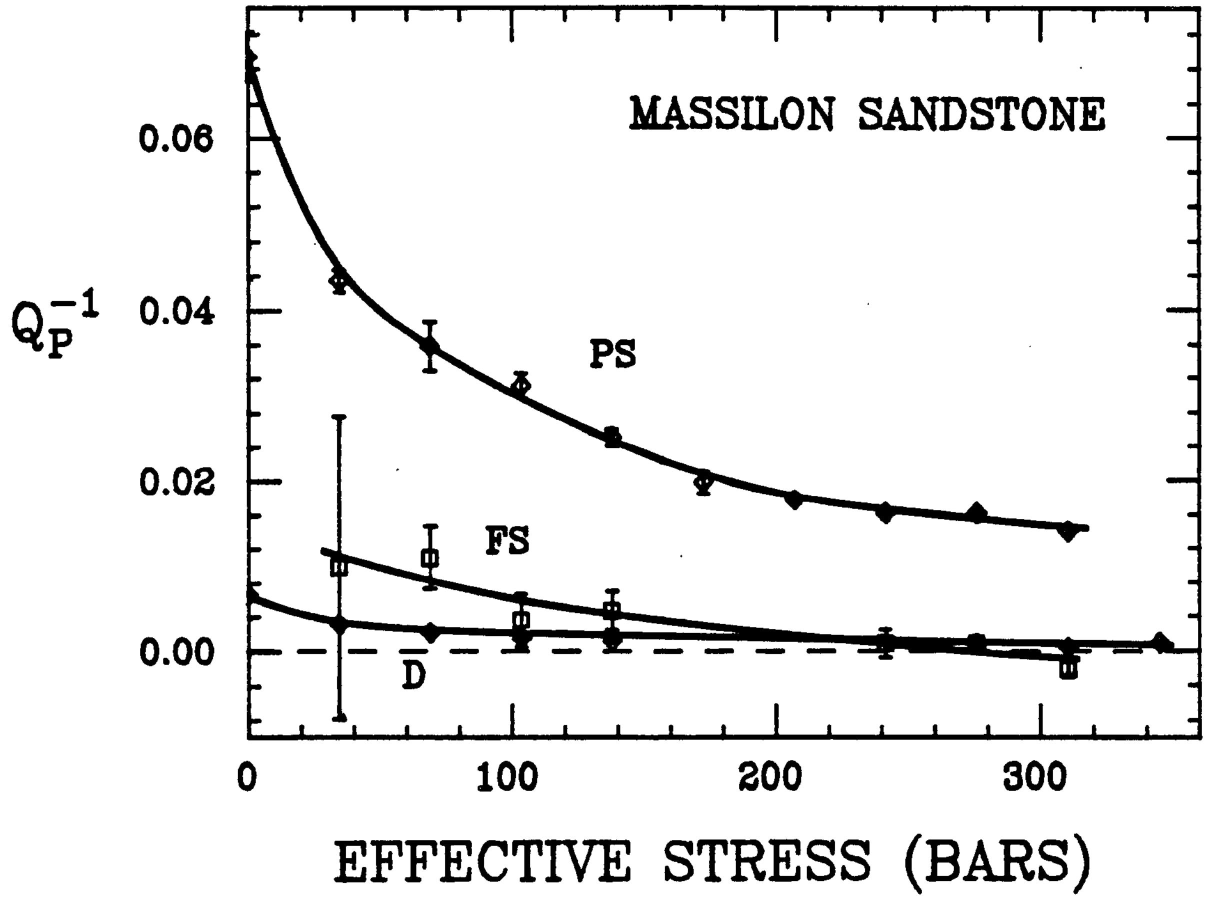

Figure (5-6). Computed bulk compressional attenuation in dry (D), partially saturated (PS), and fully saturated (FS) Massilon sandstone.

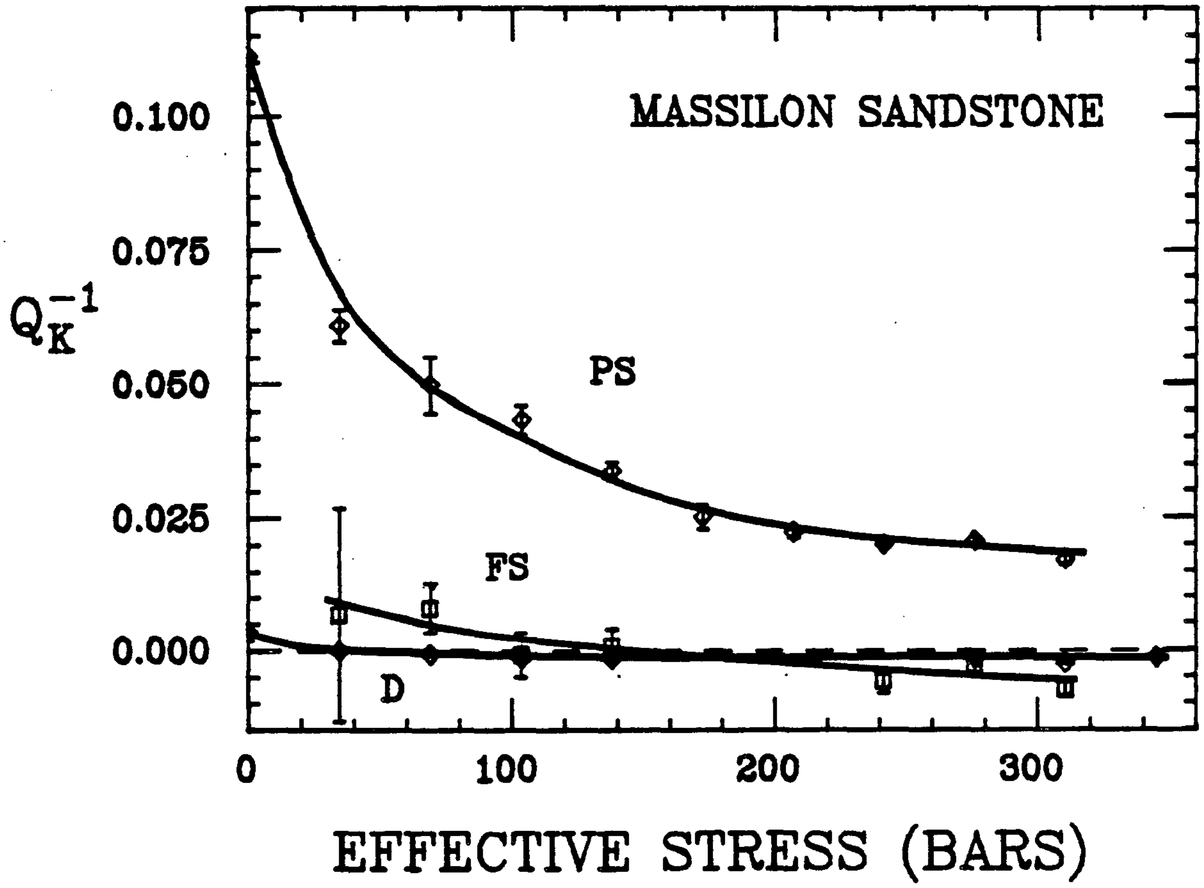

Figure (5-7). Shear (S), extensional (E), computed P-wave (P), and computed bulk compressional (K) attenuation in dry Massilon sandstone.

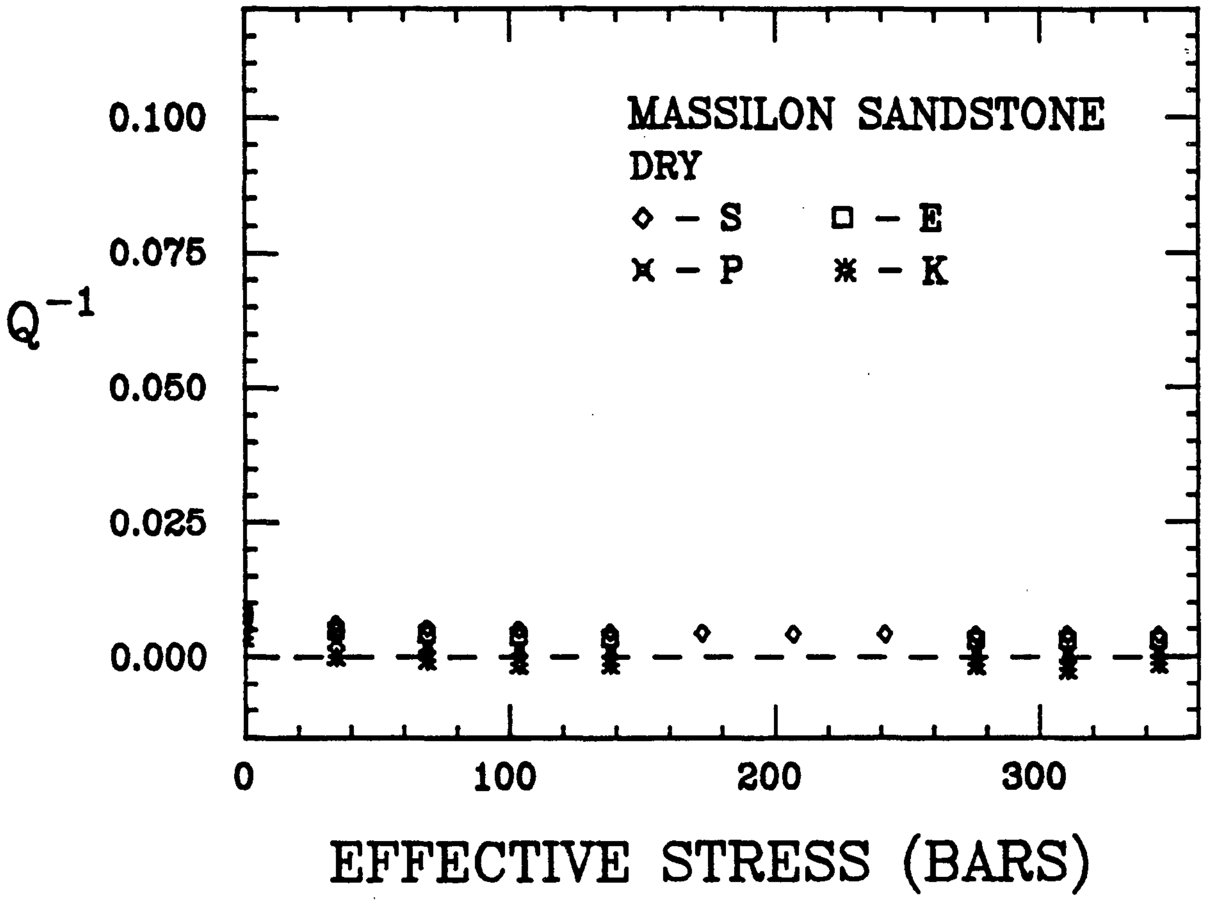

Figure Shear (S), extensional (E), computed P-wave (P), and computed bulk compressional (K) attenuation in partially saturated Massilon sandstone.

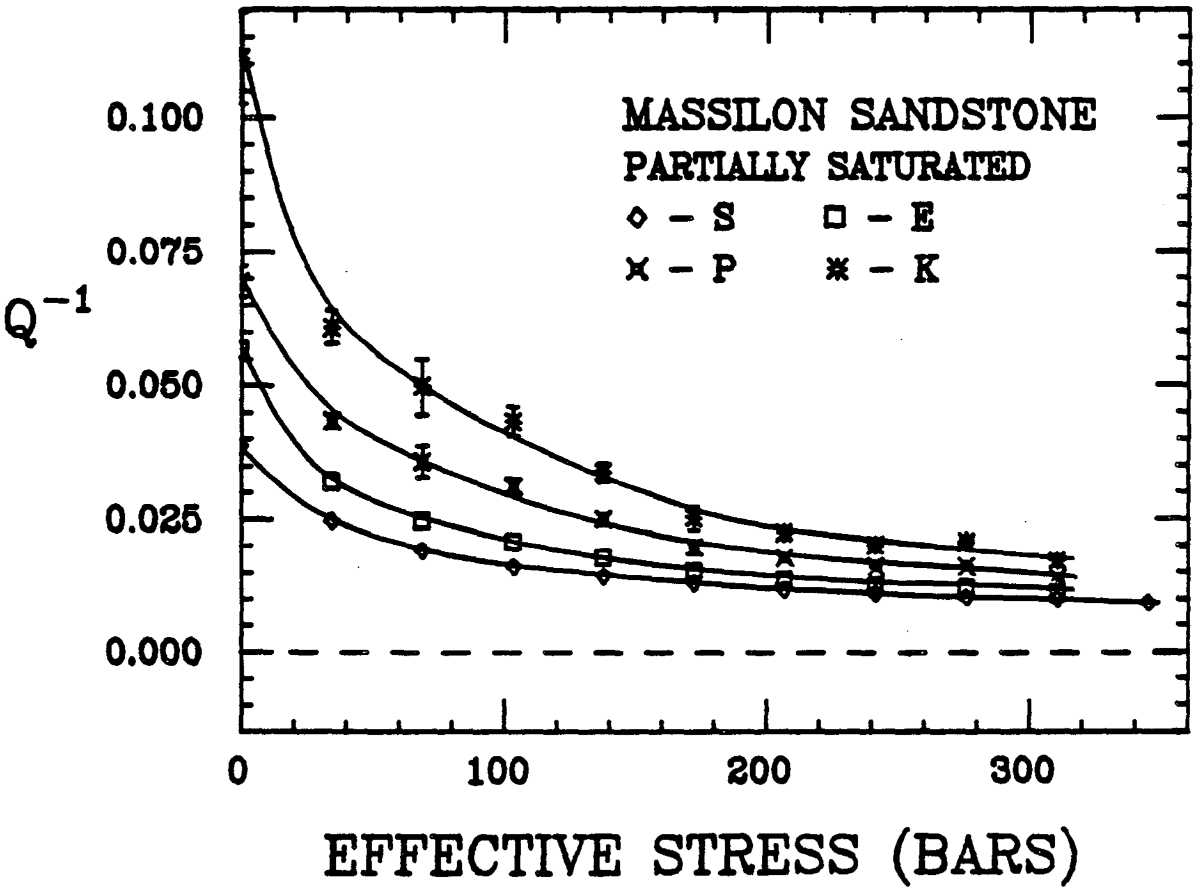

Figure (5-9). Shear (S), extensional (E), computed P-wave (P), and computed bulk compressional (K) attenuation in fully saturated Massilon sandstone.

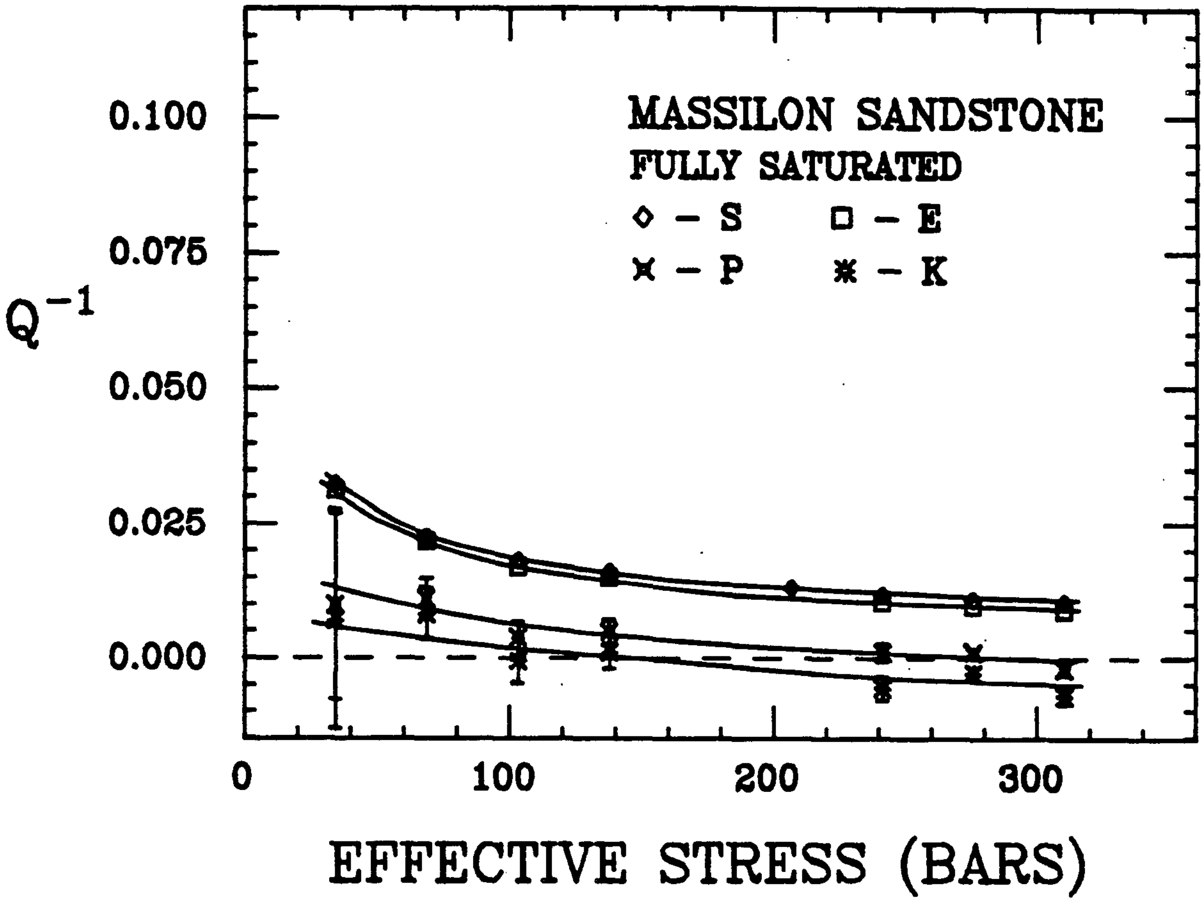

Before discussing this data we will present the results of a different experiment done on Vycor porous glass. This was a very simple experiment, and although important parameters were not controlled, the results are quite interesting. Vycor glass is described in Chapter III, but basically it is a porous glass with ~28% porosity and extremely small, rather equidimensional pores.

The experiment was performed on the benchtop with an unjacketed sample. The Vycor was saturated simply by submerging it in de-ionized water for several hours. This procedure is not sufficient to totally saturate rock, but apparently is does work with Vycor because of very strong capillary forces. As in the previous experiment, the velocity data will provide evidence that total saturation was achieved. Following saturation, both torsional and extensional attenuation and velocities were measured as the sample dried out. With this procedure we have no control over the homogeneity of the fluid distribution.

The resulting attenuation data is shown in Figure (5-10). Note that the overall level of attenuation is much less than in Massilon sandstone. As the sample dries out, shear attenuation is virtually unaffected by the degree of saturation. However, extensional attenuation rapidly increases and after seven hours reaches a peak that is more than twice as large as when fully saturated. It then slowly decreases as drying continues and eventually becomes less than the shear attenuation. Since shear attenuation is virtually constant, any variation in extensional attenuation must be due to its bulk compressional component. This is shown in Figure (5-11) where we have added to Figure (5-10) the computed P-wave and bulk compressional attenuation. These results are qualitatively similar to the results for Massilon sandstone where compressional attenuation is significantly increased by partial saturation and then reduced at total saturation. The differences between the two materials, such as the behavior of shear attenuation and the overall magnitude of attenuation, can be related to the microstructure and will be discussed later in this chapter.

Figure (5-12) shows the shear wave velocity as the Vycor dried out. Basically we see a monotonic increase in velocity as the sample dries and the density decreases. There seems to be a very small initial decrease in velocity which may be due to a stiffening effect. Figure (5-13) shows the corresponding extensional velocities and Figure (5-14) shows the P-wave velocities calculated from the shear and extensional velocities. Here we see an initial significant decrease in velocity followed by a larger increase in velocity. The decrease in velocity is caused by an increase in the compressibility of the pores as they become undersaturated. This effect is offset by a decrease in density which eventually causes the velocity to increase. For completeness we have also plotted the V_p/V_s ratio (Figure (5-15)) and Poisson's ratio (Figure (5-16)).

Several months after the experiment with Vycor, we attempted to calibrate drying time with percent saturation. A small piece of Vycor was saturated with water and allowed to dry while suspended from a balance. By recording the weight of the sample and knowing its porosity, we can calculate the percent saturation vs. time. This is shown in Figure (5-17). This curve was then used to re-plot the Vycor data against percent saturation. Admittedly, this is not the best way to measure percent saturation in the original experiment. However, the results are probably accurate to within 10-15%, and this is good enough for our present purposes.

Figure (5-18) shows the data of Figure (5-11) plotted against percent water saturation. Note that since the percent saturation curve of Figure (5-17) was not extended beyond thirty hours (due to an oversight of the author), all of the data in Figure (5-11) cannot be shown in Figure (5-18). Nevertheless, we see that compressional attenuation reaches a maximum somewhere between about 60-70% water saturation. Figures (5-19 and 5-20) show shear wave and P-wave velocities plotted against percent saturation. Note that the P-wave velocity reaches a minimum at about 50% saturation, which is less than what we expect to find in sandstone. Finally, Figure (5-21) shows the V_p/V_s ratio vs. percent saturation. We emphasize once again that the percent saturation is an average over the entire sample which ignores any heterogeneities of the pore fluid distribution.

Figure (5-10). Shear (S) and extensional (E) attenuation in Vycor vs. drying time.

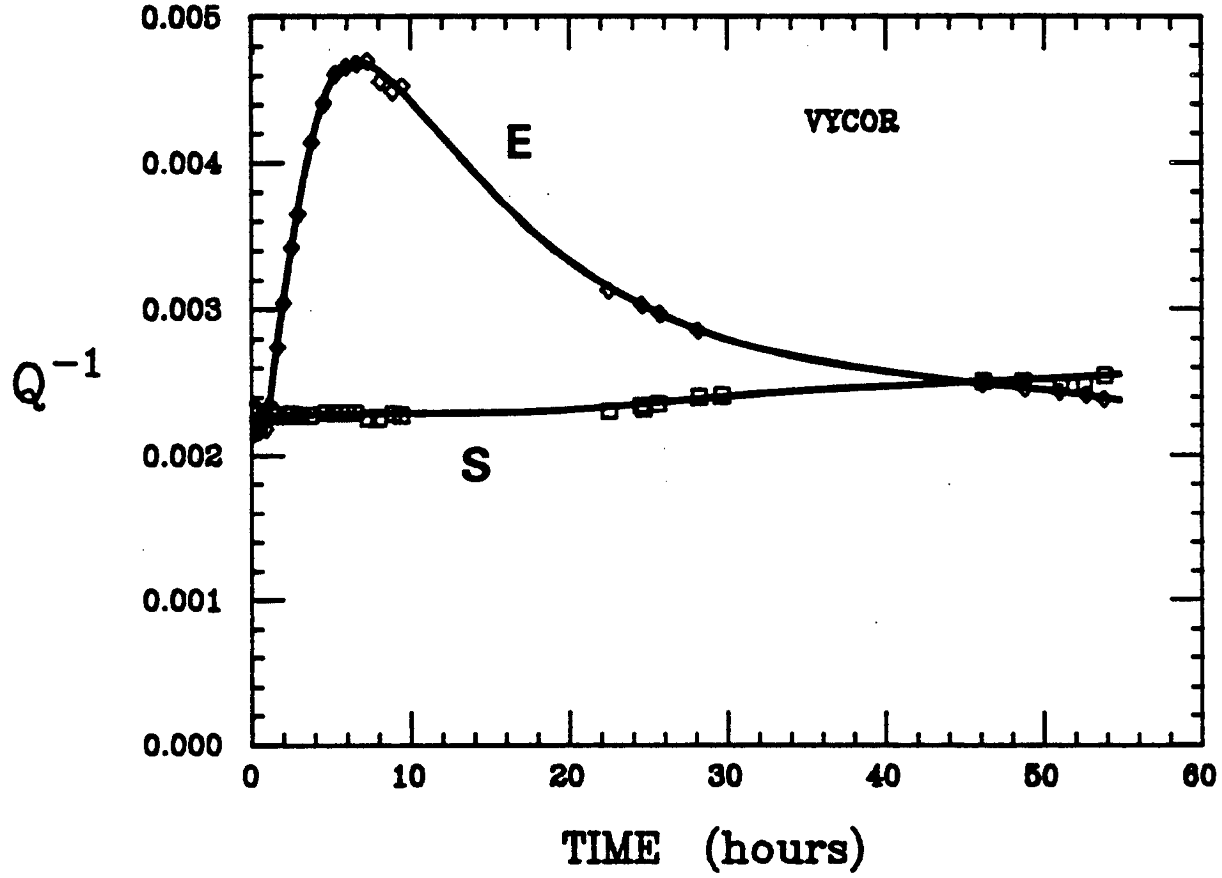

Figure (5-11). Shear (S), extensional (E), computed P-wave (P), and computed bulk compressional (K) attenuation in Vycor vs. drying time.

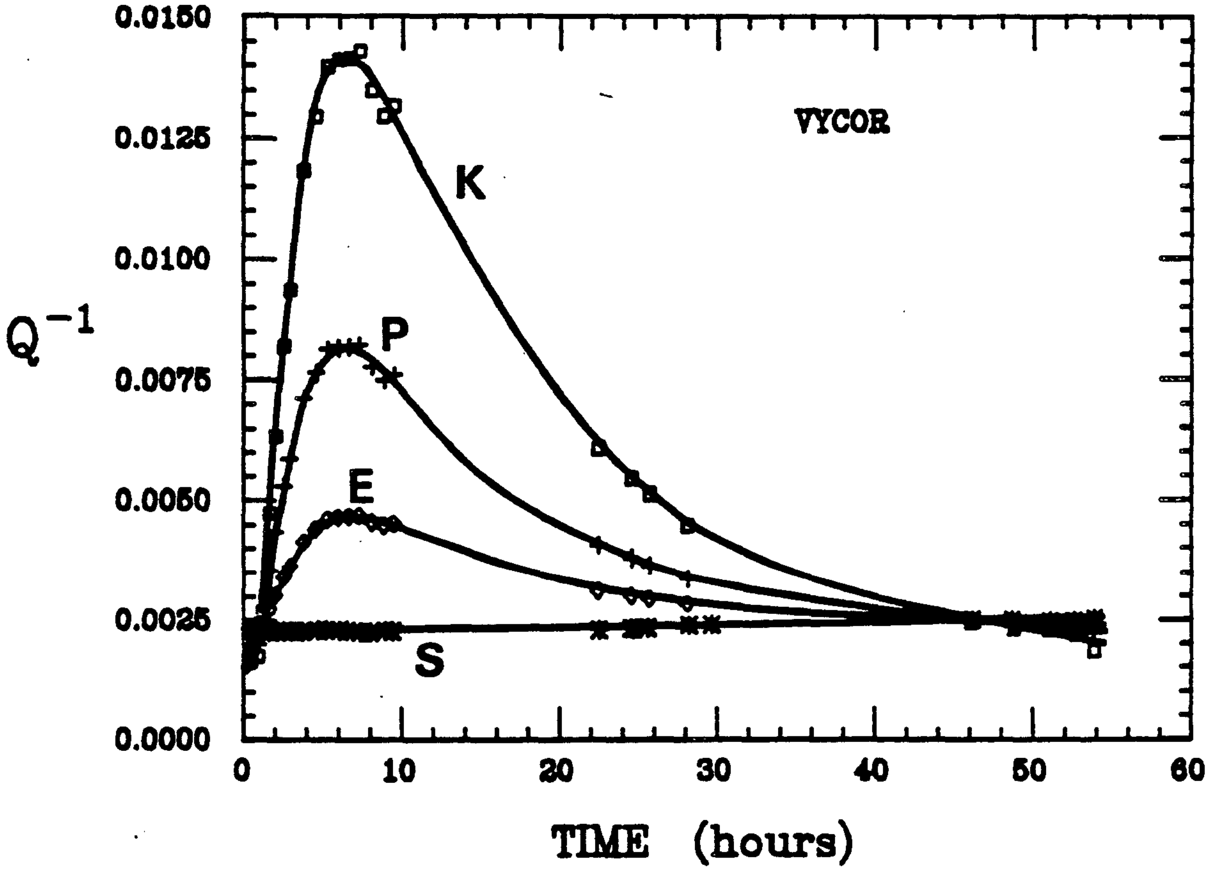

Figure (5-12). Shear velocity in Vycor vs. drying time.

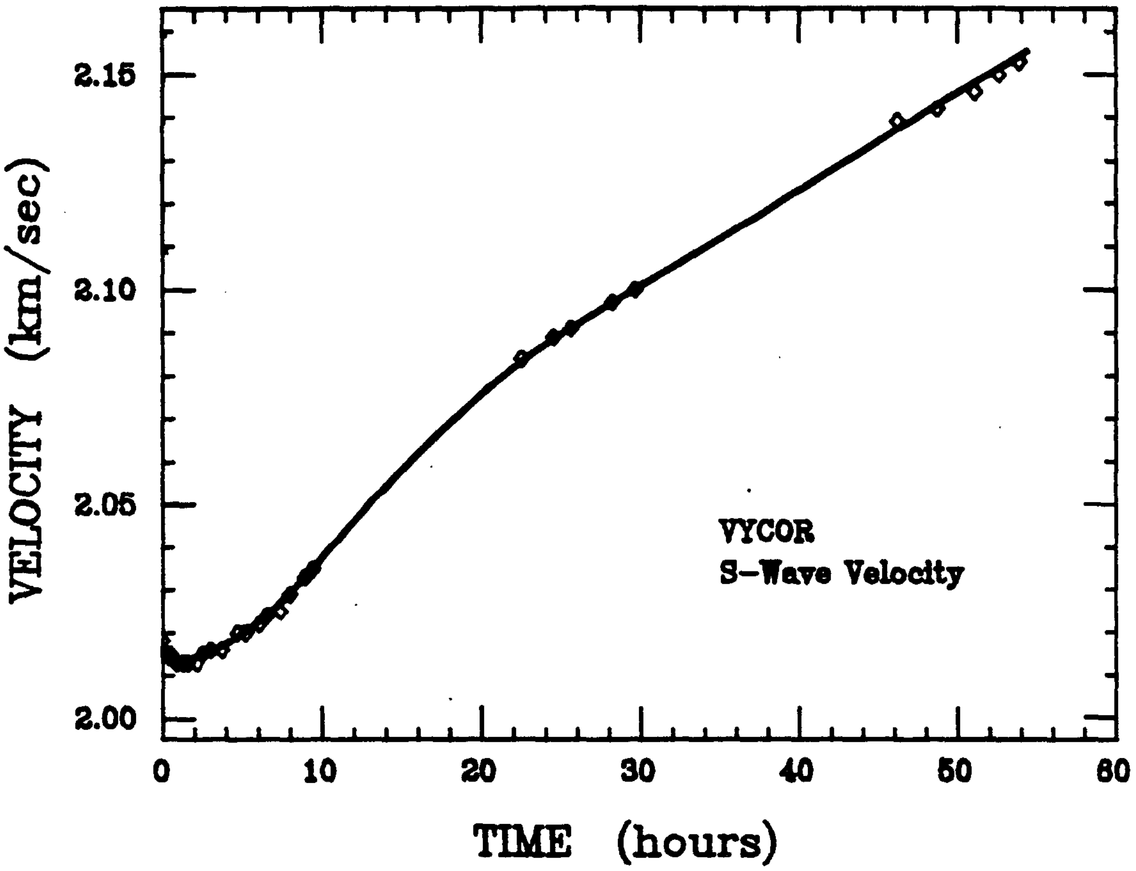

Figure (5-13). Extensional velocity in Vycor vs. drying time.

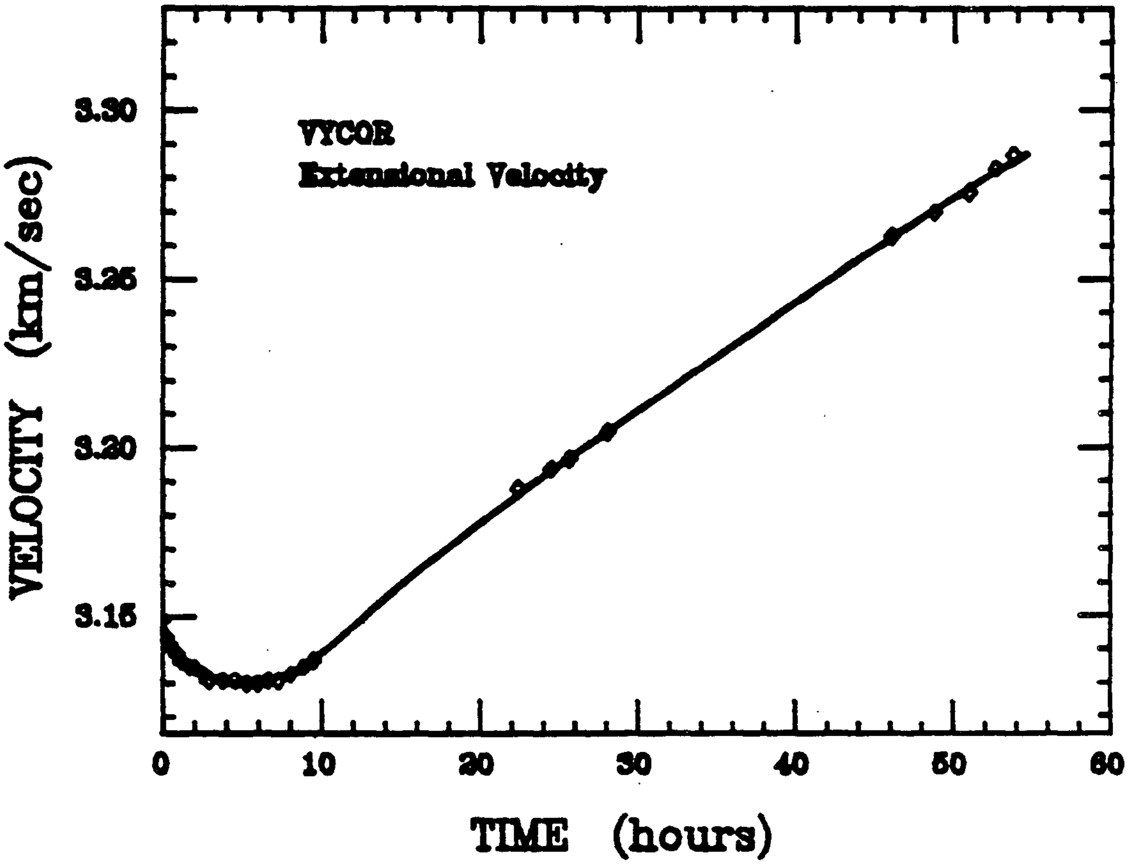

Figure (5-14). Computed P-wave velocity in Vycor vs. drying time.

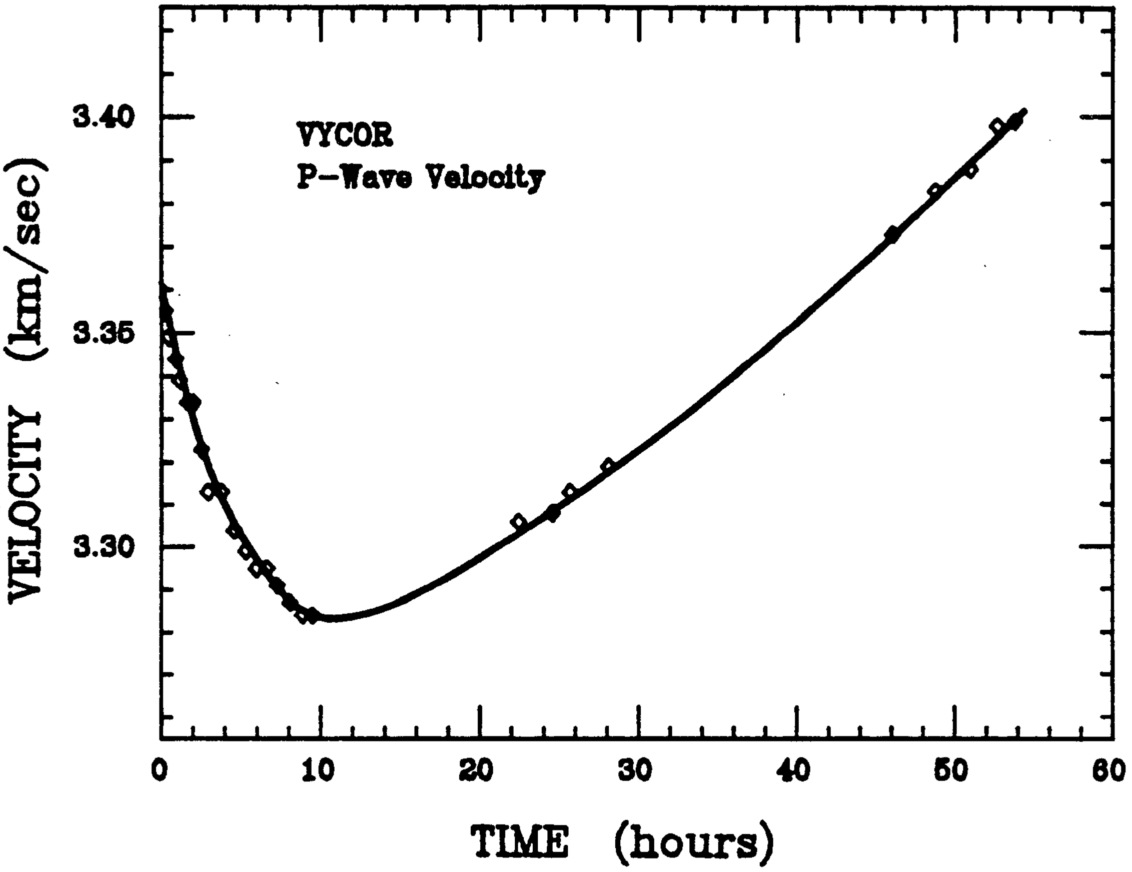

Figure (5-15). V_p/V_s ratio in Vycor vs. drying time.

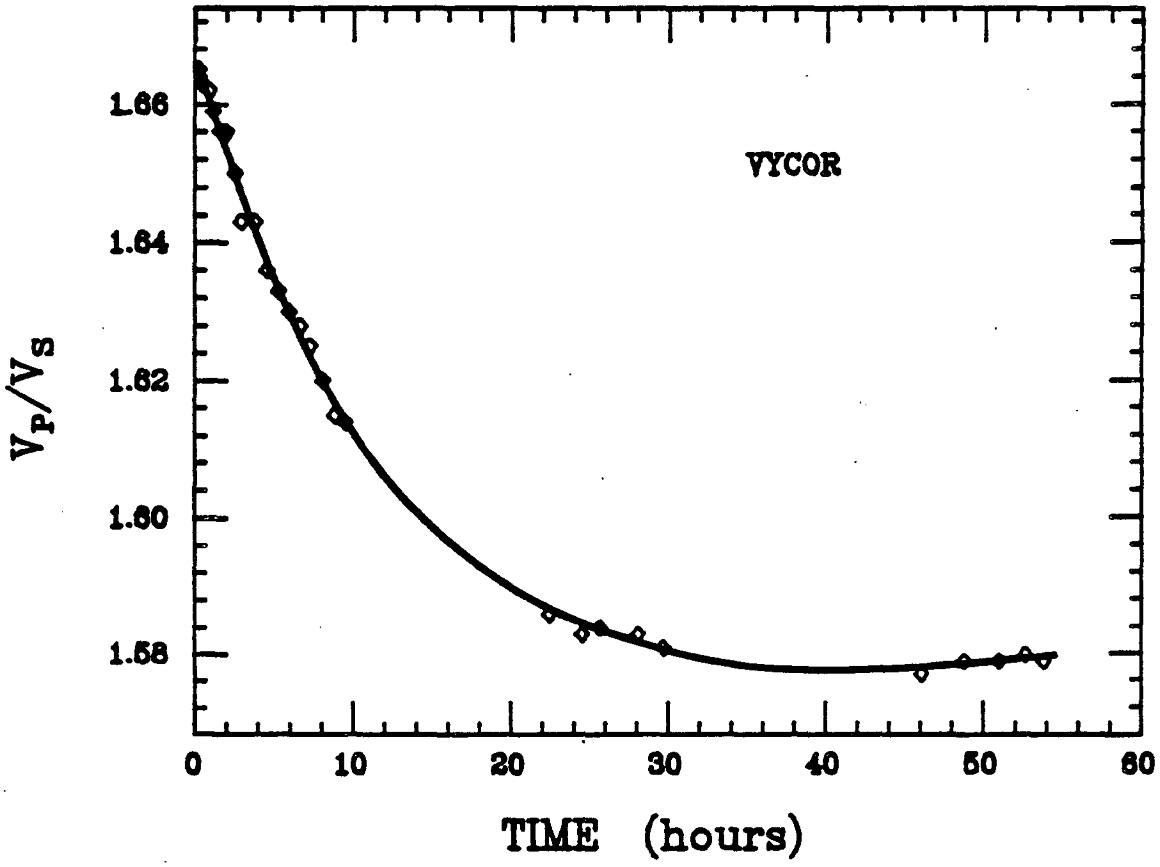

Figure (5-16). Poisson's ratio in Vycor vs. drying time.

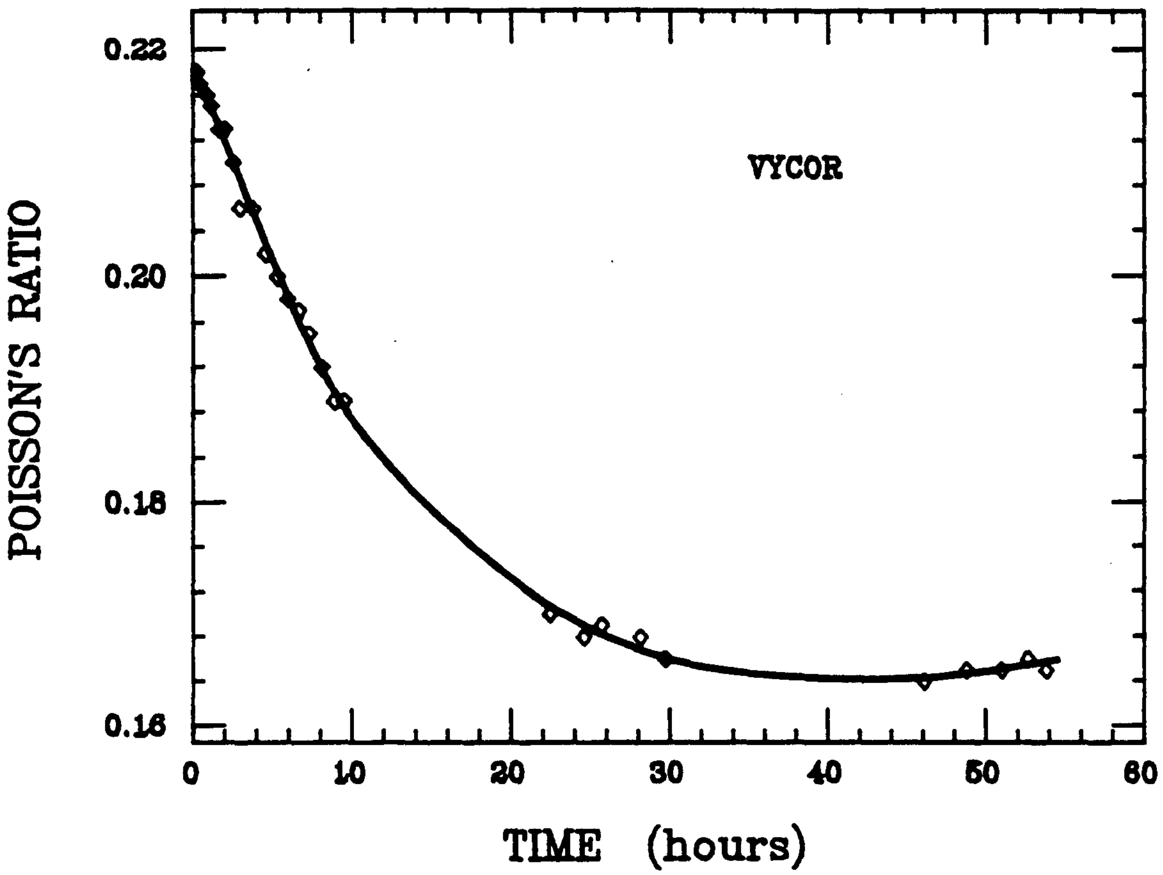

Figure (5-17). Percent water saturation vs. drying time for second Vycor sample.

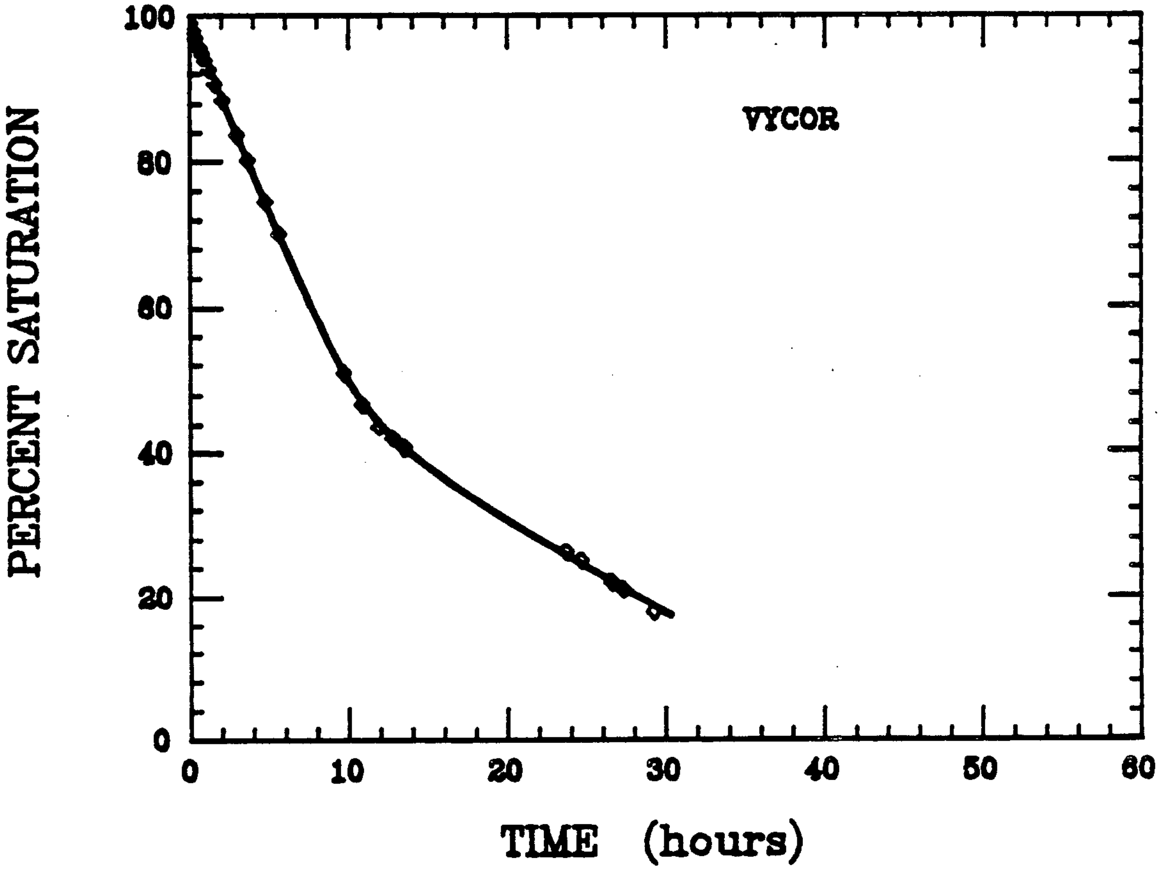

Figure (5-18). Shear (S), extensional (E), computed P-wave (P), and computed bulk compressional (K) attenuation in Vycor vs. percent water saturation.

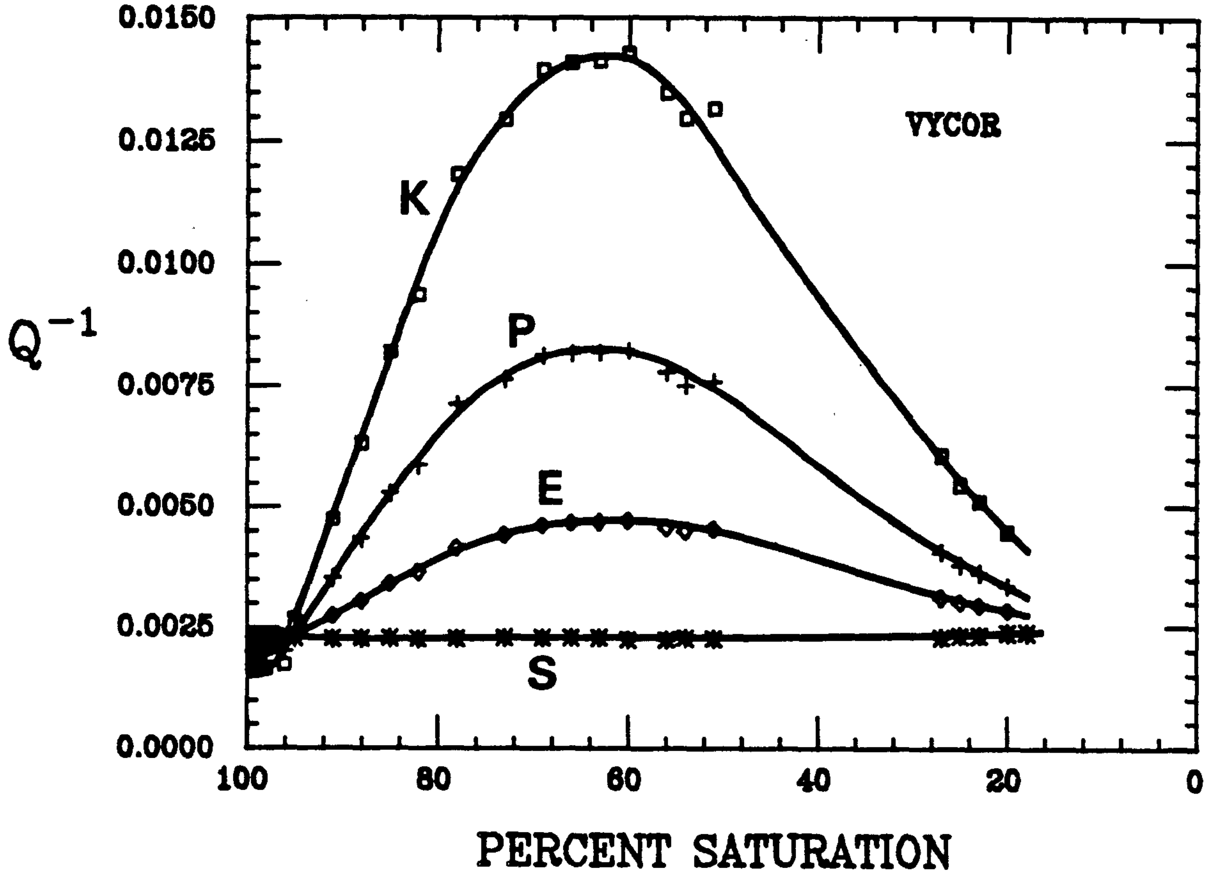

Figure (5-19). Shear velocity in Vycor vs. percent water saturation.

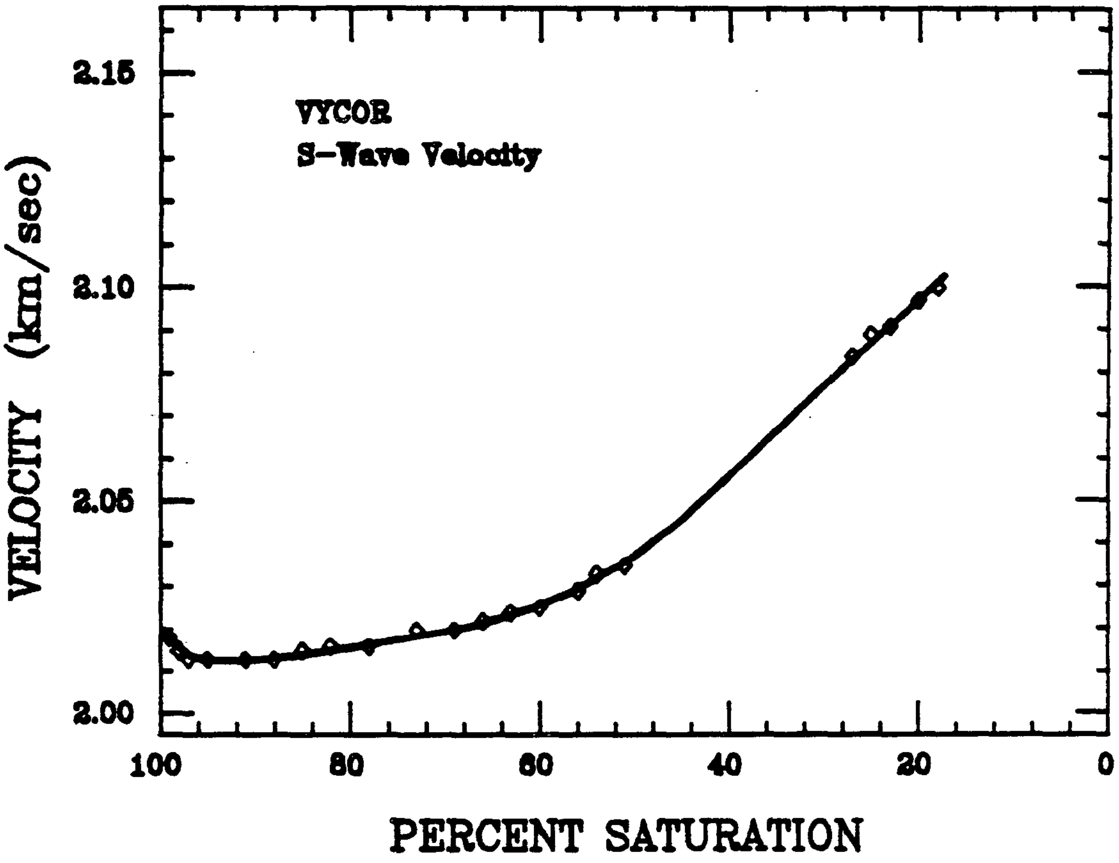

Figure (5-20). P-wave velocity in Vycor vs. percent water saturation.

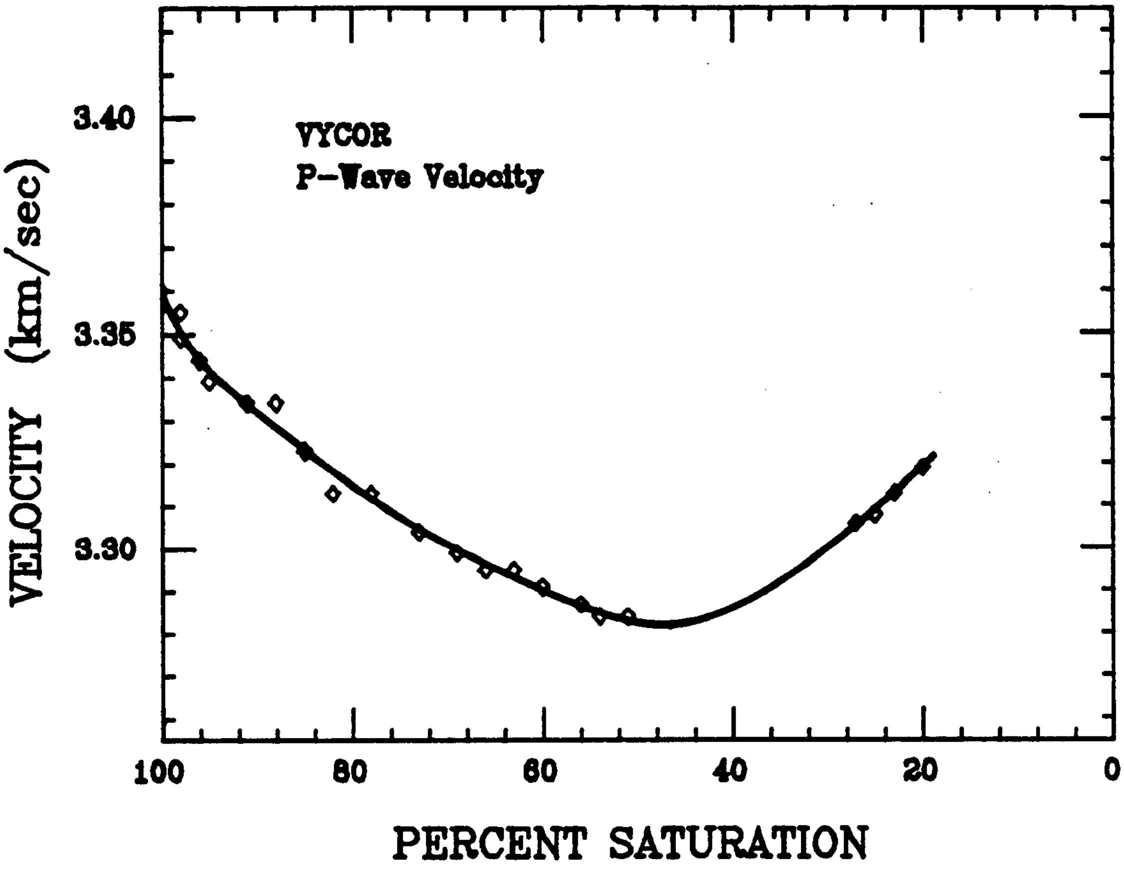

Figure (5-21). V_p/V_s ratio in Vycor vs. percent water saturation.

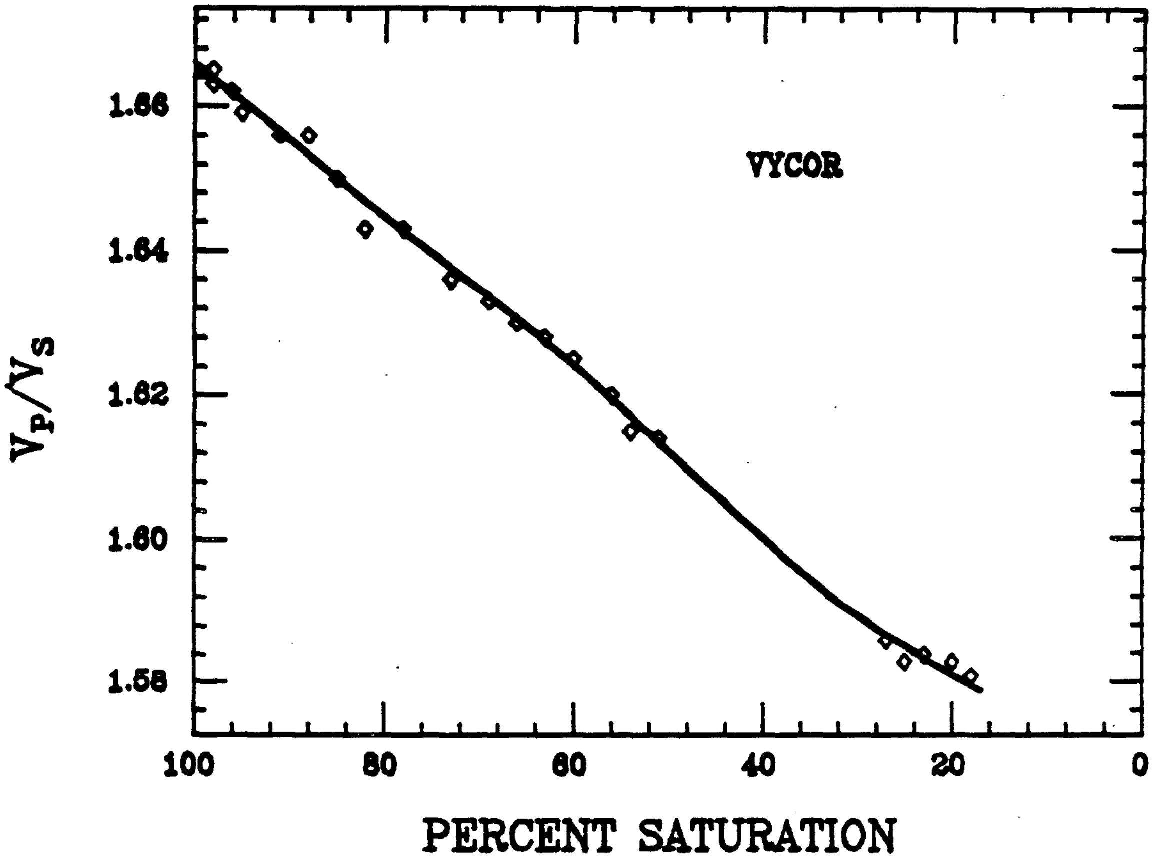

Discussion

There are two different ways in which our observations can be analyzed, one which emphasizes theory and one which emphasizes the data. Using the first approach we would take each of the theoretical models discussed in Chapter II, estimate as well as possible the various parameters in these models, and try to fit the model predictions to the data. The major weakness of this approach is that most theories require input parameters which are extremely difficult (if not impossible) to measure and can only be poorly estimated. This is especially true for models based on details of the microstructure (Walsh, 1966; O'Connell and Budiansky, 1977; Mavko and Nur, 1979), where the most difficult parameter to determine is the hypothetical distribution of crack aspect ratios. Although model parameters can always be chosen to fit observations, the choice is always non-unique. A second problem with this approach is that it assumes the theories closely approximate the real world. We actually have no idea of how well a distribution of penny-shaped cracks (or any other ideal shape) approximates the true microstructure of a rock. Although theoretical models are certainly useful for quantifying our intuitive ideas, in general they have not yet reached a stage of development where they can be used to make reliable, quantitative predictions.

The approach we will use in analyzing our data is relatively qualitative. We will make use of theory whenever possible, but will stress such features as dependence on degree of saturation or the relative amounts of attenuation in shear and bulk compression. We will show that all of our observations can be understood using a few simple and intuitively appealing (to the author, at least) concepts regarding the way in which pore fluids interact with the rock matrix during the passage of a seismic wave. Each of these concepts has been analyzed theoretically in one of the papers discussed in Chapter II, but we will not emphasize details of the theories.

The data for dry rock will be discussed in detail in Chapter VI, where additional observations will be presented. We will first consider the data for fully saturated sandstone shown in Figures (5-3 to 5-6). The most obvious feature is that attenuation decreases with increasing effective stress. This is presumably caused by the closing of microcracks. Since virtually every proposed attenuation mechanism is expected to show this sort of pressure dependence, it does not help us in evaluating the mechanisms. Of greater usefulness are the overall magnitude of the attenuation and the observation that shear waves are attenuated more strongly than P-waves, on the order of 2 to 1. Three models have been proposed to describe attenuation in fully saturated rock and all are discussed in Chapter II. Biot's (1956a,b) model involves both macroscopic flow and inertial effects. It predicts more shear wave attenuation than P-wave attenuation, and the predicted ratio is on the order of what we have observed. However, White (1965) and Johnston _et al_. (1979) have each applied Biot's theory to Berea sandstones which are very similar to Massilon sandstone, and both authors agree that at the low frequencies at which we are working, Biot's theory predicts values of attenuation which are too low by about an order of magnitude to explain our observations. Although Biot's theory itself makes some approximations, and both White (1965) and Johnston et al. (1979) had to make some assumptions when applying it, it seems unlikely that either macroscopic fluid flow or inertial effects cause significant attenuation at frequencies near (or below) one kilohertz. This, of course, does not invalidate Biot's theory. It just means that we have to look elsewhere to explain all of the attenuation we observe in fully saturated rock.

A second possible mechanism is the thermal relaxation model proposed by Kjartansson and Denlinger (1977). At room temperature this mechanism is not expected to be important in water saturated rocks because of the small difference between the adiabatic and isothermal bulk moduli of the pore fluid.

Finally, we come to the inter-crack, or "squirting", flow mechanism discussed by Mavko and Nur (1975) and O'Connell and Budiansky (1977). Cracks at different orientations to the passing wave (or cracks of different aspect ratio) will undergo different amounts of compression. This causes fluid to flow between connected cracks to re-establish pore pressure equilibrium. The fluid flow causes viscous dissipation of energy. As formulated by O'Connell and Budiansky (1977) this mechanism seems capable of giving the order of magnitude of attenuation that we have observed. We do not have enough information about the microstructure of Massilon sandstone to attempt more quantitative predictions. The theory also predicts that shear waves should be attenuated more strongly than P-waves, and the predicted ratio is reasonably close to what we have observed. It therefore seems likely that local flow of fluid between adjacent cracks is responsible for most of the attenuation observed in fully water saturated rock. However, there is ample room for improvement in the theory. For instance, O'Connell and Budiansky (1977) consider only infinitely thin cracks that respond equally to bulk compression. Thus no attenuation is expected in bulk compression. However, whenever thin cracks intersect round pores, bulk compression will cause fluid to flow from the crack into the pore. This sort of interaction will be more common in sedimentary rocks having equidimensional pores than in low porosity igneous rocks. It is not known how much additional attenuation this will cause, but the effect should be about twice as large for bulk compression as for pure shear. However, this modification to the theory is not likely to affect our conclusion that inter-crack flow dominates attenuation in water saturated rocks.

This model also adequately explains the data for Vycor shown in Figure (5-11). We are now only interested in the fully saturated sample at time zero. Again we find that shear attenuation is larger than bulk compressional attenuation, although the ratio is not as large as in sandstone. The overall magnitude of attenuation in Vycor is much less than in sandstone because the pore shapes are generally rather equidimensional. (Recall that the microstructure of Vycor approximates a packing of spheres.) An equidimensional pore is much less sensitive to compressive stresses than are flat cracks, so local pore pressure gradients are much smaller in Vycor than in sandstone. In fact, attenuation in fully saturated Vycor is comparable to that in room dry Vycor, so inter-crack flow may account for a negligible amount of attenuation in this material. It is also possible that the extremely small pores in Vycor (~4 nm) allow capillary effects to dominate over flow inducing pressure gradients. This seems likely because in packings of 700 micron glass beads we have observed total saturation to cause significant shear attenuation at ultrasonic frequencies. Therefore it is probably the small size of the pores in Vycor rather than their equidimensional shapes that inhibit attenuation in fully saturated samples.

Next we consider attenuation in partially saturated Massilon sandstone (Figures (5-3 to 5-6)) where the estimated degree of saturation is ~95%. Here we find maximum bulk compressional attenuation plus significant shear attenuation. Compressional attenuation is about twice as large as shear attenuation. Once again we have three models to consider. White (1975) proposed a model in which a material has a heterogeneous distribution of pore fluid. Macroscopic regions of total saturation are adjacent to regions of partial saturation. As the material is compressed, fluid is squeezed from the fully saturated regions into the partially saturated regions, resulting in viscous dissipation of energy. Shearing deformation causes no fluid flow because macroscopic regions are not compressed. Therefore the theory predicts substantial P-wave attenuation in partially saturated rock, but no shear wave attenuation. Since we have observed significant shear wave attenuation (Figure (5-3)), White's model does not explain our observations. However, we presumably have a homogeneous distribution of pore fluid within the sample, in which case White's model does not apply. Therefore our results do not invalidate the application of White's model to the earth, where heterogeneous pore fluid distributions may or may not exist.

The second model to consider was proposed by Mavko and Nur (1979). Rather than having macroscopic regions of total and partial saturation, each individual pore is partially saturated. On a macroscopic scale, the pore fluid is homogeneously distributed. Within a pore the fluid occurs as drops either at crack tips or at isolated points along the length of the pore. As a crack is compressed by a passing seismic wave, the fluid is squeezed and forced to flow into the regions occupied by vapor. This flow once again results in viscous dissipation of energy. During bulk compression every crack is compressed and contributes to the energy loss. However, in pure shear each crack is compressed on the average only half as much as in bulk compression. Therefore the model predicts about half as much attenuation for shear waves as for bulk compression. Comparison of Figure (5-3) and Figure (5-6) shows that this is very close to what we have observed in partially saturated Massilon sandstone. The equations developed by Mavko and Nur (1979) are extremely sensitive to poorly known parameters, so we cannot use them to make reliable estimates of absolute attenuation. However, Mavko and Nur do make estimates of how much attenuation can be expected for reasonable values of input parameters, and it seems likely that the mechanism can account for the magnitude of the attenuation we have observed.

Finally, we come to the thermoelastic mechanism discussed by Kjartansson and Denlinger (1977). We use the same conceptual model used by Mavko and Nur (1979) in which each pore contains isolated fluid drops together with a vapor phase. As a crack is compressed, we ignore the fluid flow (which is still occurring) and concentrate instead on the vapor phase. The initial compression is so rapid that the vapor heats up adiabatically (no heat flow). As heat does eventually flow into the fluid and rock matrix, the vapor cools and contracts and the crack undergoes further compression (it relaxes). This relaxation causes stress and strain to be out of phase so that during each stress cycle the wave actually performs work on the rock. The dissipated energy is seen as irreversible heat flow out of the vapor. (In the fluid flow models, relaxation occurs during the finite time which it takes for fluid to flow.) Since the thermoelastic mechanism responds to compression of thin cracks in the same way as the Mavko-Nur flow model, it too predicts that bulk compressional attenuation will be about twice as large as shear wave attenuation. In this respect it agrees with our observations. Once again, poorly known model parameters prevent us from using the theory to make reliable quantitative predictions. However, Kjartansson and Denlinger (1977) have estimated that significant attenuation may result from this mechanism, perhaps enough to explain our observations.

Therefore, we have two theoretical models that may explain our observations in partially saturated rock, Mavko and Nur's flow mechanism and Kjartansson and Denlinger's thermoelastic mechanism. Both models predict that bulk compressional attenuation should be about twice as large as shear wave attenuation, in agreement with our observations. Both models also predict that attenuation should increase with degree of fluid saturation to some maximum, and then decrease as total saturation is approached. Once again, these predictions agree with our observations. In the flow model this behavior is caused by a balance between the amount of fluid flowing and the distance over which flow occurs. In the thermal mechanism there is a balance between the amount of compression which the vapor must accomodate and the amount of vapor present. Neither theory can yet be used to make quantitative predictions that are reliable enough to let us judge the relative contributions of each mechanism. It is important to note that these mechanisms are not mutually exclusive. They probably both contribute something to the overall attenuation that we observe in partially saturated rock.

We can use Figure (5-22) to gain a more intuitive understanding of our observations. Here we have chosen ideal crack shapes and orientations to illustrate certain effects, but generalization to more random

Figure (5-22). Conceptual model of pore fluid attenuation mechanisms in rock. Inter-crack flow occurs in fully saturated rock. Intra-crack flow and/or thermal relaxation occurs in partially saturated rock.

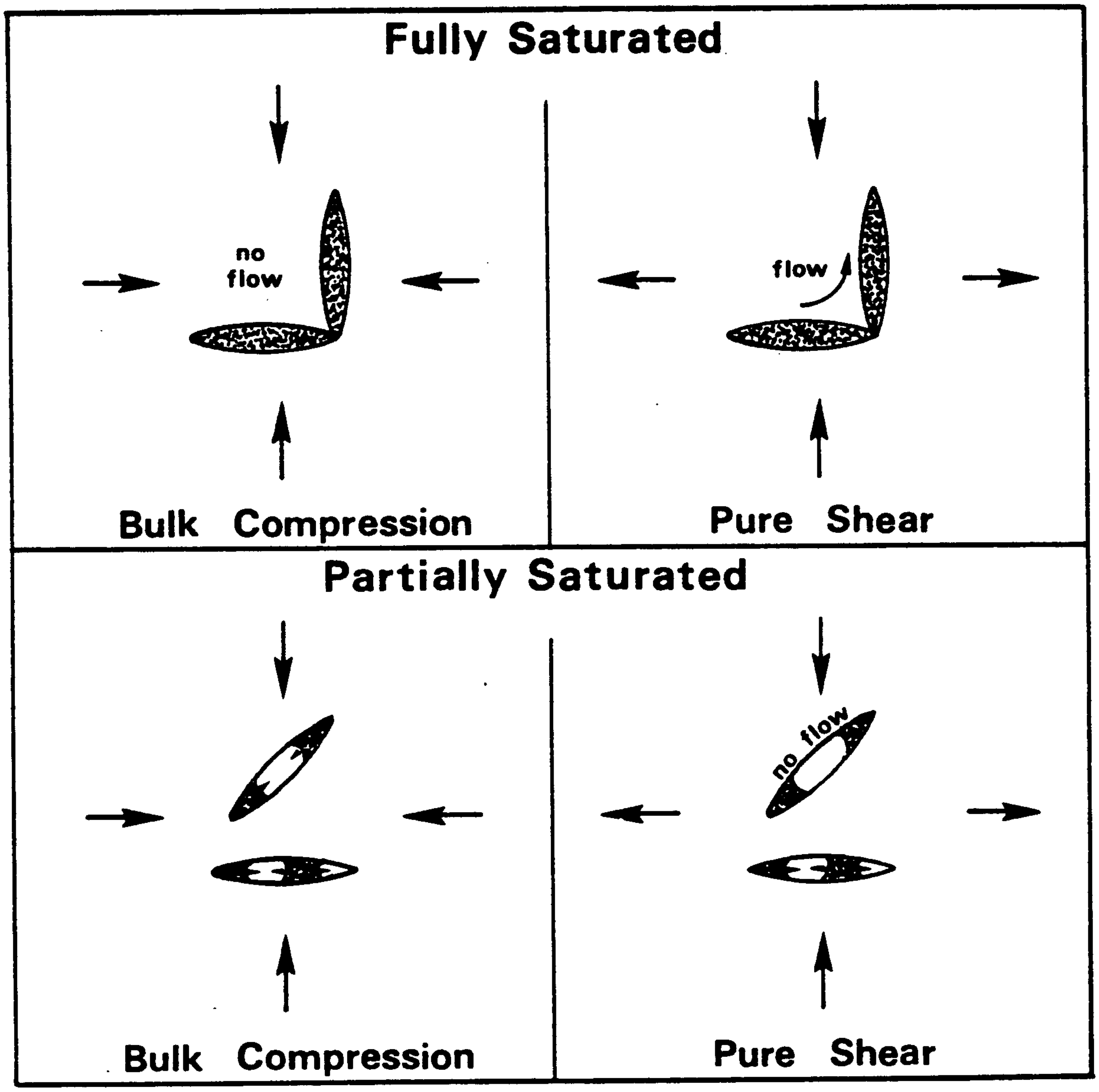

distributions wil not affect our conclusions. In the upper half of Figure (5-22) we show connected cracks which are fully saturated. As bulk compression is applied to the rock, each crack is compressed by the same amount and so there is no fluid flow between cracks. However, when pure shear is applied, one crack is compressed while the other is dilated. Fluid flows from one crack to the other. On the next half of the stress cycle, the flow direction reverses. Thus, in fully saturated rock we expect significant shear wave attenuation and much less bulk compressional attenuation. (Whenever cracks of different shapes are connected, bulk compression will cause some fluid flow.)

Now consider partially saturated cracks, shown in the lower half of Figure (5-22). The cracks here are not connected because it is not required for the mechanisms we are considering. Connecting them would not affect our discussion. Each crack is partially saturated with several isolated fluid droplets. Under bulk compression, each crack is compressed regardless of its orientation and both the flow mechanism and the thermoelastic mechanism are operative within each crack. However, under pure shear the crack oriented at 45° to the stress axes has no normal stress perpendicular to the crack faces. Therefore it is not compressed and does not contribute to the energy loss. Averaged over all crack orientations, we expect about half as much attenuation for shear waves as for bulk compression.

Another way to use Figure (5-22) is to consider only the left side showing bulk compression. As we add water to the rock the partial saturation mechanisms become operative, causing increasing attenuation as saturation increases. Although our own observations were only taken at one degree of partial saturation, we can incorporate data from Wyllie _et al_. (1962) and Gardner _et al_. (1964) to show that attenuation does increase with degree of saturation as theory predicts. Continuing on to total saturation eliminates the partial saturation mechanisms, and there is nothing to replace them. Thus total saturation causes a reduction in bulk compressional attenuation, as we have observed.

Now consider the right side of Figure (5-22) showing pure shear deformation. As we add water to the rock the partial saturation mechanisms become operative. Attenuation increases with degree of saturation, which again is verified by Wyllie _et al_. (1962) and Gardner _et al_. (1964). This continues all the way to total saturation where we have a maximum amount of fluid flow and maximum attenuation.

Since we have mentioned the work of Wyllie _et al_. (1962) and Gardner _et al_. (1964), we might also note that both studies found extensional attenuation to be greater than shear attenuation in partially saturated materials. This agrees with our own observations. Also, Toksoz _et al_. (1979) have recently shown that at ultrasonic frequencies in fully saturated rock, P-wave attenuation is less than shear wave attenuation. Although it is not clear that these results can be extrapolated to the low frequencies at which we are working, they do agree with our own observations.

Now that we have this conceptual framework in which to discuss attenuation, we can try applying it to the data on Vycor porous glass. The key here is that the microstructure of Vycor has predominantly equidimensional pores which are extremely small. Although sandstone also has many equidimensional pores, attenuation is dominated by thin flat cracks which apparently are absent in Vycor. As discussed previously, strong capillary forces probably inhibit fluid flow mechanisms in Vycor, so we will have to explain the observations with only Kjartansson and Denlinger's thermoelastic mechanism. Figure (5-23) is an analogue to Figure (5-22) in which we approximate equidimensional pores with spheres. (Note that this approximation might not be suitable for modelling flow mechanisms, where shapes similar to concave tetrahedra would have to be used.) In fully saturated pores, the thermal mechanism is not operating because there is no vapor phase. We would expect attenuation to be comparable to that in dry Vycor, which it is. When the pores become partially saturated, the thermoelastic mechanism begins operating in bulk compression. However, in pure shear the pores simply undergo a change in shape. The pores are not compressed and no attenuation occurs. Therefore, the model predicts attenuation only in bulk compression in partially saturated samples, which is what we observe in Vycor.

Figure (5-23). Conceptual model of the thermoelastic attenuation mechanism in Vycor. Roughly equidimensional pores have been grossly approximated as spheres for illustration purposes.

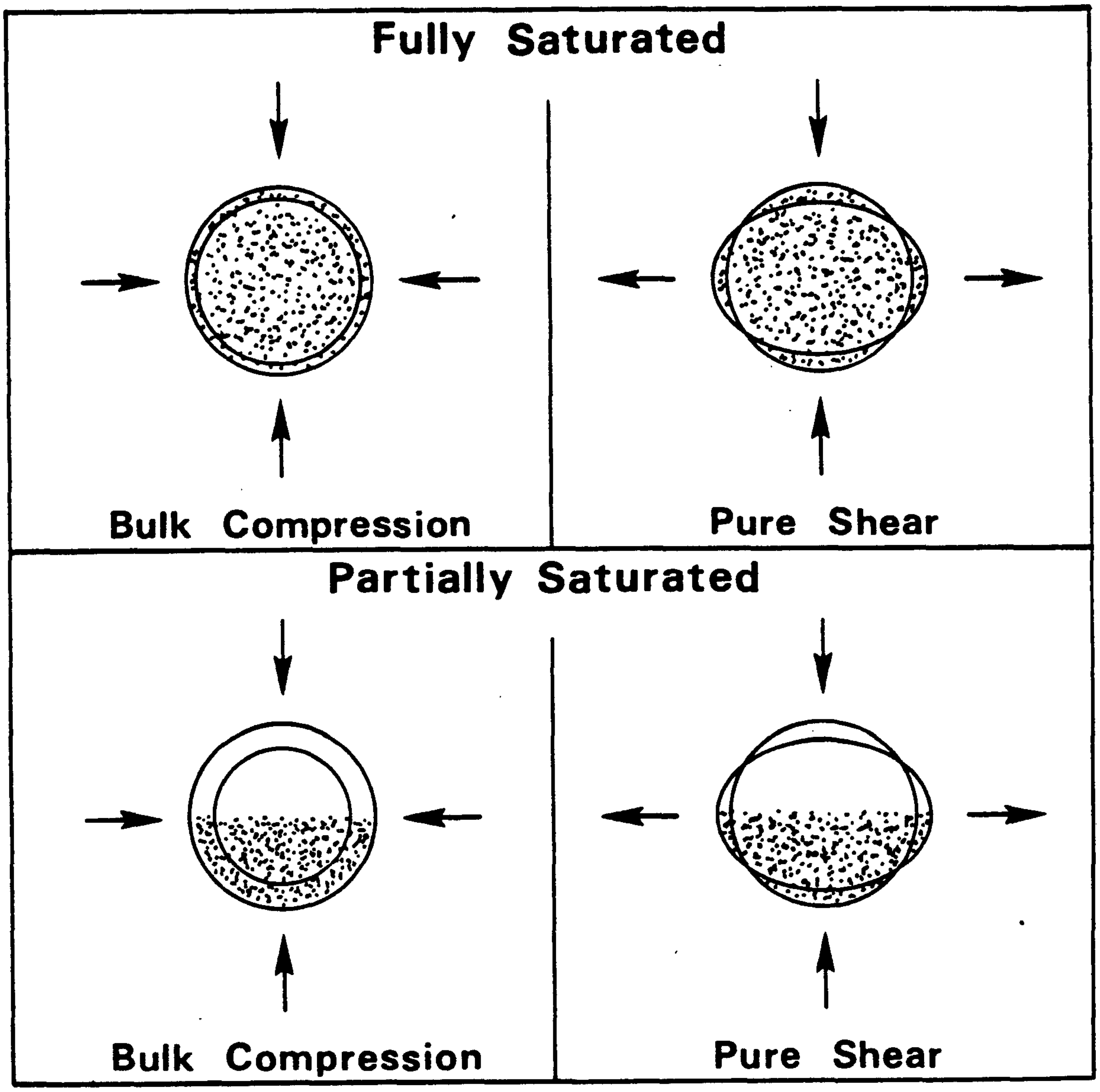

We can thus explain our observations in both Massilon sandstone and in Vycor with a few simple mechanisms applied to different microstructures. We don't claim to have proven that our interpretations are unique, but they do provide a conceptual framework with which we can understand existing observations of attenuation and plan future experimental programs.

(At first glance it might appear that White's (1975) partial saturation mechanism would explain our results for Vycor. However, we don't believe that the macroscopic pore fluid distribution required by the theory existed in the sample while it was drying. In any event, the permeability of Vycor is expected to be extremely low, which, together with the strong capillary forces, will probably inhibit fluid flow.)

Before concluding this chapter, we will take one more look at the data we have presented. Figure (5-24) shows the velocity data for Massilon sandstone (from Figure (5-2)) re-plotted as V_p vs. V_p/V_s. We see here that V_p/V_s separates the velocities in fully saturated rock from those in less than fully saturated rock. This is the basis upon which V_p/V_s is currently being used to detect partially saturated zones in the earth. Notice that V_p/V_s varies by only about 25% between the two fields and it does not significantly separate the data for dry rock from that for ~95% saturated rock. Also, the two fields can be expected to vary somewhat in V_p/V_s for various rock types, so a single determination of V_p/V_s in the earth will not always be sufficient to determine whether or not a zone is partially saturated. Figure (5-24) also shows three data points for a sample of Sierra White granite. The X with lower V_p/V_s is lightly saturated and the one with larger V_p/V_s is highly (but not fully) saturated. The V_p/V_s ratios for the granite compare well with those for under-saturated Massilon sandstone, but this is probably a coincidence and does not imply lithology independence of V_p/V_s. This data is included because it will be of interest in the following figure.

Figure (5-25) combines the data in Figures (5-2, 5-3, 5-5) to plot Q_p^{-1}/Q_s^{-1} vs. V_p/V_s. It therefore includes all the attenuation and velocity data we have for Massilon sandstone. The data is now separated into three distinct fields, one for dry rock, one for partially saturated rock, and one for fully saturated rock. Once again, V_p/V_s separates out the data for fully saturated rock. Q_p^{-1}/Q_s^{-1} now also separates out the data for partially saturated rock from the rest of the data. If we assume that dry rocks do not occur in the earth, then either V_p/V_s or Q_p^{-1}/Q_s^{-1} may be used to detect partial saturation. Partial saturation is indicated by low V_p/V_s or high Q_p^{-1}/Q_s^{-1}. There are important differences in these two methods, however. While V_p/V_s varies by only about 25% between the two fields, with the division between them probably being somewhat lithology dependent, Q_p^{-1}/Q_s^{-1} varies by about 400% with the division between the fields probably being lithology independent. This is because physical significance can be attached to a Q_p^{-1}/Q_s^{-1} ratio of one. Above this line P-waves are attenuated more strongly than shear waves, while the reverse occurs below this line. Thus, we do not necessarily have to measure attenuation absolutely in the earth to detect partial saturation, but need only determine which type of wave is attenuated more strongly. This may help offset the greater difficulty of measuring attenuation in the earth.

Figure (5-25) also contains data for Sierra White granite. The interesting thing to note here is that the data falls into the expected fields. Dry granite has $Q_p^{-1}/Q_s^{-1} < 1$ and partially saturated rock has $Q_p^{-1}/Q_s^{-1} > 1$. All the granite data was taken with no confining or pore pressure.

Also included in Figure (5-25) is the only field data we have been able to find in the literature in which both P and S velocity and attenuation were measured. This is from the study by McDonal _et al_. (1958) conducted in the Pierre shale of Colorado. This experiment was done below the water table at a depth of 150 meters. Therefore the rock was fully saturated and at fairly low pressure. Data taken at a frequency of about 100 hz is indicated by the star in Figure (5-25) ($Q_p = 32$, $Q_s = 10$, $V_p = 2164$ m/s, $V_s = 817$ m/s). This point falls just where we would expect from our own observations (in fact, the agreement is so good there must be some coincidence involved). This data would seem to extend our results to another rock type (shale) under field conditions and to lower frequencies (100 hertz is at the high end of the range used in seismic exploration).

Finally, we show in Figure (5-26) a plot of Q_p^{-1}/Q_s^{-1} vs. V_p/V_s for Vycor. As the sample dries, we move along the curve from right to left. Although the scales are quite different from Figure (5-26), we find basically the same sort of behavior that we found for Massilon sandstone. The main difference is a much larger variation in Q_p^{-1}/Q_s^{-1} and a much smaller variation in V_p/V_s.

Figure (5-24). V_p vs. V_p/V_s data for Massilon sandstone and Sierra White granite. Arrows indicate increasing effective stress. Granite data taken at atmospheric pressure.

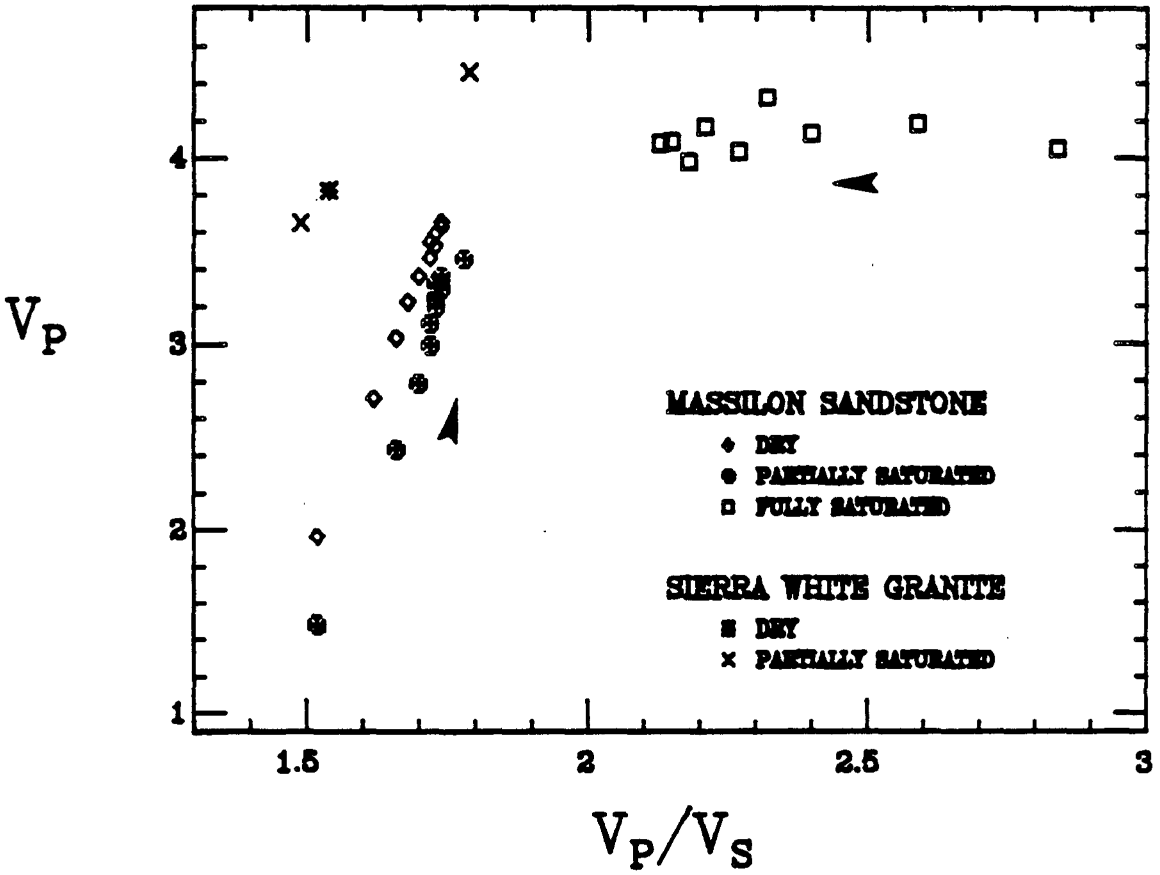

Figure (5-25). Q_P^{-1}/Q_S^{-1} vs. V_P/V_S data for Massilon sandstone, Sierra White granite, and the field data (*) from McDonal *et al*. (1958). Arrows indicate increasing effective stress. Granite data taken at atmospheric pressure.

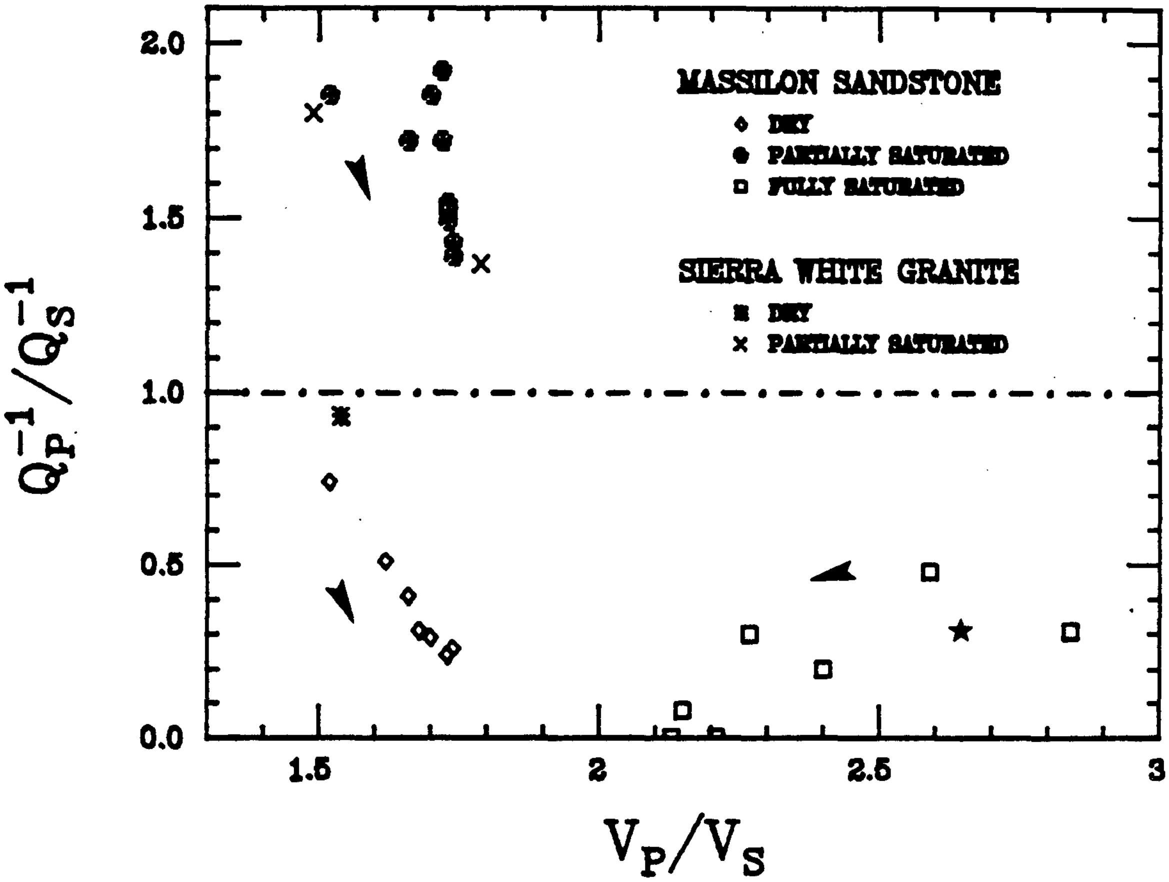

Figure (5-26). Q_P^{-1}/Q_S^{-1} vs. V_P/V_S data for Vycor. Sample is fully saturated at maximum V_P/V_S.

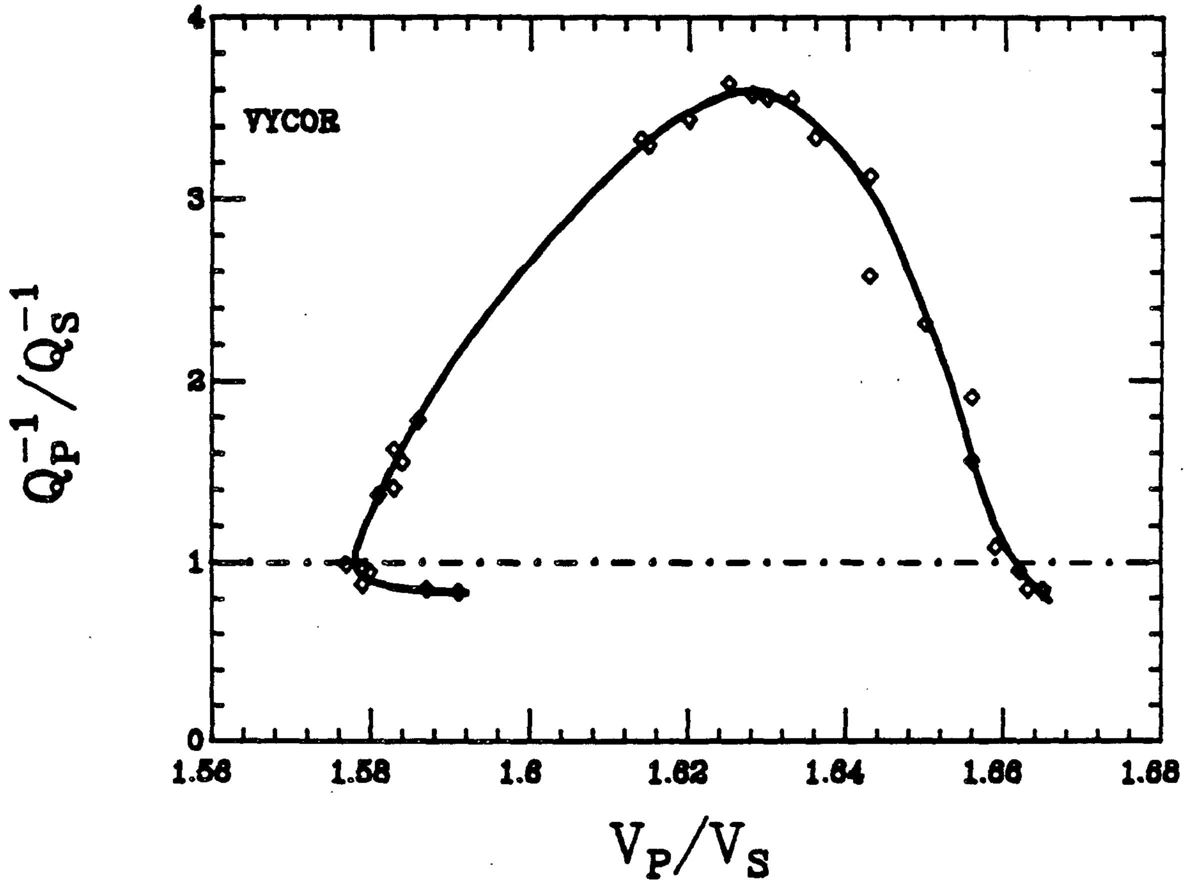

CHAPTER VI

ATTENUATION IN "DRY" ROCK

In the course of this study we have accumulated quite a bit of data on attenuation and velocity in dry rock as functions of confining pressure and pore pressure. Unfortunately, we do not have as much corresponding data for water saturated rocks. Although the data for dry rock is interesting, it is not extensive enough to let us reach any conclusions. In the title of this chapter we have put the word "dry" in quotes because it is not a well-defined term when applied to rocks and attenuation. Tittmann et al. (1972 and others) have shown that attenuation is very sensitive to trace amounts of water in rock. We have attempted, using mild heat and mild vacuum, to achieve a reproducible dry state which is probably slightly more dry than at ambient room conditions.

In Figure (6-1) we show attenuation in dry Massilon sandstone as a function of confining pressure. The pore space was open to the atmosphere. As usual, attenuation decreases with increasing pressure, and both shear and extension show similar behavior. The interesting feature is that shear attenuation is greater than extensional attenuation. This implies that shear attenuation is greater than P-wave or bulk compres-

Figure (6-1). Shear and extensional attenuation in dry Massilon sandstone.

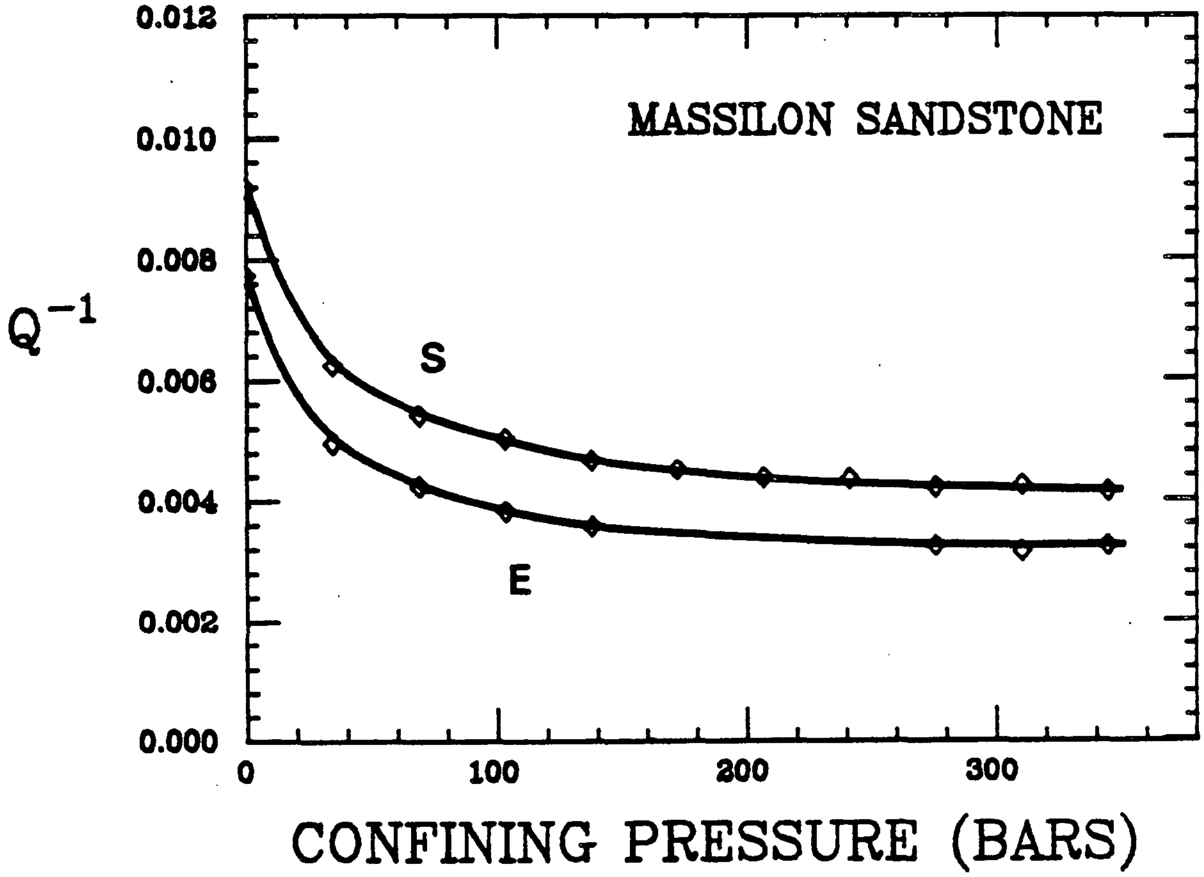

Figure (6-2). Shear and extensional velocities in dry Massilon sandstone.

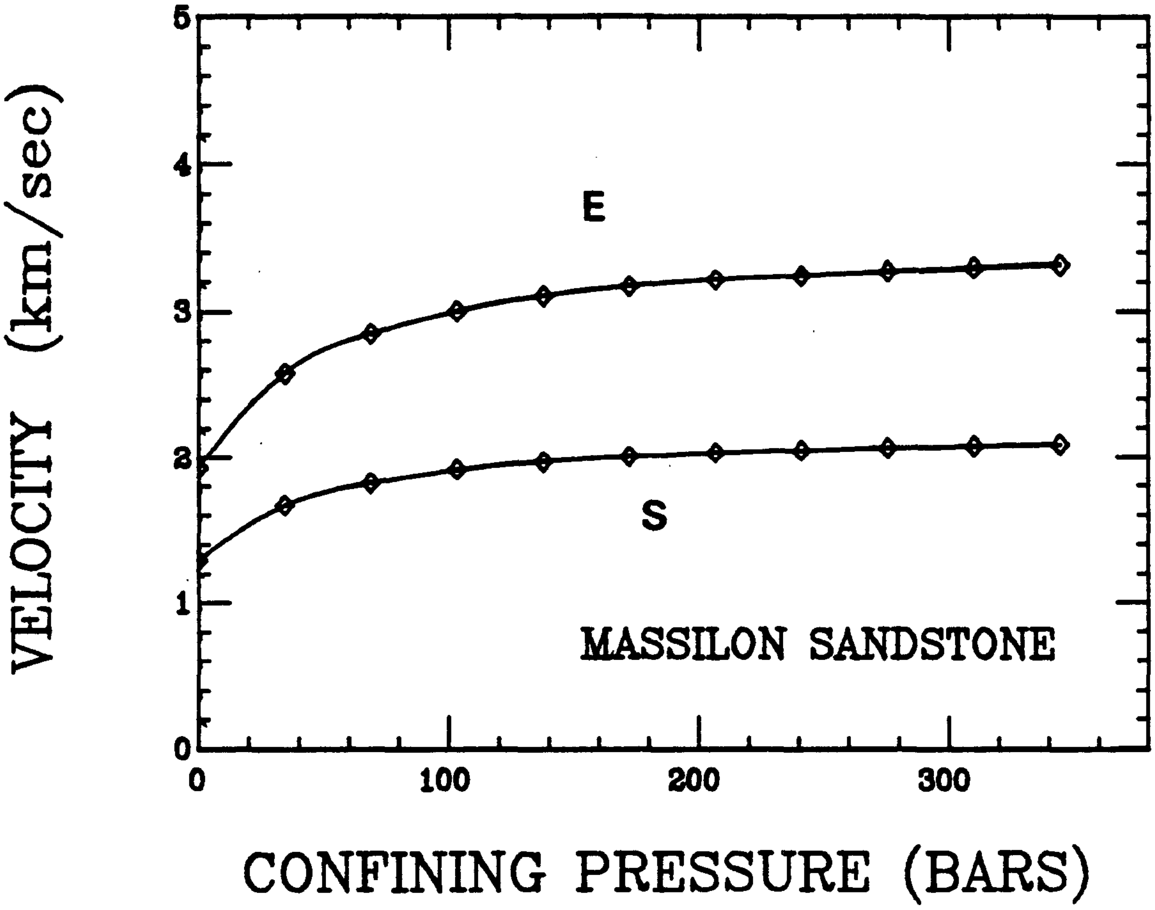

sional attenuation (see Appendix B). This feature is interesting because it is generally observed that $Q_s^{-1} \approx Q_e^{-1}$ in dry rock. We have found that in every sample we have worked with, with heat-shrink jacket, copper jacket or no jacket, we always find $Q_s^{-1} > Q_e^{-1}$ when we get the sample dry enough. As will be seen shortly, the difference between Q_s^{-1} and Q_e^{-1} is sometimes very small and we would be stretching the accuracy of our system to its limit to say that Q_s^{-1} is always greater than Q_e^{-1} in dry rock. We simply report this observation as a consistent one that is on the border of resolution. Figure (6-2) shows the velocity data that corresponds to Figure (6-1).

Figures (6-3 and 6-5) show similar attenuation data for two different Berea sandstones. The similarity between these two sets of data is rather striking. Again, $Q_s^{-1} > Q_e^{-1}$, though the difference is less than in Massilon sandstone. Overall attenuation in Massilon is somewhat greater than in Berea, with the difference being greater for shear than for extension. Figures (6-4 and 6-6) show the corresponding velocity data for the Berea sandstones. The velocities are slightly greater in Berea (600), and both Bereas have slightly higher velocities than does Massilon. These differences are almost certainly real, but probably not of great significance unless they can eventually be related to details of the microstructure.

Figure (6-3). Shear and extensional attenuation in dry Berea (350) sandstone.

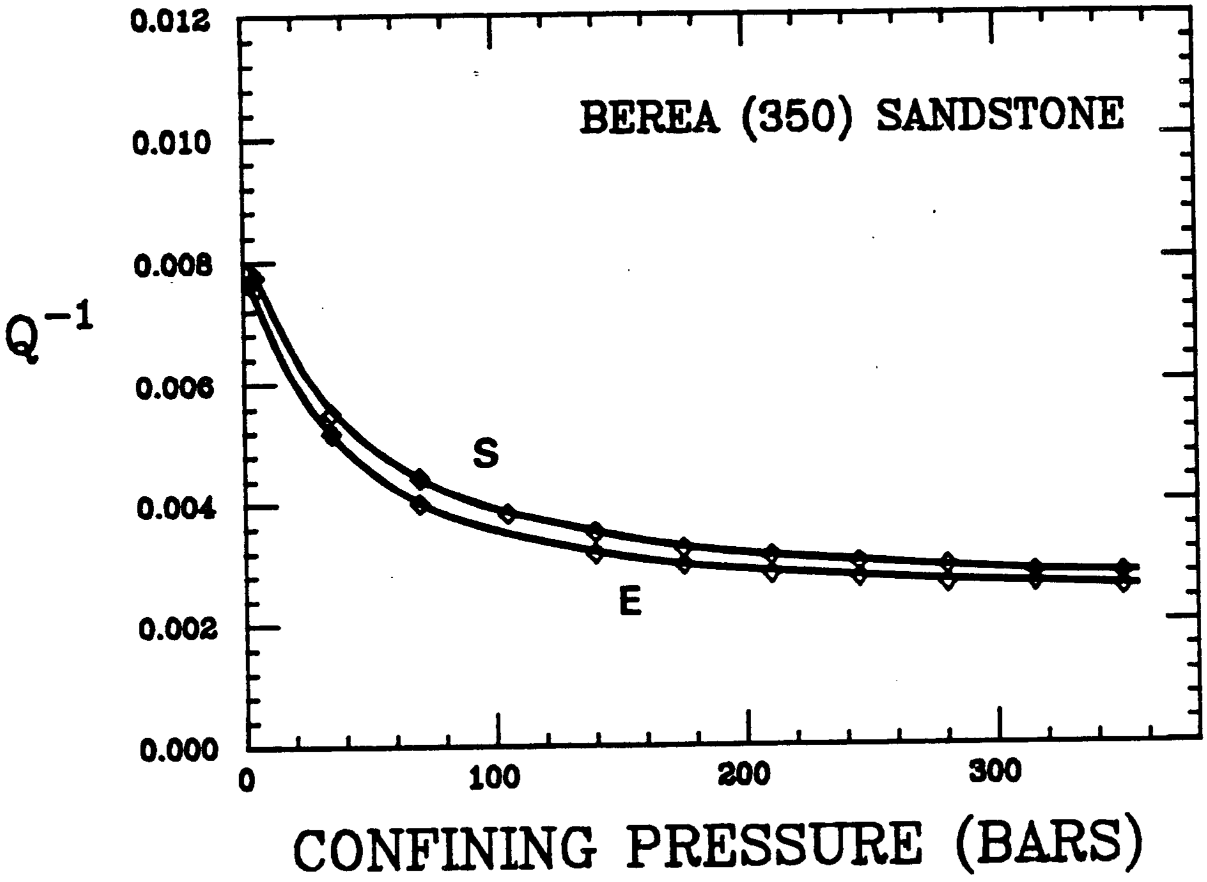

Figure (6-4). Shear and extensional velocities in dry Berea (350) sandstone.

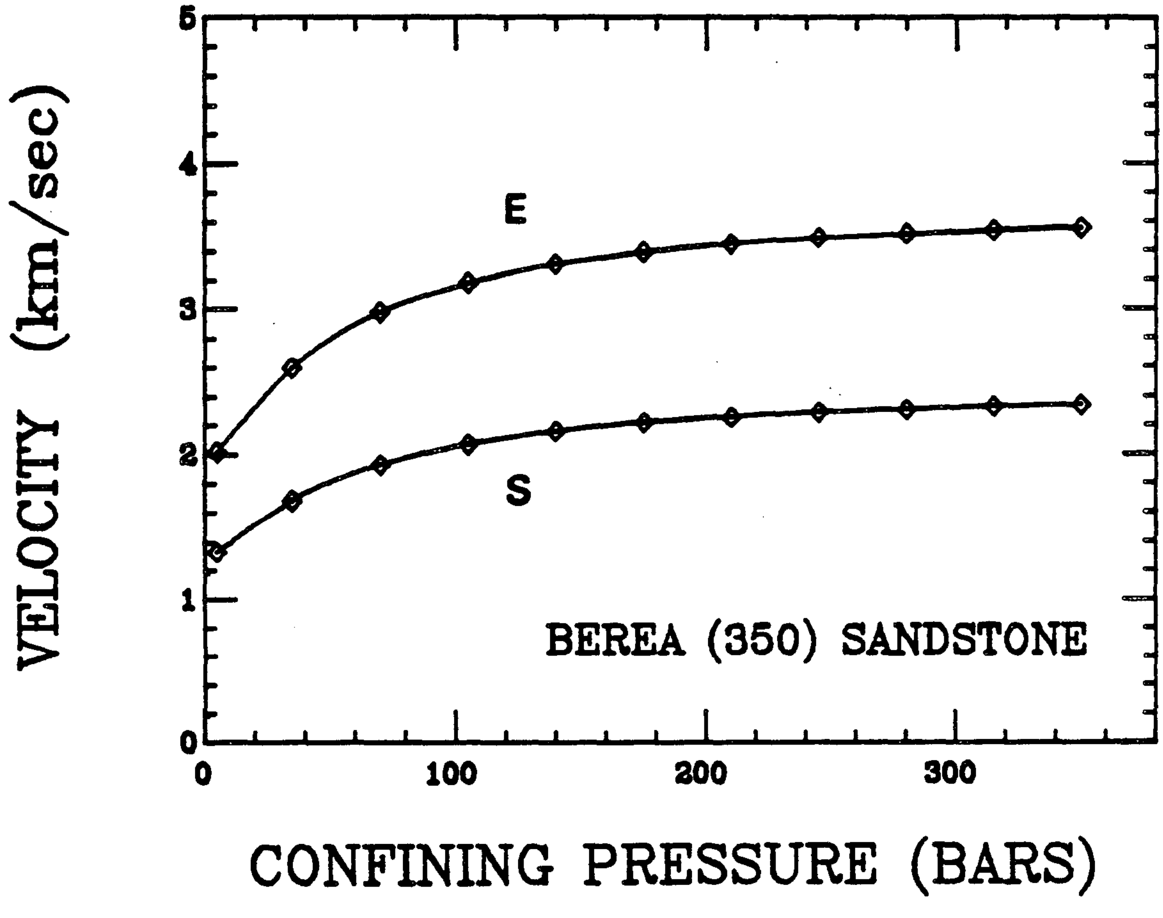

Figure (6-5). Shear and extensional attenuation in dry Berea (600) sandstone.

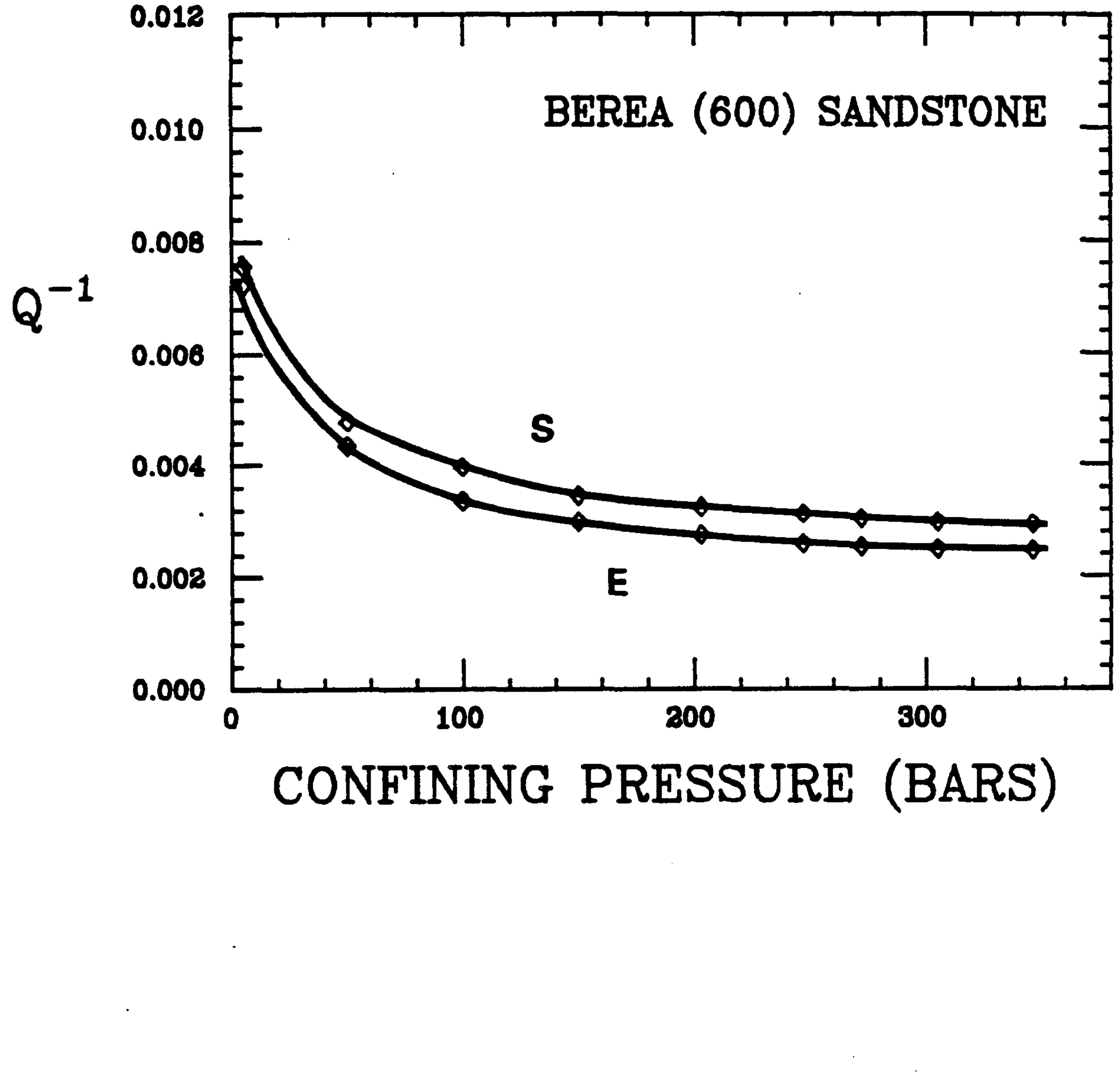

Figure (6-6). Shear and extensional velocities in dry Berea (600) sandstone.

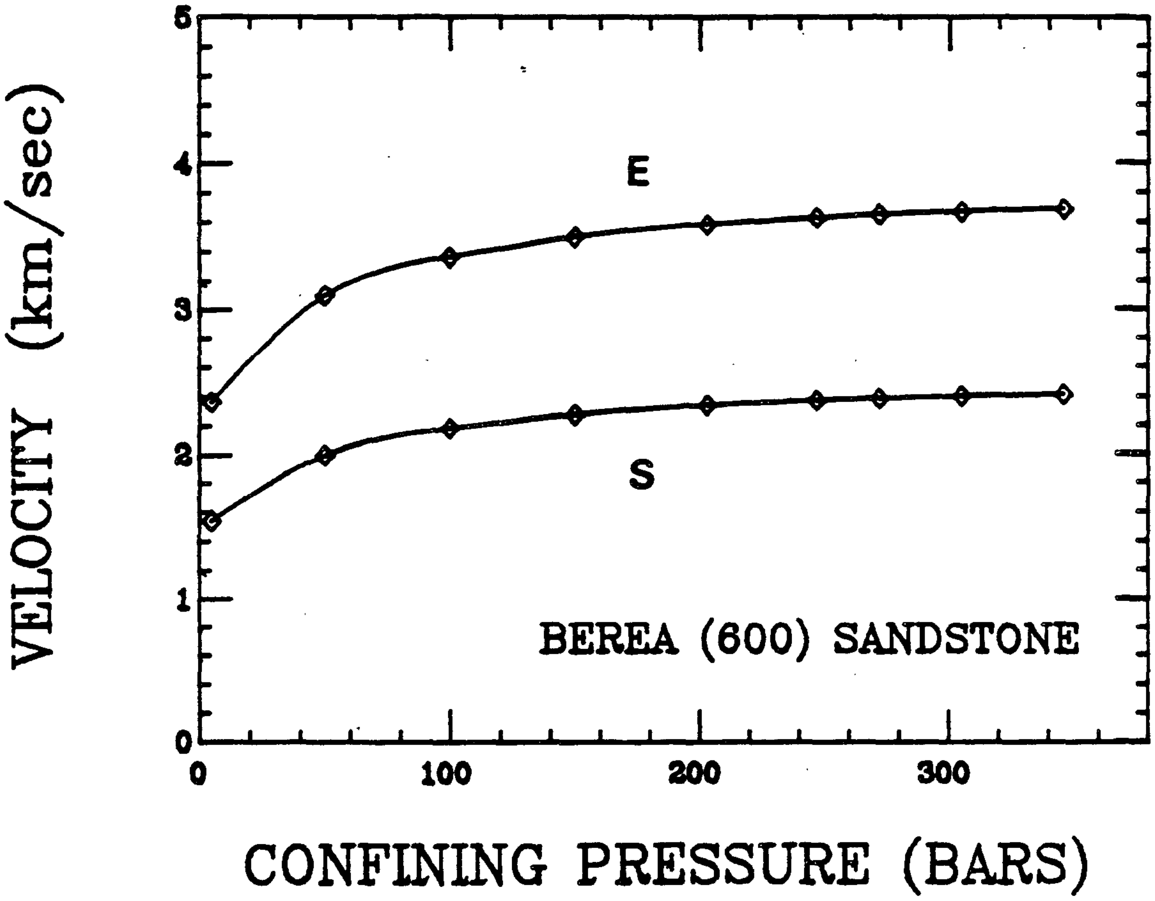

An unexpected, and as yet unexplained, observation is shown in Figures (6-7 to 6-14). We found that attenuation does not obey a simple effective stress law in dry rock, but varies with the type of gas used as the pore fluid. Figure (6-7) shows shear attenuation in Massilon sandstone. The lower curve is with zero pore pressure and the upper curve is with variable pore pressure and fixed confining pressure. The pore fluid is nitrogen gas, as is the confining pressure medium. Since the two curves are not identical, attenuation is not a unique function of effective stress (confining pressure minus pore pressure). This is not a simple hysteresis effect, because the data can be taken in any order. Several possible explanations for this effect will be discussed below. Figure (6-8) shows the shear velocities that correspond to the data in Figure (6-7). We see here that shear velocity is, to within the resolution of the data, a unique function of effective stress. This is what we expected to find. Figure (6-9) shows extensional attenuation corresponding to the data in Figure (6-7). Here again we find that attenuation is not a unique function of effective stress, and the difference between the two curves is about twice as large as for the shear data in Figure (6-7). Figure (6-10) shows that extensional velocity is probably a unique function of effective stress, just as we saw for shear velocity.

On the suspicion that the gas in the sample was somehow responsible for the increased attenuation at high pore pressures, we next repeated these experiments using different gases as pore fluids. Figure (6-11) shows shear attenuation in a Berea sandstone with helium as the confining pressure medium. Here again, attenuation is largest when the pore fluid is nitrogen under pressure. However, when the pore fluid is pressurized helium, the attenuation is virtually identical to that in rock with zero pore pressure and the same effective stress. Therefore the effect we are observing is somehow controlled by the gas used as the pore fluid. Once again, this data is independent of the order in which it is taken. Figure (6-12) shows that shear velocity is again insensitive to the pore gas and is only a function of effective stress. Figure (6-13) shows that extensional attenuation is affected in the same way as shear attenuation, though by a slightly larger amount. Figure (6-14) shows that extensional velocity is insensitive to the pore gas, as was shear velocity.

To summarize, if effective stress is maintained at a fixed level by increasing both confining pressure and pore pressure equally, attenuation will increase if the pore gas is nitrogen but will be unaffected if the pore gas is helium. The effect on extensional attenuation is slightly larger than on shear attenuation. Velocities are not affected by either pore gas.

There are several possible explanations for these effects. One is that as we increase pore pressure and confining pressure equally, attenuation increases because of greater interaction of the sample with the confining gas. However, it was shown in Chapter III that losses to the confining gas are too small by a factor of 2-3 to account for the effect seen here. More importantly, if we are simply observing losses to the confining gas, it should not be sensitive to the type of pore gas used.

Another possible explanation is that the nitrogen used as pore gas is contaminated by water vapor (or some other gas) and it is the water vapor that is affecting attenuation. This cannot be ruled out. According to the supplier's specifications, the nitrogen we used has a purity of 99.99% with traces of hydrogen and oxygen and a dew point of <-60°C. The helium has a purity of 99.995% with traces of carbon dioxide, argon, hydrogen, nitrogen and methane. It also has a dew point of <-60°C. If water vapor is causing the observed effect, it should be possible to determine this experimentally.

A final possible explanation is that the pore gas is involved in some sort of attenuation mechanism that increases with pore pressure. The low viscosity of nitrogen and helium make a flow mechanism unlikely, but some sort of thermal mechanism is a possibility. The different thermal properties of helium and nitrogen might explain why they have different effects on attenuation.

This is, however, pure speculation. A few simple, well-planned experiments will probably resolve the issue. We have not yet done this only because we preferred to concentrate on attenuation in partially and fully saturated rock.

Figure (6-7). Shear attenuation in dry Massilon sandstone as a function of effective stress. Lower curve - $P_p = 0$, variable confining pressure. Upper curve - $P_c = 345$ bars, variable pore pressure. Pore gas is nitrogen.

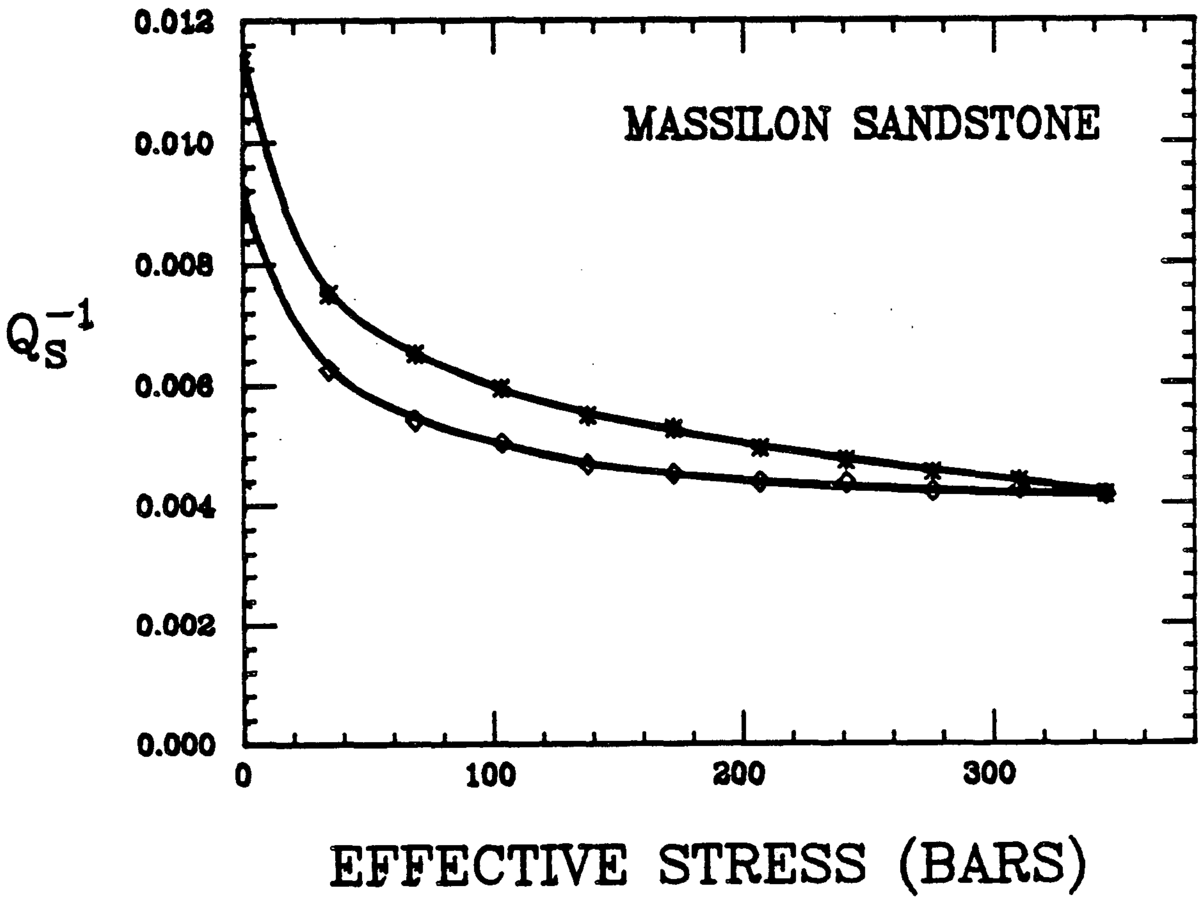

Figure (6-8). Shear velocities corresponding to Figure (6-7).

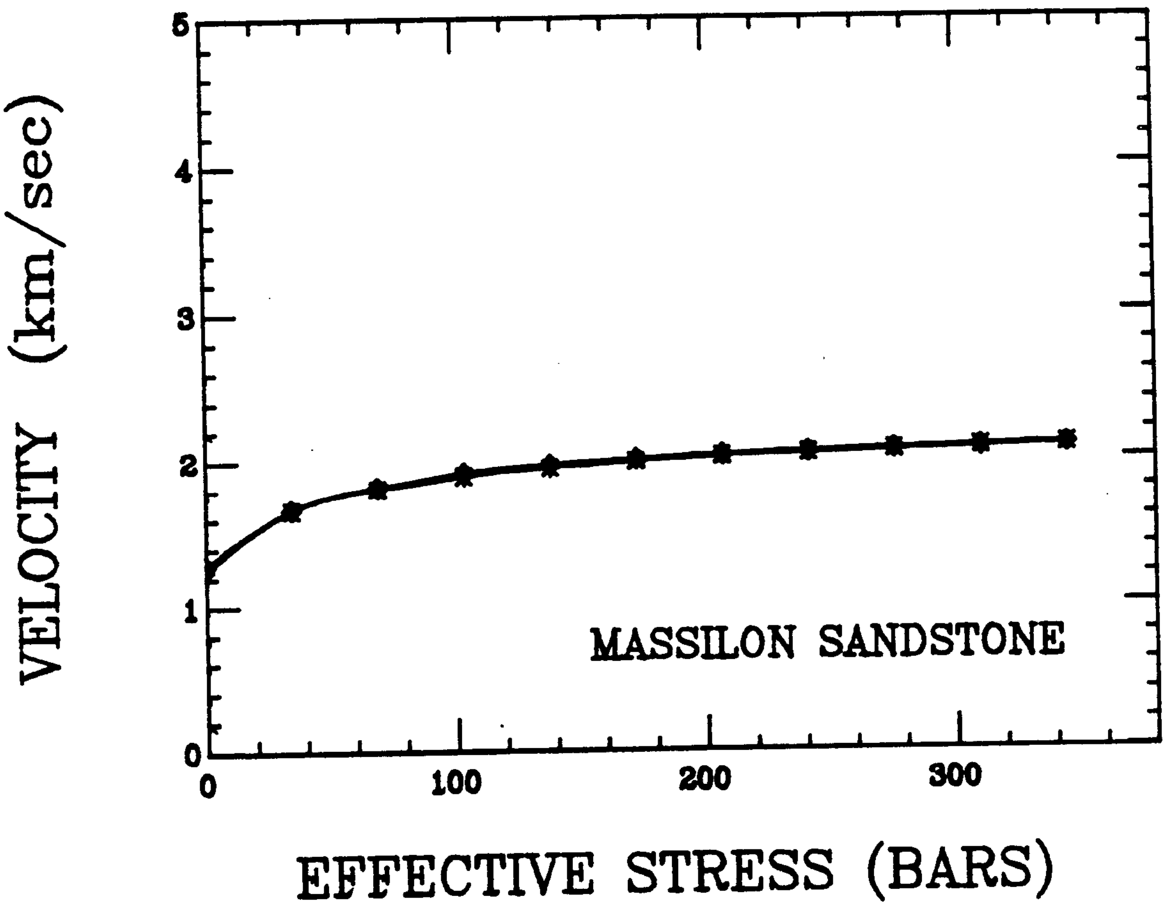

Figure (6-9). Extensional attenuation corresponding to Figure (6-7).

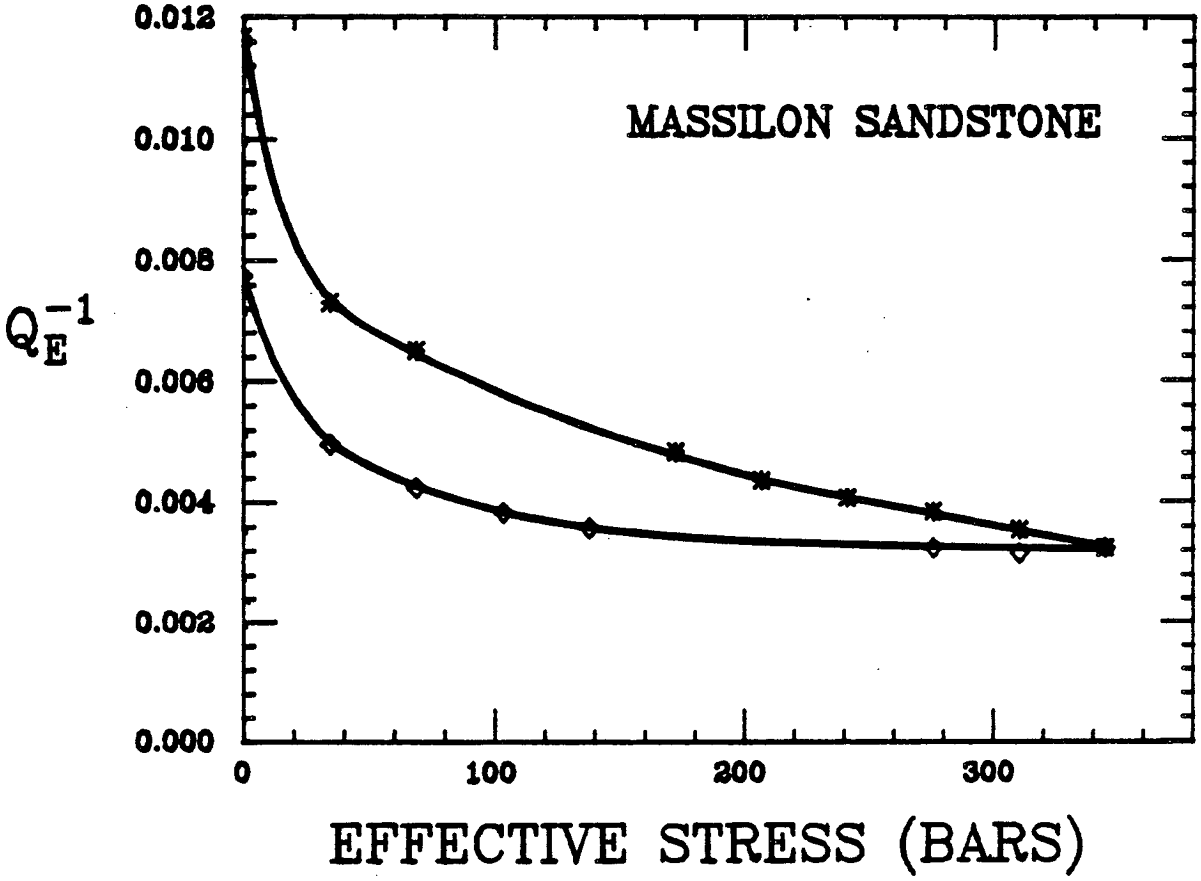

Figure (6-10). Extensional velocities corresponding to Figure (6-9).

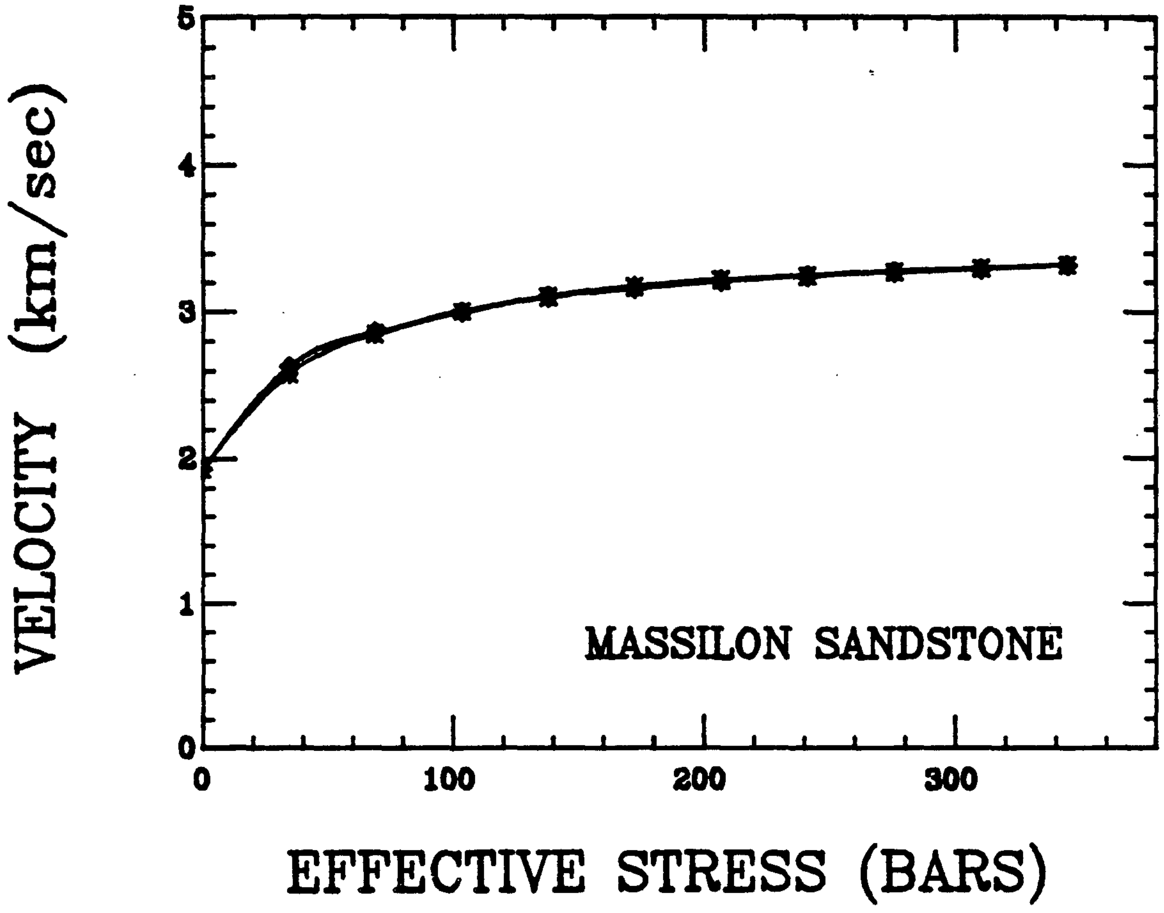

Figure (6-11). Shear attenuation in dry Berea (350) sandstone. Diamonds - $P_p = 0$, variable confining pressure; squares - P_c = 350 bars, variable pore pressure of helium gas; stars - P_c = 350 bars, variable pore pressure of nitrogen gas.

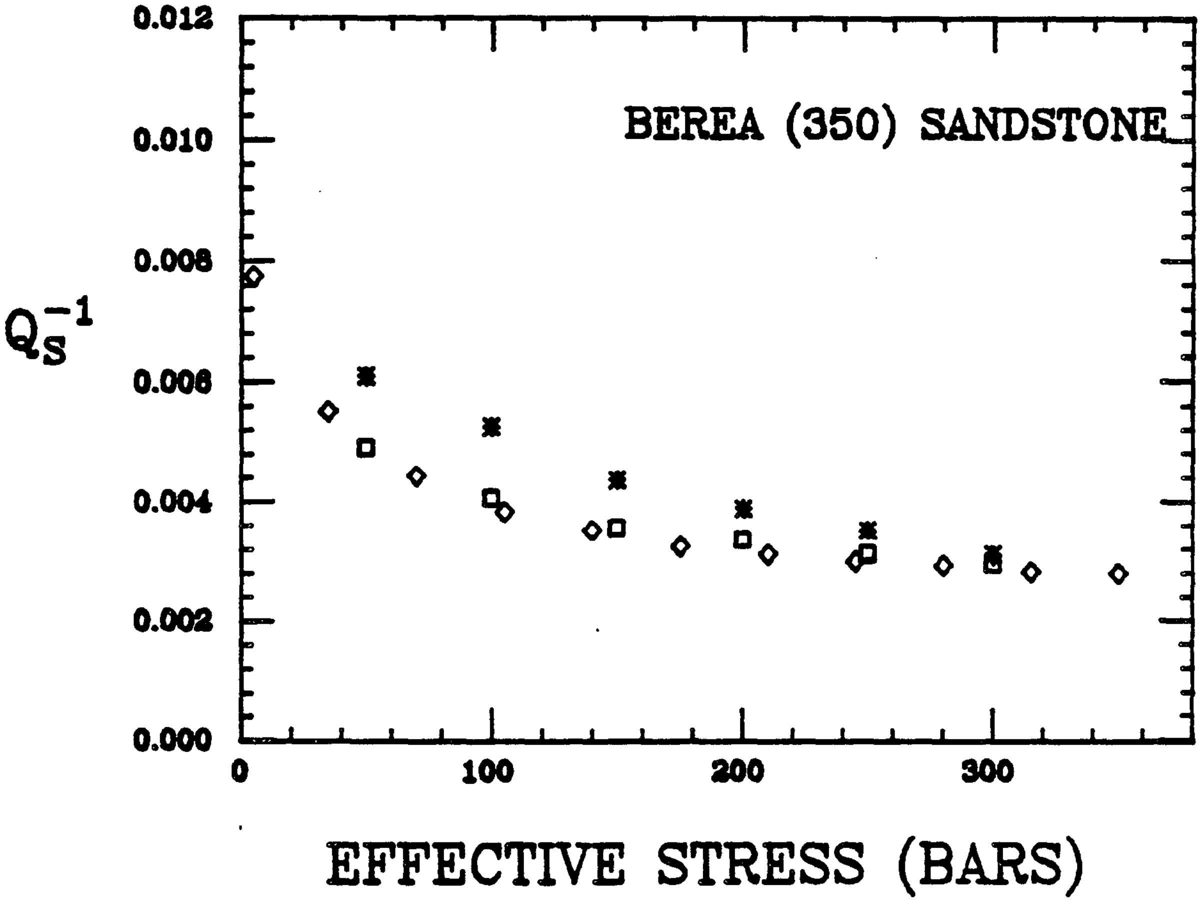

Figure (6-12). Shear velocities corresponding to Figure (6-11).

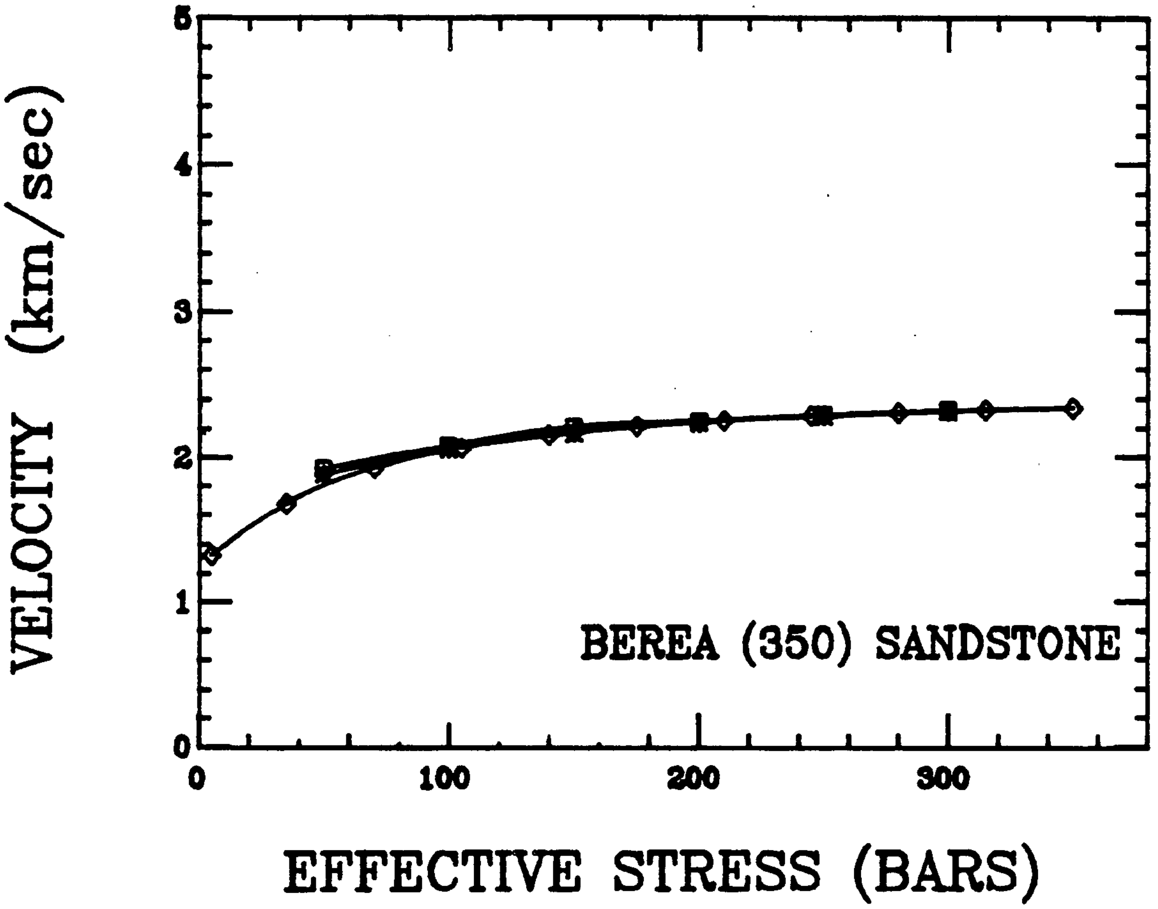

Figure (6-13). Extensional attenuation corresponding to Figure (6-11).

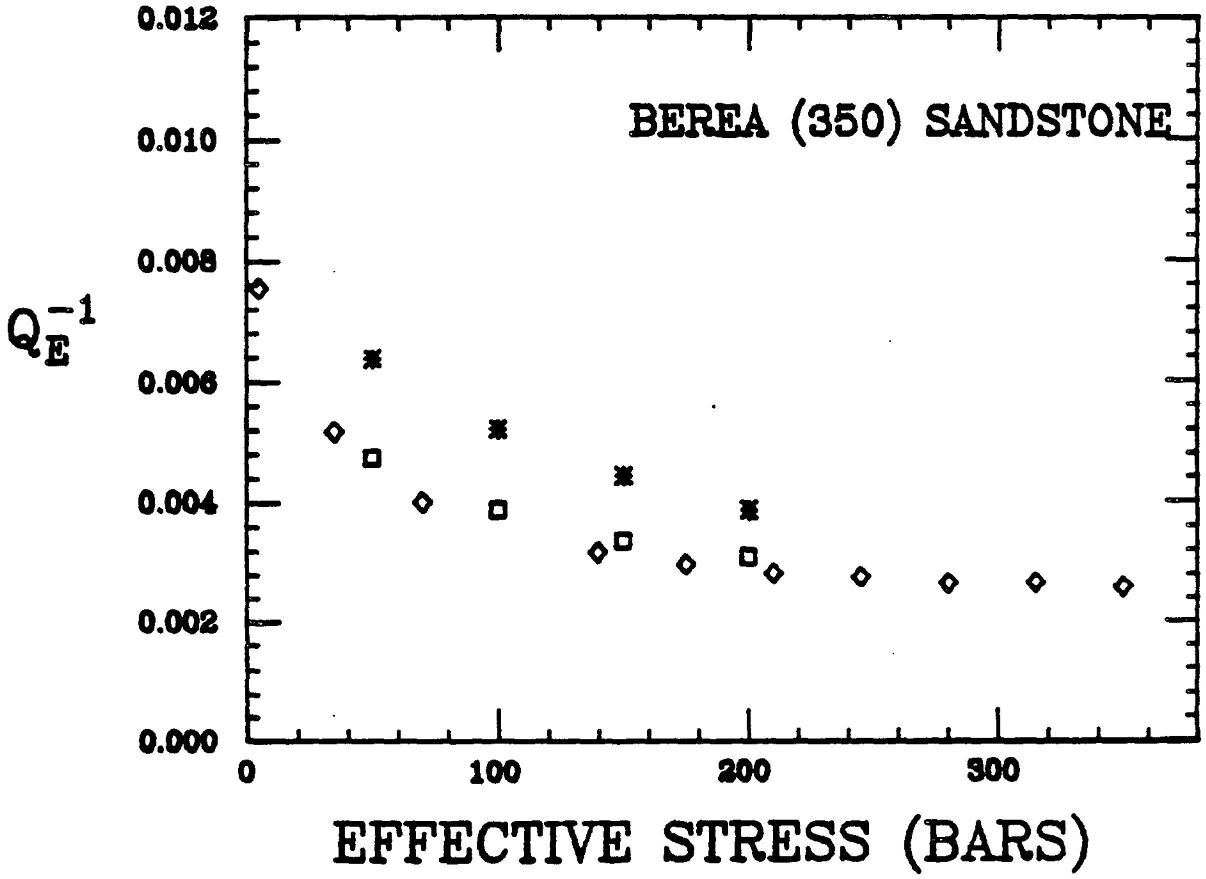

Figure (6-14). Extensional velocities corresponding to Figure (6-13).

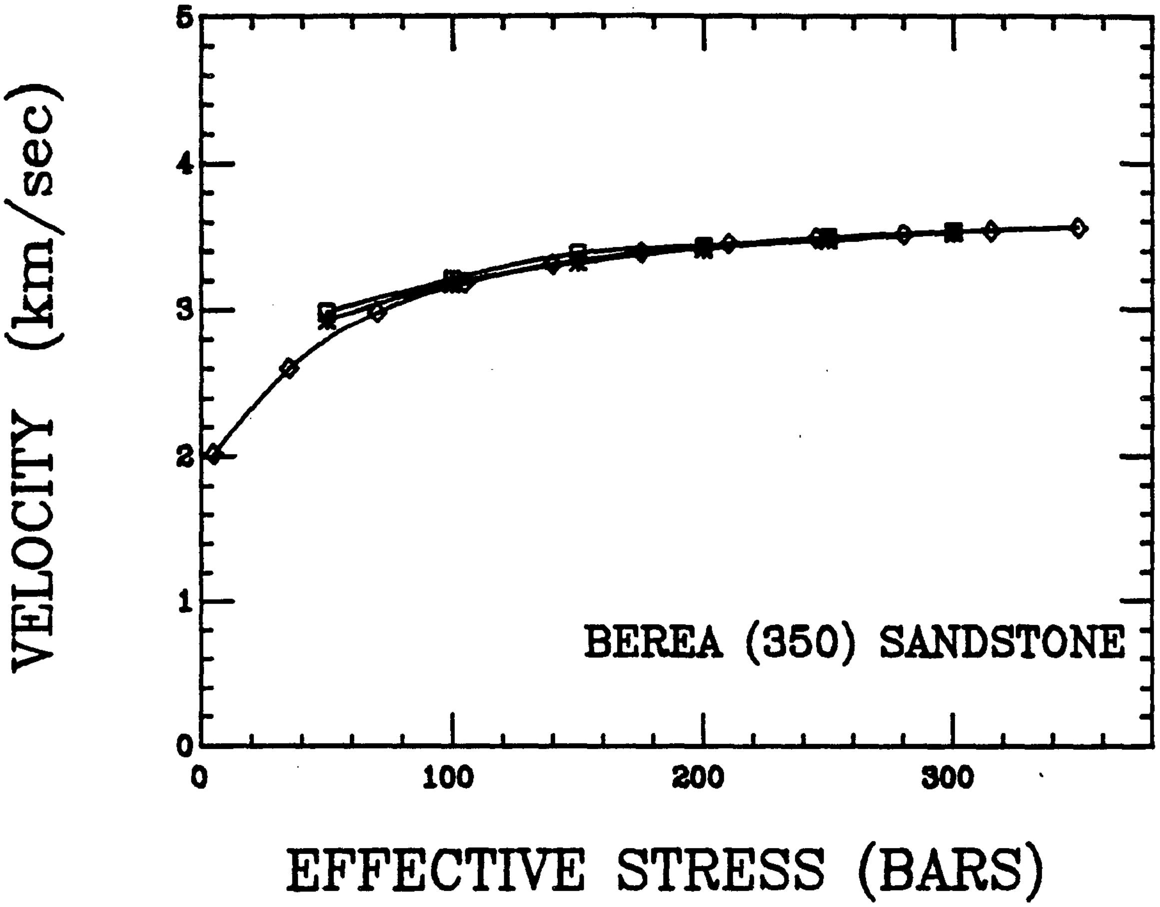

CHAPTER VII

SUMMARY AND CONCLUSIONS

During the past fifty years or so, a considerable amount of experimental work has been done to study seismic attenuation. In more recent years this work has been supplemented by various theoretical models of attenuation mechanisms in rock. In light of this effort to understand seismic attenuation, it is somewhat remarkable that no consensus of opinion has been reached on what physical mechanisms dominate seismic attenuation under laboratory conditions and in the earth's crust. In particular, observations are variously interpreted in terms of frictional sliding or fluid flow mechanisms. The objectives of the present study have been to determine which physical mechanisms are most important in seismic attenuation and to look in particular at the effects of pore fluids on the attenuation of P and S-waves. To do this we have set up a high precision bar resonance experiment. Controlled parameters include confining pressure, pore pressure, degree of saturation, and strain amplitude. This is the first study of attenuation in which dry, partially saturated, and fully saturated rocks have been studied under controlled conditions.

Our first major result was to show that frictional sliding does not contribute significantly to seismic attenuation in the earth's crust. Several theoretical models have shown that friction should cause nonlinear, amplitude dependent attenuation of seismic waves. We verified previous observations of amplitude dependent attenuation at large strains and amplitude independence at low strains. In addition, we also showed that velocity and attenuation exhibit simultaneous dependence on strain amplitude, that pore fluids affect the amplitude dependence, that moderate confining pressures eliminate the amplitude dependence, and that materials not containing flat cracks do not show any amplitude dependence at the strains used in this study. These results all agree with the predictions of frictional attenuation mechanisms and imply that at the low strain amplitudes of seismic waves and the high confining pressures found in the earth, nonlinear frictional sliding will not be an important attenuation mechanism.

Our second set of results involves the effects that pore fluids have on seismic attenuation. Adding pore water to dry rock to about 95% saturation causes attenuation of P and S-waves to increase by a factor of three to four, the effect being larger on P-waves than on shear waves. Further addition of pore water to total saturation causes shear wave attenuation to reach a maximum, but causes a significant reduction in P-wave attenuation. As a result, in partially saturated rock P-waves are attenuated more strongly than shear waves, whereas in fully saturated rock, shear waves are attenuated more strongly.

Our results are interpreted in terms of several different mechanisms involving pore fluids. In fully saturated rock fluid flow occurs between cracks at different orientations to the passing wave or between cracks having different shapes. In partially saturated rock, attenuation is caused by one or both of two possible mechanisms. Fluid droplets in partially saturated cracks will flow in response to compression of the crack, resulting in viscous dissipation of energy. Alternatively, thermal relaxation will occur as gas in partially saturated cracks is adiabatically heated, followed by irreversible flow of heat into the rock matrix.

Most previous experimental results are consistent with our own observations and can probably be explained using the same mechanisms we have used. Of course, frequency dependence of these mechanisms must be considered when extrapolating our results much beyond the frequency range of our experiments (500-1700 hz). The only complete set of field data available (McDonal *et al*., 1958), taken at ~100 hz, is also consistent with our observations.

Detailed application of our results to the field must await development of techniques to measure P and S attenuation more precisely than is now possible. However, our results indicate that simple relative measures of attenuation may be of some use. In particular, waves passing through partially saturated rock should show greater P-wave attenuation than shear wave attenuation. Anomalously high P-wave attenuation may thus be used as an indication of hydrocarbon gas or geothermal steam reservoirs.

Our results can also be used to explain several field observations. It has been suspected, though not proven, that partially saturated gas sands are sources of high P-wave attenuation. Sheriff (1975) presents an example in which a gas sand apparently attenuates the seismic wave and so creates a shadow zone below the gas pocket. In borehole sonic logs the phenomenon of "cycle skipping" is often observed opposite partially saturated gas sands (Pirson, 1963). Here the sonic wave is attenuated so much that the second half-cycle of the wave is picked as a first arrival, thus yielding an anomalously low velocity. Pirson (1963) also presents a so-called SATA log (signal attenuation, transmitted amplitude). This log was responsible for the discovery of a gas reservoir because of increased attenuation opposite the gas-bearing zone. This is what our experimental results would predict, assuming the gas sand is partially saturated and not completely dry. To our knowledge, this sort of attenuation log is not a standard logging tool. However, our results may allow this to become a more quantitative, less empirical well logging technique.

It is hoped that the results of this study will provide a conceptual framework in which to discuss seismic attenuation in partially and fully saturated rock. As with most scientific investigations, we have created at least as many questions as we have answered. Precise control over degree of saturation must be obtained in order to determine the exact variation of P and S attenuation with pore fluid content. Experiments must be performed at lower frequencies to confirm our suspicion that the results we have obtained also apply at seismic frequencies. Experiments at higher temperatures should be performed to fully evaluate Kjartansson and Denlinger's (1977) thermoelastic mechanism. Our experiments should be repeated with different rock types and different pore fluids. Correlations between attenuation and other rock properties should be attempted. And the list goes on.

APPENDIX A

DEFINITIONS

Seismic attenuation can be studied using several different methods, and each method has generated an "attenuation parameter" that is most conveniently suited to it. For instance, traveling plane waves show an amplitude decrease proportional to $\exp(-\alpha x)$, where α is often called the "attenuation coefficient". Although the natural units for α are nepers/unit length, it is often converted to decibels/unit length with the relation $\alpha' = (20\log_{10}e)\alpha = 8.686\alpha$. If we observe a single peak of a traveling plane wave (or alternatively the amplitude of a resonating system), we find that the amplitude decrease with time is proportional to $\exp(-\gamma t)$. Since $\gamma t = \alpha x$, we can easily relate γ and α through

$$\gamma = \alpha x/t = \alpha v$$

where v is the phase velocity of the wave.

When studying resonating systems, the "sharpness" of a resonance is often used as a measure of energy loss. The dimensionless parameter Q is generally used to quantify the sharpness of a resonance, with $Q = f/\Delta f$. Here f is the resonance frequency and Δf is the width of a resonance peak at one-half the maximum power, or, for small attenuation, $1/\sqrt{2}$ times the maximum output signal (displacement, velocity or acceleration). This is discussed in more detail in Appendix C.

Attenuation can also be related to the fractional energy loss per stress cycle. It can be shown that for small attenuation, Q can be related to this energy loss through the relation $Q = 2\pi E/\Delta E$ where E is the maximum energy stored during the stress cycle and ΔE is the energy dissipated during that cycle. An alternative relation, valid for large Q, is $Q = 4\pi E_{av}/\Delta E$ where E_{av} is the average energy stored during the stress cycle.

Another means of representing attenuation is with the log decrement. If A_1 and A_2 represent successive peaks of a traveling plane wave, or successive maxima of a decaying resonance, then the log decrement, δ, is given by

$$\delta = \ln(A_1/A_2)$$

Any linear medium exhibiting attenuation can be characterized by a complex modulus relating stress and strain. For an elastic material with no loss, the modulus is real. If stress and strain are related through a complex modulus, then they are necessarily out of phase. This phase angle, ϕ, is another measure of attenuation. If the complex modulus is written as $M = M_1 + iM_2$, then $\tan \phi = M_2/M_1$.

Fortunately, for materials with a reasonably small amount of attenuation ($Q > \sim 10$), the various parameters we have discussed can be easily related. Derivations of these relations can be found in many papers and texts, including Zener (1948), Kolsky (1963), and O'Connell and Budiansky (1978). We shall simply summarize them below.

$$Q^{-1} = \tan\phi = M_2/M_1$$

$$Q^{-1} = \Delta E/2\pi E = \Delta E/4\pi E_{av}$$

$$Q^{-1} = \Delta f/f$$

$$\alpha = \pi f/Qv$$

$$\gamma = \pi f/Q$$

$$\delta = \pi/Q$$

APPENDIX B

RELATIONS BETWEEN Q_s, Q_e, Q_p, Q_k

In bar resonance experiments we measure the attenuation of extensional and torsional waves, whereas in the earth we are generally interested in compressional and shear wave attenuation. It would be useful to be able to convert attenuation data between different wave types. In this appendix we will derive relations between Q_s, Q_e, Q_p, and Q_k where these are the specific attenuation factors for shear waves, extensional waves, compressional (P) waves, and bulk compression, respectively.

We make several important assumptions in the following derivations. The first is that the solid can be described using complex moduli with small imaginary components. By small we mean that to first order we can ignore products of imaginary components compared to products of real components. We also adopt the definition of Q given by $Q^{-1} = \mathrm{Im}(M)/\mathrm{Re}(M)$ where M represents a complex modulus controlling a certain type of wave propagation. We will also make use of the correspondence principle (Fung, 1965) which lets us substitute complex moduli for their corresponding moduli in the equations of linear elasticity.

In order to apply the resulting equations to our resonance data, we must assume that the bars are very thin and infinitely long. This allows us to use Young's modulus (E) and the shear modulus (μ) to completely describe extensional waves and torsional waves, respectively, without the need of second order corrections. Of course, this assumption is never met in practice, but by maintaining a large length to diameter ratio the approximation is very good. Note that this assumption puts a limit on the application of the resulting equations, but not on the validity of the equations themselves.

Analysis

Our analysis will consist of three parts. The first will relate Q_k, Q_p, and Q_s, the second will relate Q_k, Q_e, and Q_p, and the third will discuss some consequences of the relations.

Part 1

Let $M = \lambda + 2\mu$ be the elastic modulus associated with P-wave velocity. If ν is Poisson's ratio, it can be shown that

$$M = \frac{2(\nu-1)}{2\nu-1}\,\mu. \tag{1}$$

Eq.(1) will be used later. If K is the bulk modulus it can also be shown that

$$K = M - (4/3)\mu \tag{2}$$

Using the correspondence principle, we can re-write Eq.(2) using complex moduli.

$$K + iK^* = (M + iM^*) - (4/3)(\mu + i\mu^*) \tag{3}$$

$$K + iK^* = [M - (4/3)\mu] + i[M^* - (4/3)\mu^*] \tag{4}$$

On each side of Eq.(4), divide the imaginary part by the real part.

$$\frac{K^*}{K} = \frac{M^* - (4/3)\mu^*}{M - (4/3)\mu} \tag{5}$$

$$\frac{K^*}{K} = \frac{M^*}{M - (4/3)\mu} - \frac{(4/3)\mu^*}{M - (4/3)\mu}$$

It will be shown later that Eq.(1) is also true if M, ν, μ are the real parts of complex moduli having small imaginary components. Then we can use Eq.(1) to re-write the denominators.

$$\frac{K^*}{K} = \frac{M^*}{M - \frac{2(2\nu-1)M}{3(\nu-1)}} - \frac{(4/3)\mu^*}{\frac{2(\nu-1)\mu}{2\nu-1} - \frac{4\mu}{3}}$$

$$\frac{K^*}{K} = \frac{M^*}{M\left[1 - \frac{2(2\nu-1)}{3(\nu-1)}\right]} - \frac{(4/3)\mu^*}{\mu\left[\frac{2(\nu-1)}{2\nu-1} - (4/3)\right]}$$

Now, $Q_k^{-1} = K^*/K$, $Q_p^{-1} = M^*/M$, $Q_s^{-1} = \mu^*/\mu$, so

$$\frac{1}{Q_k} = \frac{1}{Q_p\left[1 - \frac{2(2\nu-1)}{3(\nu-1)}\right]} - \frac{1}{Q_s\left[\frac{3(\nu-1)}{2(2\nu-1)} - 1\right]}$$

This can be re-arranged to give

$$\frac{1+\nu}{Q_k} = \frac{3(1-\nu)}{Q_p} - \frac{2(1-2\nu)}{Q_s} \qquad (6)$$

This is our relation between Q_k, Q_p, and Q_s.

Part 2

It can be shown that

$$E = 2\mu(\nu+1) \qquad (7)$$

As with Eq.(1), Eq.(7) is true both for real moduli and for the real parts of complex moduli having small imaginary components. We will use Eq.(7) later. It can also be shown that

$$3K = E\mu/(3\mu-E) \qquad (8)$$

Again, we will re-write Eq.(8) using complex moduli.

$$3(K + iK^*) = \frac{(E + iE^*)(\mu + i\mu^*)}{3(\mu + i\mu^*) - (E + iE^*)} \tag{9}$$

$$= \frac{(E\mu - E^*\mu^*) + i(E^*\mu + E\mu^*)}{(3\mu - E) + i(3\mu^* - E^*)}$$

$$= \frac{[(E\mu - E^*\mu^*) + i(E^*\mu + E\mu^*)][(3\mu - E) - i(3\mu^* - E^*)]}{(3\mu - E)^2 + (3\mu^* - E^*)^2}$$

$$= \frac{[3E\mu^2 - E^2\mu - \mu(E^*)^2 + 3E(\mu^*)^2] + i[3E^*\mu^2 - E^2\mu^* - \mu^*(E^*)^2 + 3E^*(\mu^*)^2]}{\text{real denominator}}$$

This equation simplifies when we neglect multiples of starred terms. This is allowed since we have assumed small attenuation.

$$3(K + iK^*) = \frac{(3E\mu^2 - E^2\mu) + i(3E^*\mu^2 - E^2\mu^*)}{\text{real denominator}}$$

On each side of this equation, divide the imaginary part by the real part.

$$\frac{K^*}{K} = \frac{3E^*\mu^2 - E^2\mu^*}{3E\mu^2 - E^2\mu}$$

$$\frac{K^*}{K} = \frac{3E^*\mu^2}{3E\mu^2 - E^2\mu} - \frac{E^2\mu^*}{3E\mu^2 - E^2\mu} \tag{10}$$

Now use Eq.(7) to re-write the terms on the right side of Eq.(10).

$$\frac{K^*}{K} = \frac{3E^*E^2/[4(\nu+1)^2]}{\dfrac{3E^3}{4(\nu+1)^2} - \dfrac{E^3}{2(\nu+1)}} - \frac{4\mu^2(\nu+1)^2\mu^*}{6\mu^3(\nu+1) - 4\mu^3(\nu+1)^2} \tag{11}$$

Eq.(11) can be re-arranged to give

$$\frac{K^*}{K} = \frac{3E^*}{(1-2\nu)E} - \frac{2(\nu+1)\mu^*}{(1-2\nu)\mu}$$

Since $Q_k^{-1} = K^*/K$, $Q_e^{-1} = E^*/E$ and $Q_s^{-1} = \mu^*/\mu$, we have

$$\frac{1-2\nu}{Q_k} = \frac{3}{Q_e} - \frac{2(\nu+1)}{Q_s} \qquad (12)$$

This is our relation between Q_k, Q_e, and Q_s.

Part 3

It is obvious that Eq.(6) and Eq.(12) can be combined to eliminate Q_k and obtain a relation between Q_e, Q_s, and Q_p. Without going through the algebra, the result is

$$\frac{(1-\nu)(1-2\nu)}{Q_p} = \frac{1+\nu}{Q_e} - \frac{2\nu(2-\nu)}{Q_s} \qquad (13)$$

For a Poisson solid we have $\nu = 0.25$ and our relations become

$$5/Q_k = 9/Q_p - 4/Q_s \qquad (14)$$

$$1/Q_k = 6/Q_e - 5/Q_s \qquad (15)$$

$$3/Q_p = 10/Q_e - 7/Q_s \qquad (16)$$

It might be noted that Eq.(14) agrees with a result stated by Knopoff (1964). Several other relations that he gives come directly from Eqs.(14-16).

We can also derive a simple relation between the relative magnitudes of Q_k, Q_p, Q_e, and Q_s. Start with Eq.(13).

$$\frac{(1-\nu)(1-2\nu)}{Q_p} = \frac{1+\nu}{Q_e} - \frac{2\nu(2-\nu)}{Q_s}$$

$$\frac{Q_e}{Q_p}\frac{(1-\nu)(1-2\nu)}{1+\nu} = 1 - \frac{Q_e}{Q_s}\frac{2\nu(2-\nu)}{1+\nu}$$

$$1 = \frac{Q_e}{Q_p}\frac{(1-\nu)(1-2\nu)}{1+\nu} + \frac{Q_e}{Q_s}\frac{2\nu(2-\nu)}{1+\nu}$$

$$1 = A(Q_e/Q_p) + B(Q_e/Q_s) \qquad (17)$$

where $A = (1-\nu)(1-2\nu)/(1+\nu)$ and $B = 2\nu(2-\nu)/(1+\nu)$. (18)

It is readily verified that $A + B = 1$. (19)

If we require that $0 \leq \nu \leq 1/2$ then it is clear from Eq.(18) that

$$A \geq 0, \quad B \geq 0 \qquad (20)$$

To summarize, we now have

$$A(Q_e/Q_p) + B(Q_e/Q_s) = 1 \qquad (17)$$

$$A + B = 1 \qquad (19)$$

$$A \geq 0, \quad B \geq 0 \qquad (20)$$

It is clear that if $Q_e > Q_p$, then $Q_e < Q_s$, or if $Q_e < Q_p$, then $Q_e > Q_s$. One of the following must then be true.

$$Q_p > Q_e > Q_s \quad \text{or} \quad Q_p < Q_e < Q_s \tag{21}$$

A similar calculation will show that one of the following must be true.

$$Q_k > Q_p > Q_s \quad \text{or} \quad Q_k < Q_p < Q_s \tag{22}$$

Combining (21) and (22) gives our final result.

$$Q_k > Q_p > Q_e > Q_s \tag{23}$$

or

$$Q_k < Q_p < Q_e < Q_s \tag{24}$$

It can also be shown that the possibility exists for

$Q_k = Q_p = Q_e = Q_s$

Summary

Given the assumptions of small attenuation described by complex moduli related through the correspondence principle, the following results have been derived.

$$\frac{(1-\nu)(1-2\nu)}{Q_p} = \frac{1+\nu}{Q_e} - \frac{2\nu(2-\nu)}{Q_s}$$

$$\frac{1+\nu}{Q_k} = \frac{3(1-\nu)}{Q_p} - \frac{2(1-2\nu)}{Q_s}$$

$$\frac{1-2\nu}{Q_k} = \frac{3}{Q_e} - \frac{2(\nu+1)}{Q_s}$$

$$Q_k > Q_p > Q_e > Q_s$$

or $Q_k < Q_p < Q_e < Q_s$

or $Q_k = Q_p = Q_e = Q_s$

For a Poisson solid with $\nu = 0.25$ the first three results reduce to-

$3/Q_p = 10/Q_e - 7/Q_s$

$5/Q_k = 9/Q_p - 4/Q_s$

$1/Q_k = 6/Q_e - 5/Q_s$

Note- to use the general form of these results we need to know Poisson's ratio.

$$\nu = (E/2\mu) - 1$$

In bar resonance experiments, E and μ can be found from the extensional and torsional resonance frequencies. Spinner and Tefft (1961) give formulae and tables that include correction factors based on sample geometry. Using these the moduli, and thus ν, can be found with good precision.

In lab or field experiments using P and S body waves, ν can be found directly from the velocities.

$$\nu = \frac{V_p^2 - 2V_s^2}{2(V_p^2 - V_s^2)} \qquad (25)$$

We will now show that Eq.1 is valid if M, ν, μ are real parts of complex moduli with small imaginary components. This result was used in the preceding derivation.

Re-write Eq.(1) using complex moduli.

$$M + iM^* = \frac{2(\nu + i\nu^* - 1)(\mu + i\mu^*)}{2(\nu + i\nu^*) - 1}$$

$$(M + iM^*)[2(\nu + i\nu^*) - 1] = 2(\nu + i\nu^* - 1)(\mu + i\mu^*)$$

Equate the real parts on each side.

$$2M\nu - M - 2M^*\nu^* = 2(\nu\mu - \nu^*\mu^* - \mu)$$

$$M(2\nu - 1) - 2M^*\nu^* = 2\mu(\nu - 1) - 2\nu^*\mu^*$$

Since we have assumed small imaginary components, we can neglect products of these terms.

$$M(2\nu - 1) = 2\mu(\nu - 1)$$

$$M = \frac{2(\nu - 1)}{2\nu - 1}\mu$$

This is the same as Eq.(1).

It is also easily shown that Eq.(7) is valid whether E, μ and ν are real elastic moduli or the real parts of complex moduli. Therefore the ν that is used in the relations between Q's is the real part of a complex Poisson's ratio. Since we calculate ν from the real parts of complex velocities, we are in fact calculating the real part of a complex ν (assuming small attenuation). It is easily shown that, assuming small attenuation, Eq.(25) is true whether the variables are real elastic parameters or the real parts of complex parameters.

APPENDIX C

THEORY BEHIND THE RESONANT BAR TECHNIQUE

Simple resonating systems are most easily analyzed by studying a damped harmonic oscillator. (See note at the end of this appendix.) This has bee done in detail by many authors (e.g. Barger and Olsson, 1973; Symon, 1960; Morse, 1948). In the following we shall outline the analysis and discuss some interesting features that relate to measurements of attenuation.

The equation of motion of a damped harmonic oscillator can be expressed as

$$m(d^2x/dt^2) = -kx - b(dx/dt) \tag{1}$$

where m is the mass, k is the stiffness, and b is the damping coefficient. Here kx is the elastic restoring force given by Hooke's Law and b(dx/dt) is a viscous damping force. Eq.(1) is often re-written as

$$d^2x/dt^2 + 2\gamma(dx/dt) + \omega_0{}^2x = 0 \tag{2}$$

where $\gamma = b/2m$ and $\omega_0^2 = k/m$. ω_0 is the natural frequency of the oscillator with no damping. We are interested in cases of small damping for which $\gamma > \omega_0$, generally referred to as underdamped. A solution to Eq.(2) is then

$$x(t) = a \exp(-\gamma t) \cos[(\omega_0^2-\gamma^2)^{1/2}t + \alpha] \tag{3}$$

where 'a' and 'α' are determined by the initial conditions. This solution is a sinusoid decaying exponentially with time constant γ^{-1}. We might point out that the frequency of the decay is not ω_0, but $\omega_f = (\omega_0 - \gamma^2)^{1/2}$. However, for small damping the difference is negligible. For instance, if $Q = 10$ then $\omega_f = 0.9987\omega_0$.

It can be shown that for small attenuation, the total energy in the system decays as $E = E_0 \exp(-2\gamma t)$. This might be expected if the maximum energy is proportional to the square of the maximum amplitude. It then follows that

$$E^{-1}(dE/dt) = -2\gamma$$

If we let E be the maximum (or initial) energy in the system during one stress cycle, we can approximate dE/dt by $\Delta E/\Delta t$ where $-\Delta E$ is the energy dissipated during the cycle and $\Delta t = 1/f$ is the period of the cycle. Then

$$E^{-1}(\Delta E/\Delta t) = 2\gamma$$

$\Delta E/E = 2\gamma\Delta t = 2\gamma/f$

$\Delta E/2\pi E = \gamma/\pi f$

In Appendix A we show that $Q^{-1} = \Delta E/2\pi E$, so

$Q^{-1} = \gamma/\pi f$

$\gamma = \pi f/Q$

This result was also stated in Appendix A.

Thus by measuring the time constant of a decay of resonance, the Q of the system can be determined. When applying this method to a bar-shaped sample, the bar is driven at or near resonance to build up a large initial amplitude. When the driving force is turned off, the bar has no memory of the frequency at which it was being driven but begins to vibrate at its resonant frequency. In practice we deviate from this theoretical analysis in that the driving force is concentrated at the end of the bar. Ideally we would like to have a driving force that varies sinusoidally along the length of the bar so that each mass element can be treated as a damped harmonic oscillator. What actually happens when the driving force is turned off is that the bar begins to vibrate in a combination of all of its normal modes, and so the decay is actually a combination of many different exponential decays. Fortunately, by driving the bar near a resonance frequency we can excite a particular mode (or harmonic) much more strongly than other modes (or harmonics). The observed decay is very nearly that of a pure resonance mode.

The resonance decay technique discussed above is essentially a time domain technique. A frequency domain technique may also be used in which the amplitude of the oscillator is recorded as a function of the driving frequency. The equation of motion of a driven damped harmonic oscillator is

$$m(d^2x/dt^2) = -kx - b(dx/dt) + F_0\cos(\omega t) ,$$

or, after re-arranging as before,

$$d^2x/dt^2 + 2\gamma(dx/dt) + \omega_0{}^2x = (F_0/m)\cos(\omega t) \qquad (4)$$

Here $F_0\cos(\omega t)$ is the driving force. A particular solution to Eq.(4) is

$$x(\omega,t) = (F_0/m)[(\omega_0{}^2 - \omega^2)^2 + 4\gamma^2\omega^2]^{-1/2} \sin(\omega t + \beta) \qquad (5)$$

where $\beta = \tan^{-1}[(\omega_0{}^2 - \omega^2)/2\gamma\omega]$.

When studying a resonance peak we are only interested in the amplitude of the vibrations given by

$$|x| = (F_0/m)[(\omega_0{}^2 - \omega^2)^2 + 4\gamma^2\omega^2]^{-1/2} \qquad (6)$$

Since γ is related to Q, we can in principle determine Q by measuring $|x|$, F_0, m, ω_0 and ω and substituting these into Eq.(6). However, it is much easier to make use of the shape of the amplitude response given by Eq.(6), which has a maximum near $\omega = \omega_0$. This is most easily done by making a simplifying approximation to Eq.(6), in which we assume that $\omega \approx \omega_0$. Then

$$|x| = (F_0/m)[(\omega_0-\omega)^2(\omega_0+\omega)^2 + 4\gamma^2\omega^2]^{-1/2}$$

$$|x| \approx (F_0/m)[(\omega_0-\omega)^2(2\omega_0)^2 + (2\omega_0)^2\gamma^2]^{-1/2}$$

$$|x| \approx (F_0/2\omega_0 m)[(\omega_0-\omega)^2 + \gamma^2]^{-1/2} \qquad (7)$$

This is an approximation to the resonance peak which is symmetric about ω_0.

Let $|x_0|$ equal $|x|$ at $\omega = \omega_0$. Then from Eq.(7),

$$|x_0| = F_0/2\omega_0 m\gamma$$

The normalized response is then given by

$$R = |x|/|x_0| = \gamma/[(\omega_0-\omega)^2 + \gamma^2]^{1/2}$$

This can be re-arranged to give

$$|\omega_0-\omega| = (R^{-2}-1)^{1/2}\gamma$$

Using the relation $\gamma = \pi f/Q = \omega/2Q$ gives

$$Q = (R^{-2}-1)^{1/2}\ \omega/2|\omega_0-\omega|$$

or

$$Q = (R^{-2}-1)^{1/2}\ f/2|f_0-f|$$

If we require that $Q = f/2|f_0-f|$ then it follows that $R = 1/\sqrt{2}$. Therefore if we choose $|x|/|x_0|$ such that $|x| = |x_0|/\sqrt{2}$, then $Q = f/2|f_0-f|$ where f is measured at amplitude $|x|$. Since the approximate response given by Eq.(6) is symmetric about $f = f_0$, we can ignore the difference between $f>f_0$ and $f<f_0$ and define $\Delta f \equiv 2|f_0-f|$, in which case

$$Q = f/\Delta f. \tag{8}$$

Here Δf is the width of the resonance peak measured at an amplitude which is $1/\sqrt{2}$ times the maximum amplitude of the peak and is known as the half-width of the resonance peak.

We could stop here and use Eq.(8) to measure attenuation, making the assumption that we have small attenuation. However, we thought it would be interesting to plot some resonance peaks using both the exact and approximate equations (Eqs.(6 and 7)), and find out how good the approximation is. Also, it would be interesting to plot resonance peaks of the velocity response and the acceleration response of the oscillator. This is of practical importance because vibrations can be detected with transducers that respond to either displacement, velocity, or acceleration. For instance, in the present study we have used piezoelectric transducers (phonograph pick-ups) fixed at one end of the bar so that they respond to displacement. Transducers using moving coils, moving magnets, or variable reluctance, (such as magnetic phonograph pick-ups or so-called magnetic pick-ups used to count gear teeth) respond to velocity. Piezoelectric transducers having one free surface and the opposite face cemented to the sample will respond to acceleration.

Differentiating Eq.(3) with respect to time shows that during a resonance decay both velocity and acceleration fall off as exp(-γt), so this measurement is the same regardless of the type of transducer used. To find the response of velocity and acceleration during resonance, we simply differentiate Eq.(5) with respect to time, yielding

$$v(\omega,t) = \omega x(\omega,t) \tag{9}$$

$$a(\omega,t) = \omega v(\omega,t) = \omega^2 x(\omega,t) \tag{10}$$

As before, we are only interested in the amplitude of the vibrations.

$$|x| = (F_0/m)[(\omega_0{}^2-\omega^2)^2 + 4\gamma^2\omega^2]^{-1/2} \tag{6}$$

$$|v| = \omega|x| \tag{11}$$

$$|a| = \omega^2|x| \tag{12}$$

We have used Eq.(6, 11, and 12) to plot resonance peaks of displacement, velocity and acceleration for several values of Q. In addition we have plotted points on the approximate displacement resonance peak given by Eq.(7). These are shown in Figures (C1-C4). The horizontal scales are normalized frequency, ω/ω_0, and the vertical scale is normalized amplitude. For programming convenience, all peaks have been normalized to an amplitude of one at $\omega/\omega_0 = 1$. The peaks do not necessarily have a maximum at $\omega/\omega_0 = 1$. The figures also have horizontal lines at an amplitude of $1/\sqrt{2}$ which is where the half-width would be measured. The main point to be obtained from these figures is that for reasonably large values of Q ($Q>\sim 10$) we will get virtually the same value of Q, using $Q = f/\Delta f$, from resonance peaks of displacement, velocity, or acceleration.

Note - In this appendix we have modelled a resonating bar with a simple damped harmonic oscillator, which is essentially a Kelvin solid (spring and dashpot in parallel). However, we are definitely not assuming that our samples are Kelvin solids (they are not). Regardless of the exact constitutive relation we assume, if it is linear and if we assume that we have small attenuation, similar results will be obtained to those that we have derived. O'Connell and Budiansky (1978) discuss this in more detail. We have used a damped harmonic oscillator model only because it is the simplest model available.

Figure (C1). Q = 10. Theoretical resonance peaks for displacement (D), velocity (V), and acceleration (A). X's indicate approximation to displacement resonance peak.

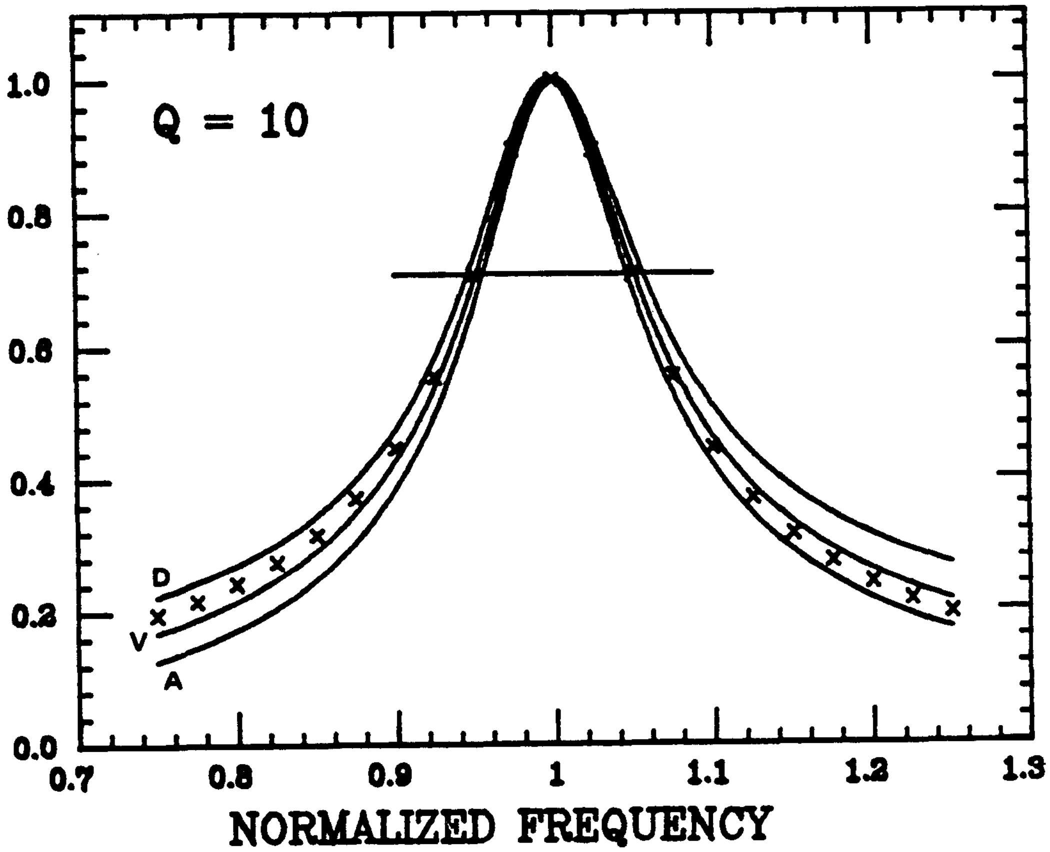

Figure (C2). Q = 25. Theoretical resonance peaks for displacement (D), velocity (V), and acceleration (A). X's indicate approximation to displacement resonance peak.

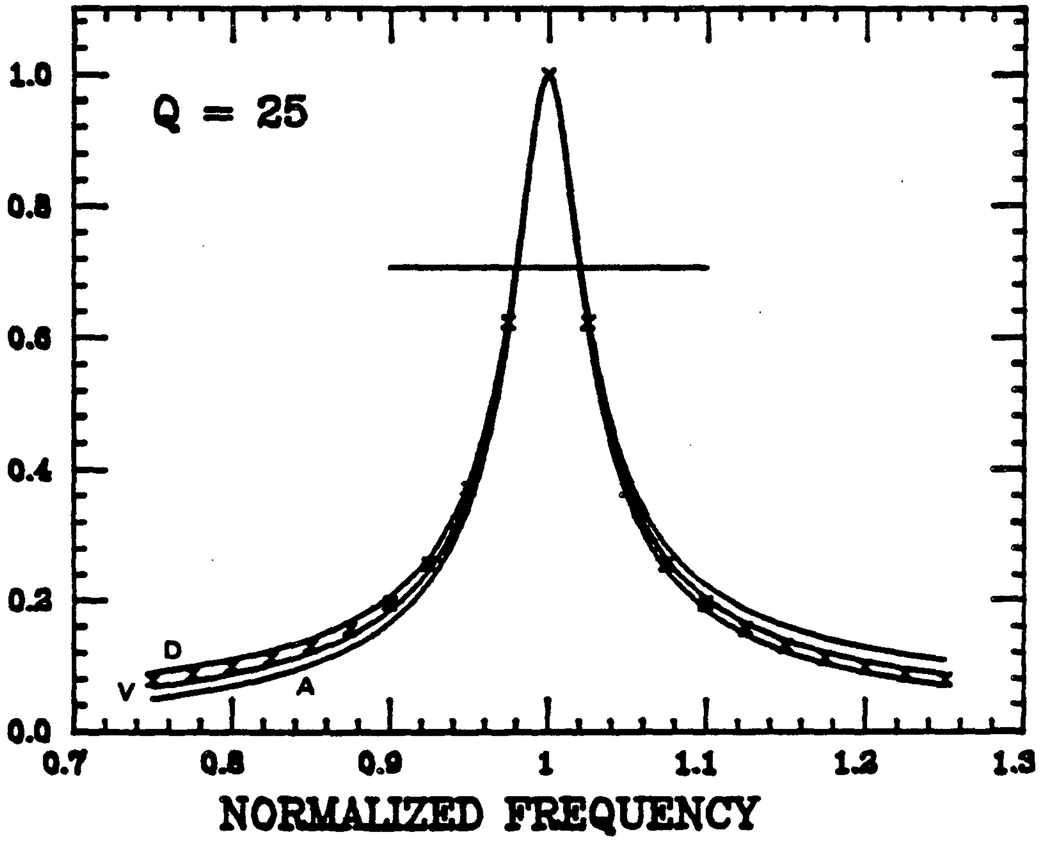

Figure (C3). Q = 50. Theoretical resonance peaks for displacement (D), velocity (V), and acceleration (A). X's indicate approximation to displacement resonance peak.

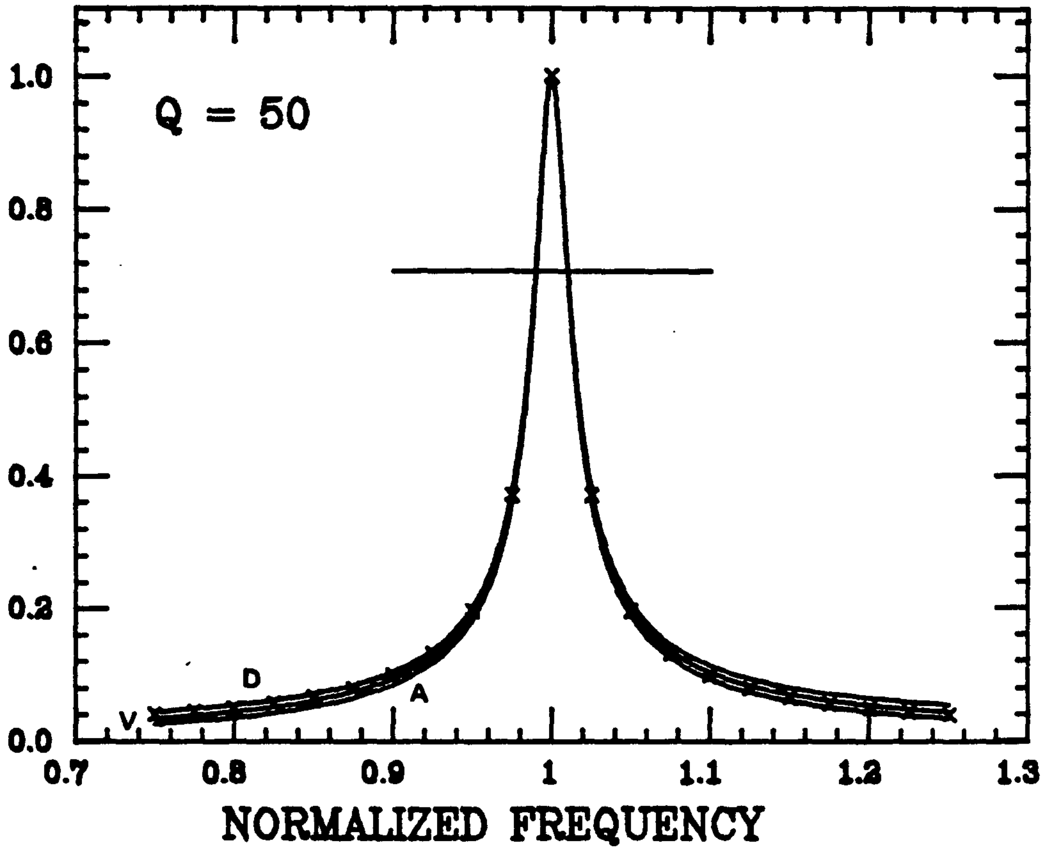

Figure (C4). Q = 100. Theoretical resonance peaks for displacement (D), velocity (V), and acceleration (A). X's indicate approximation to displacement resonance peak.

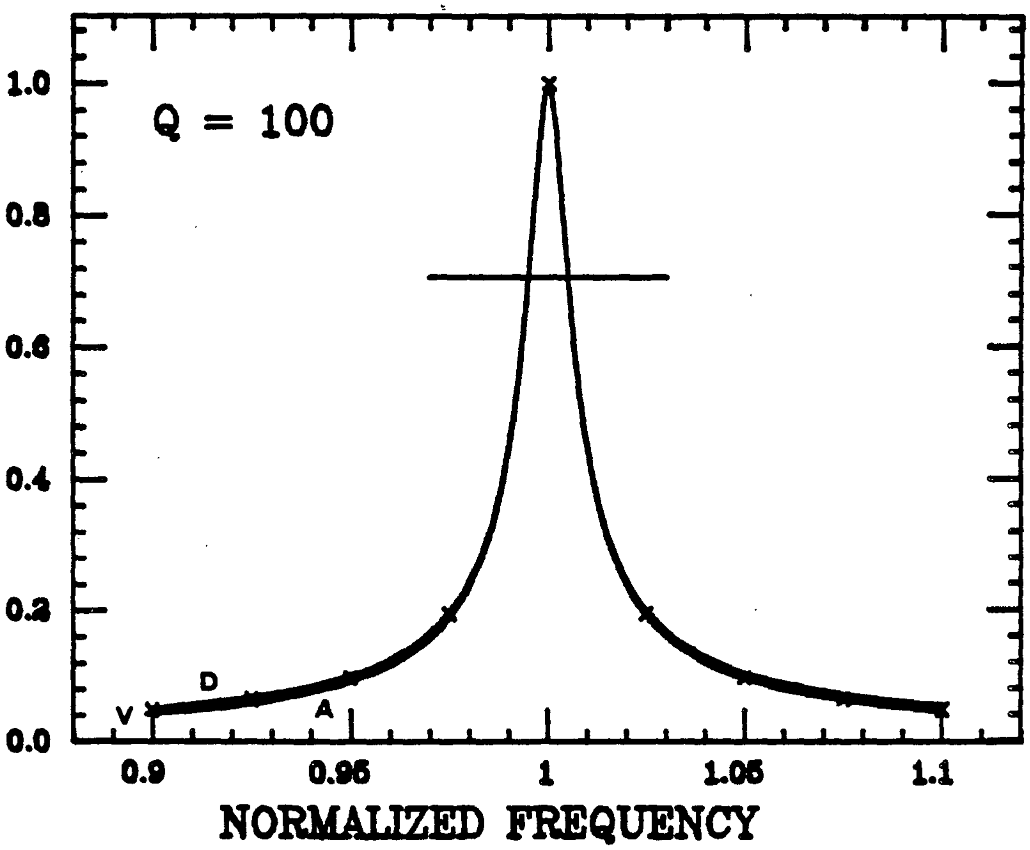

APPENDIX D

Equipment Listing

1. phonograph pick-up - Electo-Voice #5572D stereo cartridge with diamond needle #2428DS
2. function generator A - Krohn-Hite model 5400B
3. function generator B - Wavetek model 180
4. frequency counter - Hewlett-Packard model 5212A
5. gate - General Radio tone burst generator model 1396-B
6. power amplifier - California Instruments Invertron model 101T
7. amplifier - Hewlett-Packard model 465A
8. filter - Krohn-Hite model 3550
9. X-Y plotter - Hewlett-Packard model 7004-B with 17174B DC offset, 17171A DC pre-amplifier and 17177A AC/DC converter, DC pre-amplifier
10. oscilloscope - Tektronix model 5440 with 5A48 dual trace amplifier and 5B42 delaying time base
11. camera - Tektronix C-59
12. pressure gauge - Heise CMM, 0-600 bars, 12 inch face
13. differential pressure gauge - Celesco P3D, ±5000 psi with model CD10 carrier demodulator
14. calculator - Hewlett-Packard model HP-97
15. heat-shrink tubing - Raychem Thermofit type RNF-100

16. epoxy - Klenk's fast set epoxy, Raychem S-1009, and Emerson and Cuming's 264-F
17. pore pressure intensifier - High Pressure Equipment model 37-6-30
18. gas intensifier - Teledyne Sprague model S-3600WB-60
19. digitizer - millimeter scale plus a sharp eye
20. strain gage - Kulite Semiconductor type DHP-10000-500; gage factor = 175±5%
21. capillary tubing - Small Parts # CTX-6220, type 316 SS, 0.0625" OD, 0.020" ID

APPENDIX E

Selected Data Listing

For the convenience of anyone wishing to work with the data we have collected, data for dry, partially saturated, and fully saturated Massilon sandstone is listed below. Most of this data has been plotted in Chapter V. The data is listed in blocks, each block containing all the data taken at a particular value of effective stress. The organization of each block is given at the top of each page. As usual, the subscripts S, E, P, and K refer to shear, extension, P-wave, and bulk compression, respectively. P_c is confining pressure, P_p is pore pressure, and P_{eff} is effective stress (P_c-P_p). Poisson's ratio is indicated by ν. The conversions between velocity and resonant frequency are $V_e=2f_e$ and $V_s=2.181f_t$.

Pressures are given in bars and velocities are given in meters/second. Values of attenuation (Q^{-1}) have been multiplied by 1000. The unusual spacing of the pressures (in bars) is because the actual spacing used was 500 psi (34.5 bars).

Dry Massilon Sandstone

P_{eff} P_c P_p	Q_s^{-1} Q_e^{-1} Q_p^{-1} Q_k^{-1}	Q_s Q_e Q_p Q_k	V_s V_e V_p	ν V_p/V_s
0	9.23	108	1291	0.118
0	7.80	128	1930	1.52
0	6.68	150	1961	
	3.50	286		
34	6.21	161	1672	0.190
34	4.93	203	2580	1.62
0	3.18	314	2704	
	-0.01	---		
69	5.41	185	1827	0.215
69	4.30	233	2848	1.66
0	2.23	448	3033	
	-0.64	---		
103	5.09	196	1918	0.226
103	3.82	262	3004	1.68
0	1.59	629	3224	
	-1.43	---		
138	4.62	216	1977	0.235
138	3.50	286	3108	1.70
0	1.27	787	3361	
	---	---		
172	4.46	224	2012	0.244
172	---	---	3174	1.72
0	---	---	3458	
	---	---		

Dry Massilon Sandstone

P_{eff} P_c P_p	Q_s^{-1} Q_e^{-1} Q_p^{-1} Q_k^{-1}	Q_s Q_e Q_p Q_k	V_s V_e V_p	ν V_p/V_s
207	4.30	233	2038	0.248
207	---	---	3220	1.73
0	---	---	3520	
	---	---		
241	4.30	233	2056	0.247
241	---	---	3246	1.72
0	---	---	3545	
	---	---		
276	4.14	242	2073	0.250
276	3.18	314	3278	1.73
0	0.95	1050	3591	
	-1.59	---		
310	4.30	233	2086	0.253
310	3.18	314	3302	1.74
0	0.48	2080	3626	
	-2.39	---		
345	4.14	242	2099	0.254
345	3.18	314	3324	1.74
0	1.11	901	3653	
	-1.27	---		

Partially Saturated Massilon Sandstone

P_{eff} P_c P_p	Q_s^{-1} Q_e^{-1} Q_p^{-1} Q_k^{-1}	Q_s Q_e Q_p Q_k	V_s V_e V_p	ν V_p/V_s
0	38.7	25.8	972	0.122
0	56.8	17.6	1456	1.52
0	69.4	14.4	1481	
	111.0	9.0		
34	24.8	40.3	1463	0.217
34	32.2	31.1	2282	1.66
0	43.5	23.0	2433	
	61.0	16.4		
69	19.3	51.8	1637	0.236
69	24.7	40.5	2574	1.70
0	35.8	27.9	2785	
	50.0	20.0		
138	14.5	69.0	1803	0.246
138	17.8	56.2	2846	1.72
0	25.2	39.7	3106	
	33.9	29.5		
172	13.2	75.8	1844	0.250
172	15.3	65.4	2916	1.73
0	19.9	50.3	3194	
	25.3	39.5		
207	11.9	84.0	1875	0.250
207	13.7	73.0	2964	1.73
0	17.8	56.2	3246	
	22.6	44.2		

Partially Saturated Massilon Sandstone

P_{eff} P_c P_p	Q_s^{-1} Q_e^{-1} Q_p^{-1} Q_k^{-1}	Q_s Q_e Q_p Q_k	V_s V_e V_p	ν V_p/V_s -
241	11.3	88.5	1899	0.251
241	12.7	78.7	3004	1.74
0	16.2	61.7	3295	
	20.2	49.5		
276	10.5	95.2	1918	0.249
276	12.3	81.3	3032	1.73
0	16.2	61.7	3318	
	20.9	47.8		
310	10.2	98.0	1934	0.252
310	11.3	88.5	3060	1.74
0	14.2	70.4	3359	
	17.4	57.5		
345	9.55	105	1942	0.269
345	---	---	3094	1.78
0	---	---	3454	
	---	---		

Fully Saturated Massilon Sandstone

P_{eff} P_c P_p	Q_s^{-1} Q_e^{-1} Q_p^{-1} Q_k^{-1}	Q_s Q_e Q_p Q_k	V_s V_e V_p	ν V_p/V_s
35	32.5	30.8	1428	0.428
345	31.2	32.1	2414	2.81
310	9.9	101	4015	
	6.8	147		
69	22.6	44.2	1620	0.412
345	21.8	45.9	2722	2.59
276	11.0	90.9	4188	
	8.1	123		
104	18.3	54.6	1724	0.395
345	17.0	58.8	2880	2.40
241	3.7	270	4135	
	-0.6	---		
138	16.2	61.7	1781	0.379
345	15.0	66.7	2958	2.27
207	4.8	208	4037	
	1.0	1000		
173	---	---	1827	0.366
345	---	---	3020	2.18
172	---	---	3979	
	---	---		
207	13.1	76.3	1862	0.386
345	---	---	3100	2.32
138	---	---	4326	
	---	---		

Fully Saturated Massilon Sandstone

P_{eff} P_c P_p	Q_s^{-1} Q_e^{-1} Q_p^{-1} Q_k^{-1}	Q_s Q_e Q_p Q_k	V_s V_e V_p	ν V_p/V_s
242	11.8	84.7	1884	0.372
345	10.3	97.1	3120	2.21
103	1.0	1000	4171	
	-5.7	---		
276	11.0	90.9	1905	0.361
345	9.7	103	3144	2.15
69	1.0	1000	4090	
	-3.0	---		
311	10.5	95.2	1918	0.358
345	8.9	112	3162	2.13
34	-2.1	---	4083	
	-7.2	---		

REFERENCES

Barger, V. and M. Olsson, Classical Mechanics: A Modern Perspective, McGraw-Hill, 1973.

Bear, J., Dynamics of Fluids in Porous Media, Elsevier, N.Y., 1972.

Bevington, P.R., Data Reduction and Error Analysis for the Physical Sciences, McGraw-Hill, 1969.

Biot, M.A., Theory of propagation of elastic waves in a fluid saturated, porous solid. Low-frequency range, J. Acoust. Soc. Am., 28, 168-178, 1956a.

Biot, M.A., Theory of propagation of elastic waves in a fluid saturated, porous solid. II. Higher frequency range, J. Acoust. Soc. Am., 28, 179-191, 1956b.

Birch, F., Velocity and attenuation from resonant vibrations of spheres of rock, glass, and steel, J. Geophys. Res., 80, 756-764, 1975.

Birch, F. and D. Bancroft, Elasticity and internal friction in a long column of granite, Bull. Seis. Soc. Am., 28, 243-254, 1938.

Born, W.T., The attenuation constant of earth materials, _Geophysics_, _6_, 132-148, 1941.

Brennan, B.J. and F.D. Stacey, Frequency dependence of elasticity of rock - test of seismic velocity dispersion, _Nature_, _268_, 220-222, 1977.

Bruckshaw, J.M. and P.C. Mahanta, The variation of the elastic constants of rocks with frequency, _Petroleum_, _17_, 14-18, 1954.

Byerlee, J.D., Frictional characteristics of granite under high confining pressure, _J. Geophys. Res._, _72_, 3639-3648, 1967.

Collins, F. and C.C. Lee, Seismic wave attenuation characteristics from pulse experiments, _Geophysics_, _21_, 16-40, 1956.

Darcy, H., _Les Fontaines Publiques de la Ville de Dijon_, Dalmont, Paris, 1856.

Domenico, N.S., Effect of brine-gas mixture on velocity in an unconsolidated sand reservoir, _Geophysics_, _41_, 5, 882-894, 1976.

Elliot, S.E. and B.F. Wiley, Compressional velocities of partially saturated unconsolidated sands, _Geophysics_, _40_, 6, 949-954, 1975.

Fung, Y.C., Foundations of Solid Mechanics, Prentice-Hall, 1965.

Gardner, G.H.F. and M.H. Harris, Velocity and attenuation of elastic waves in sands, SPWLA Ninth Annual Logging Symposium, 1-18, 1968.

Gardner, G.H.F., M.R.J. Wyllie, and D.M. Droschak, Effects of pressure and fluid saturation on the attenuation of elastic waves in sands, J. Petrol. Tech., 16, 189-198, 1964.

Goodman, L.E. and C.B. Brown, Energy dissipation in contact friction: constant normal and cyclic tangential loading, J. Appl. Mech., 29, 17-22, 1962.

Gordon, R.B., Mechanical relaxation spectrum of crystalline rock containing water, J. Geophys. Res., 79, 2129-2131, 1974.

Gordon, R.B. and L.A. Davis, Velocity and attenuation of seismic waves in imperfectly elastic rock, J. Geophys. Res., 73, 3917-3935, 1968.

Gordon, R.B. and C.W. Nelson, Anelastic properties of the earth, Rev. Geophys., 4, 457-474, 1966.

Gordon, R.B. and D. Rader, Imperfect elasticity of rock: its influence on the velocity of stress waves, in Structure and Physical Properties of the Earth's Crust, Geophys. Monograph Ser., Vol. 14, ed. by J. Heacock, 235-242, 1971.

Gregory, A.R., Fluid saturation effects on dynamic elastic properties of sedimentary rocks, Geophysics, 41, 895-921, 1976.

Hadley, K., Comparison of calculated and observed crack densities and seismic velocities in Westerly granite, J. Geophys. Res., 81, 3484-3494, 1976.

Horn, H.M. and D.U. Deere, Frictional characteristics of minerals, Geotechnique, 12, 319-335, 1962.

Hueter, T.F. and R.H. Bolt, Sonics, J. Wiley & Sons, N.Y., 19, 1955.

Jackson, D.D. and D.L. Anderson, Physical mechanisms of seismic wave attenuation, Rev. Geophys. Space Phys., 8, 1-63, 1970.

Jaegar, J.C. and N.G.W. Cook, Fundamentals of Rock Mechanics, Halsted Press, N.Y., 1976.

Johnston, D.H., M.N. Toksoz, and A. Timur, Attenuation of seismic waves in dry and saturated rocks: II. Mechanisms, Geophysics, 44, 691-711, 1979.

Kjartansson, E., Constant Q - wave propagation and attenuation, J. Geophys. Res., in press, 1979.

Kjartansson, E., and R. Denlinger, Seismic wave attenuation due to thermal relaxation in porous media (abstract), *Geophysics*, *42*, 7, 1516, 1977.

Knopoff, L., Q, *Rev. Geophys.*, *2*, 625-660, 1964.

Knopoff, L. and G.J.F. MacDonald, Models for acoustic loss in solids, *J. Geophys. Res.*, *65*, 2191-2197, 1960.

Kolsky, H., *Stress Waves in Solids*, Dover, 1963.

Lockner, D.A., J.B. Walsh, and J.D. Byerlee, Changes in seismic velocity and attenuation during deformation of granite, *J. Geophys. Res.*, *82*, 5374-5378, 1977.

Lomnitz, C., Creep measurements in igneous rocks, *J. Geol.*, *64*, 473-479, 1956.

Lomnitz, C., Linear dissipation in solids, *J. Appl. Phys.*, *28*, 201-205, 1957.

Mason, W.P., Internal friction mechanism that produces an attenuation in the earth's crust proportional to the frequency, *J. Geophys. Res.*, *74*, 4963-4966, 1969.

Mason, W.P, Internal friction at low frequencies due to dislocations: Applications to metals and rock mechanics, in *Physical Acoustics: Principles and Methods, Vol. 8*, ed. by W.P. Mason and R.N. Thurston, Academic Press, N.Y., 1971a.

Mason, W.P., Internal friction in moon and earth rocks, *Nature*, *234*, 461-463, 1971b.

Mason, W.P., D.N. Beshers, and J.T. Kuo, Internal friction in Westerly granite: Relation to dislocation theory, *J. Appl. Phys.*, *41*, 5206-5209, 1970.

Mason, W.P. and J.T. Kuo, Internal friction of Pennsylvania slate, *J. Geophys. Res.*, *76*, 2084-2089, 1971.

Mason, W.P., K.J. Marfurt, D.N. Beshers, and J.T. Kuo, Internal friction in rocks, *J. Acous. Soc. Am.*, *63*, 1596-1603, 1978.

Mavko, G., Frictional attenuation: An inherent amplitude dependence, *J. Geophys. Res.*, in press, 1979.

Mavko, G. and E. Kjartansson, The effect of friction on velocity and attenuation (abstract), *Geophysics*, *44*, 333, 1979.

Mavko, G., E. Kjartansson, and K. Winkler, Seismic wave attenuation in rocks, *Rev. Geophys. Space Phys.*, in press, 1979.

Mavko, G. and A. Nur, Melt squirt in the asthenosphere, *J. Geophys. Res.*, *80*, 1444-1448, 1975.

Mavko, G. and A. Nur, Wave attenuation in partially saturated rocks, *Geophysics*, *44*, 161-178, 1979.

McDonal, F.J., F.A. Angona, R.L. Mills, R.L. Sengbush, R.A. van Nostrand, and J.E. White, Attenuation of shear and compressional waves in Pierre shale, *Geophysics*, *23*, 421-439, 1958.

McKavanagh, B. and F.D. Stacey, Mechanical hysteresis in rocks at low strain amplitudes and seismic frequencies, *Phys. Earth. Planet Int.*, *8*, 246-250, 1974.

Mindlin, R.D. and H. Deresiewicz, Elastic spheres in contact under varying oblique forces, *J. Appl. Mech.*, *20*, 327-344, 1953.

Mindlin, R.D., W.P. Mason, T.F. Osmer, and H. Deresiewicz, Effects of an oscillating tangential force on the contact surfaces of elastic spheres, *Proc. First U.S. Nat. Cong. Appl. Mech.*, 203-208, 1951.

Morse, P.M., *Vibration and Sound*, McGraw-Hill, 1948.

Nur, A., Viscous phase in rocks and the low-velocity zone, J. Geophys. Res., 76, 1270-1277, 1971.

Nur, A., Dilatancy, pore fluids and premonitory variations in T_s/T_p travel times, Bull. Seis. Soc. Am., 62, 1217-1222, 1972.

Nur, A. and G. Simmons, The effect of saturation on velocity in low porosity rocks, Earth. Plan. Sci. Lett., 7, 183-193, 1969.

Nur, A. and G. Simmons, The effect of viscosity of a fluid phase on velocity in low porosity rocks, Earth Planet. Sci. Lett., 7, 99-108, 1970.

O'Connell, R.J. and B. Budiansky, Viscoelastic properties of fluid-saturated cracked solids, J. Geophys. Res., 82, 36, 5719-5736, 1977.

O'Connell, R.J. and B. Budiansky, Measures of dissipation in viscoelastic media, Geophys. Res. Lett., 5, 1, 5-8, 1978.

Pandit, B.I. and J.C. Savage, An experimental test of Lomnitz's theory of internal friction in rocks, J. Geophys. Res., 78, 6097-6099, 1973.

Peselnick, L. and W.F. Outerbridge, Internal friction in shear and shear modulus of Solenhofen limestone over a frequency range of 10^7 cycles per second, J. Geophys. Res., 66, 581-588, 1961.

Peselnick, L. and I. Zietz, Internal friction of fine grained limestones at ultrasonic frequencies, Geophysics, 24, 285-296, 1959.

Pirson, S.J., Handbook of Well Log Analysis, Prentice-Hall, 1963.

Randall, M.J., Attenuative dispersion and frequency shifts of the Earth's free oscillations, Phys. Earth Planet. Int., 12, 1-4, 1976.

Ricker, N., The form and laws of propagation of seismic wavelets, Geophysics, 18, 10-40, 1953.

Savage, J.C., Comments on paper by R.B. Gordon and L.A. Davis, 'Velocity and attenuation of seismic waves in imperfectly elastic rock', J. Geophys. Res., 74, 726-728, 1969.

Savage, J.C. and H.S. Hasegawa, Evidence for a linear attenuation mechanism, Geophysics, 22, 1003-1014, 1967.

Sheriff, R.E., Factors affecting seismic amplitudes, Geophys. Pros., 23, 125-138, 1975.

Spetzler, H. and D.L. Anderson, The effect of temperature and partial melting on velocity and attenuation in a simple binary system, _J_. _Geophys_. _Res_., _73_, 6051-6060, 1968.

Spinner, S. and W.E. Tefft, A method for determining mechanical resonance frequencies and for calculating elastic moduli from these frequencies, _Proc_. _A_._S_._T_._M_., _61_, 1221-1238, 1961.

Stacey, F.D., M.T. Gladwin, B. McKavanagh, A.T. Linde, and L.M. Hastie. Anelastic damping of acoustic and seismic pulses, _Geophys_. _Surveys_, _2_, 133-151, 1975.

Stocker, R.L. and R.B. Gordon, Velocity and internal friction in partial melts, _J_. _Geophys_. _Res_., _80_, 4828-4836, 1975.

Stoll, R.D., Acoustic waves in saturated sediments, in _Physics_ _of_ _Sound_ _in_ _Marine_ _Sediments_, ed. by L. Hampton, Plenum Press, N.Y., 1974.

Stoll, R.D., Acoustic waves in ocean sediments, _Geophysics_, _42_, 715-725, 1977.

Stoll, R.D., and G.M. Bryan, Wave attenuaton in saturated sediments, _J_. _Acoust_. _Soc_. _Am_., _47_, 1440-1447, 1970.

Symon, K.R., _Mechanics_, Addison-Wesley, 1953.

Tittmann, B.R., Lunar rock seismic Q in 3000-5000 range achieved in laboratory, Phil. Trans. R. Soc. Lond. A, 285, 475-479, 1977.

Tittmann, B.R., Internal friction measurements and their implications in seismic Q structure models of the earth's crust, in The Earth's Crust, Geophys. Monog. Series, Vol. 20, ed. by J. Heacock, 197-213, 1978.

Tittmann, B.R., M. Abdel-Gawad, and R.M. Housley, Elastic velocity and Q measurements on Apollo 12, 14, and 15 rocks, Proc. Lunar Sci. Conf. 3rd, 2565-2575, 1972.

Tittmann, B.R., L. Ahlberg, and J. Curnow, Internal friction and velocity measurements, Proc. Lunar Sci. Conf. 7th, 3123-3132, 1976.

Tittmann, B.R., J.M. Curnow, and R.M. Housley, Internal friction quality factor Q>3100 achieved in lunar rock 70215,85, Proc. Lunar Sci. Conf. 6th, 3217-3226, 1975.

Tittmann, B.R., R.M. Housley, G.A. Algers, and E.H. Cirlin, Internal friction in rocks and its relationship to volatiles on the moon, Proc. Lunar Sci. Conf. 5th, 2913-2918, 1974.

Tittmann, B.R. R.M. Housley, and E.H. Cirlin, Internal friction of rocks and volatiles on the moon, Proc. Lunar Sci. Conf. 4th, 2631-2637, 1973.

Toksoz, M.N., D.H. Johnston, and A. Timur, Attenuation of seismic waves in dry and saturated rocks: I. Laboratory measurements, Geophysics, 44, 681-690, 1979.

Walsh, J.B., Seismic wave attenuation in rock due to friction, J. Geophys. Res., 71, 2591-2599, 1966.

Walsh, J.B., Attenuation in partially melted material, J. Geophys. Res., 73, 2209-2219, 1968.

Walsh, J.B., New analysis of attenuation in partially melted rock, J. Geophys. Res., 74, 4333-4337, 1969.

White, J.E., Seismic waves: Radiation, Transmission and Attenuation, McGraw-Hill, 1965.

White, J.E., Static friction as a source of seismic attenuation, Geophysics, 31, 333-339, 1966.

White, J.E., Computed seismic speeds and attenuation in rocks with partial gas saturation, Geophysics, 40, 224-232, 1975.

Winkler, K. and A. Nur, Depth constraints on dilatancy induced velocity anomalies, J. Phys. Earth, 25, Suppl., 231-241, 1977.

Winkler, K. and A. Nur, Pore fluids and seismic attenuation in rocks, Geophys. Res. Lett., 6, 1-4, 1979.

Winkler, K., A. Nur, and M. Gladwin, Friction and seismic attenuation in rocks, Nature, 277, 528-531, 1979.

Wyllie, M.R.J., G.H.F. Gardner, and A.R. Gregory, Studies of elastic wave propagation in porous media, Geophysics, 27, 569-589, 1962.

Zemanek, J. and I. Rudnick, Attenuation and dispersion of elastic waves in a cylindrical bar, J. Acoust. Soc. Am., 33, 1283-1288, 1961.

Zener, C.M., Elasticity and Anelasticity of Metals, Univ. of Chicago Press, 1948.